UCSF

UC San Francisco Electronic Theses and Dissertations

Title

The innate immune response to Mycobacterium tuberculosis infection

Permalink

https://escholarship.org/uc/item/94q0p9wz

Author

Manzanillo, Paolo Solano

Publication Date

2013

Peer reviewed|Thesis/dissertation

The innate immune response to *Mycobacterium tuberculosis*

infection

by

Paolo Solano Manzanillo

DISSERTATION

Submitted in partial satisfaction of the requirements for the degree of

DOCTOR OF PHILOSOPHY

in

Biochemistry and Molecular Biology

in the

GRADUATE DIVISION

of the

UNIVERSITY OF CALIFORNIA, SAN FRANCISCO

Chapter 1 of this thesis contains previously published material from the following article:

Manzanillo PS, Shiloh MU, Portnoy DA, Cox JS (2011). *Mycobacterium tuberculosis* activates the DNA-dependent cytoslic surveillance pathway within macrophages. *Cell Host and Microbe*. 2012 May 17;11(5):469-80.

Chapter 2 of this thesis contains previously published material from the following article:

Watson RO*, **Manzanillo PS*,** Cox JS. Detection of mycobacterial DNA activates ubiquitin-mediated autophagy and is essential for control of *M. tuberculosis* infection. ***Co-first authors**. *Cell*. 2012 Aug 17;150(4):803-15.

Chapter 3 contains material currently in submission for publication:

Manzanillo PS, Ayres JS, Watson RO, Souza G, Rae CS, Schneider DS, Nakamura K, Cox JS. The ubiquitin ligase PARKIN is required for autophagy and host resistance to intracellular pathogens.

<div align="center">**Abstract**</div>

<div align="center">**The innate immune response to *Mycobacterium tuberculosis* infection.**</div>

<div align="center">**Paolo Solano Manzanillo**</div>

Mycobacterium tuberculosis is one of the world's most successful human pathogens, infecting over 1.7 billion people worldwide. A key to its success is the ability to survive and replicate within macrophages through the use of a type VII secretion system, ESX-1. Upon phagocytosis, *M. tuberculosis* establishes a specialized phagosomal environment within macrophages, allowing for intracellular replication, persistence, and communication with the host cytoslic environment. Mycobacterial mutants defective in genes necessary for ESX-1 secretion are attenuated within infected macrophages and animal models of infection. While much work has been done to detail the molecular mechanism of ESX-1 secretion, little is still known about how the ESX-1 system modulates and affects the host-response during *M. tuberculosis* infection.

Through the use of gene expression arrays and microscopy analysis we demonstrate that the ESX-1 system of *M. tuberculosis* activates two key innate immune responses during infection of macrophages. One response is the transcription of type I interferons and induction of interferon stimulated genes (ISGs). The second response is ubiquitin mediated selective autophagy of the mycobacterial phagosome. Surprisingly, we demonstrate that both pathways are activated through a common mechanism via ESX-1 dependent release of mycobacterial DNA within the host cytosol.   Activation of host DNA sensing machinery by mycobacterial DNA stimulates the STING-TBK1 pathway

which simultaneous activates both the transcriptional induction of ISGs and recruitment

of autophagic adaptors.

Table of Contents

List of Tables

List of Figures

Chapter 1.

Mycobacterium tuberculosis activates the DNA-dependent cytosolic surveillance pathway within macrophages.

Abstract

Cytosolic bacterial pathogens activate the unique cytosolic surveillance pathway (CSP), but how the host detects vacuolar pathogens like *Mycobacterium tuberculosis* is not well understood. Here we show that *M. tuberculosis* also initiates the CSP upon macrophage infection via limited perforation of the phagosome membrane mediated by the ESX-1 secretion system. Mixing of phagosomal and cytoplasmic compartments allows extracellular mycobacterial DNA access to host cytosolic receptors that initiate signaling through the STING/TBK1/IRF3 axis. Hence, although *M. tuberculosis* remains membrane bound, it gains access to the cytoplasm early after infection, blurring the distinction between "vacuolar" and "cytosolic" pathogen. Surprisingly, *IRF3*$^{-/-}$ mice, which cannot respond to cytosolic DNA, are profoundly resistant to long-term *M. tuberculosis* infection. DNA sensing represents the molecular basis for increased type I IFN during infection of mice, and is likely responsible for the high type I IFN signature in human tuberculosis.

Introduction

Infection with *Mycobacterium tuberculosis* causes enormous worldwide morbidity and mortality, and global incidence continues to rise [1]. A key mediator of *M. tuberculosis* pathogenesis is the ESX-1 specialized secretion system that modulates host-cell functions, presumably by translocating bacterial effectors into the host [2]. Mutants lacking ESX-1 are defective for replication within macrophages and are severely attenuated in animal models of infection, but the mechanism by which this system functions to promote infection remains unclear [3-5]. A growing body of work indicates

2

that ESX-1 contributes to *M. tuberculosis* virulence by modulating host innate immune responses of macrophages. For example, elicitation of type I interferon (IFN) by *M. tuberculosis* infection of both murine and human macrophages requires the ESX-1 secretion system [6, 7]. Although type II IFN (IFN-γ) is critical for activating host defenses, type I IFNs (IFN-α and IFN-β) can negatively regulate host resistance to *M. tuberculosis* in mouse models of infection [8], though the overall effect of type I IFN signaling appears to be relatively minor [6].

Bacterial pathogens that replicate in the cytoplasm of macrophages, such as *Listeria monocytogenes* and *Franciscella tularensis*, induce IFN-β transcription as part of a large transcriptional response controlled by the "cytosolic surveillance pathway" (CSP) [9, 10]. CSP activation by these species occurs early after infection specifically by cytoplasmic bacteria, whereas mutants unable to access the cytosol and trapped in phagosomes fail to induce transcription [9, 11]. The CSP is controlled by the host transcription factor interferon regulatory factor 3 (IRF3), which is activated via phosphorylation by the TBK1 kinase. It is thought that upon phagosomal membrane rupture, bacterial products are granted cytosolic access and recognized by cytosolic receptors that lead to IRF3 activation [12]. Although IRF3 activation of the CSP induces transcription of a wide range of immune response genes, including many known to be important for antiviral defense, the role of the CSP during bacterial infection is still unclear [13].

IRF3 is activated by multiple pattern recognition receptors (PRRs), including Toll like receptors (TLRs), RIG like receptors (RLRs) and cytosolic DNA receptors [14]. Two putative DNA receptors, DAI [15] and IFI204 (the mouse homolog of IFI16, [16]), have been proposed to be sensors that initiate the CSP, though the requirement for DAI is cell-

3

line dependent [17]. Despite some controversies over the nature of DNA receptors, STING is a critical adapter that clearly functions downstream of the putative sensor in the pathway, linking TBK1 and IRF3 [18]. Interestingly, though the host requirements for CSP activation by intracellular *L. monocytogenes* is identical to that of cytosolic DNA, recent work has implicated bacterial derived cyclic-di-AMP as the relevant trigger [19].

In contrast to cytosolic bacterial pathogens, *M. tuberculosis* has long thought to reside within membrane-bound phagosomes of host cells [20]. However, one group recently reported that *M. tuberculosis* translocates into the host cytosol and that the ESX-1 system is required for this process [21]. *Mycobacterium marinum*, an ectothermic pathogen related to *M. tuberculosis* which has been well documented to escape from the vacuole, also requires ESX-1 secretion for cytosolic access [22]. Because ESAT-6, a major secreted protein of the ESX-1 system, has membrane lytic properties at high concentrations [4, 23], it has been suggested that this protein is responsible for ESX-1 mediated cytosolic access. However, this notion has been difficult to test during infection since inactivation of the ESAT-6 gene has pleiotropic effects on secretion of all other ESX-1 substrates [24].

Here we report that *M. tuberculosis* induces the transcription of a broad range of interferon-stimulated genes (ISGs) immediately after macrophage infection via activation of the IRF3-dependent cytosolic surveillance response. Importantly, CSP activation by *M. tuberculosis* requires the ESX-1 secretion system and is dependent on the IFI204 DNA receptor which stimulates the STING-TBK1-IRF3 signaling axis, the same host components as required for the interferon stimulatory DNA (ISD) pathway [18, 25]. This is in contrast to previously published work describing an obligate role for peptidoglycan

mediated Nod signaling in IFN induction [26], a pathway which can modulate IFN-β

transcription but is not required to initiate IFN production [11]. We provide multiple

pieces of evidence that extracellular mycobacterial DNA is the critical ligand for CSP

activation and that the ESX-1 system allows extracellular mycobacterial DNA access to

cytoplasmic DNA receptors. Surprisingly, CSP activation is required for the *M.*

tuberculosis pathogenesis as *IRF3*^{-/-} mice are profoundly resistant to infection.

Results

M. tuberculosis elicits the CSP via ESX-1 secretion

To understand how the host responds to infection with ESX-1^{+} *M. tuberculosis*, we

used microarrays to probe the early transcriptional response of murine bone marrow-

derived macrophages (BMDMs) to infection with either wild-type or ESX-1 mutant

(Tn*5370::Rv3877/EccD1*) *M. tuberculosis* cells. Overall, the transcriptional profile of

macrophages in response to either strain was remarkably similar, with signatures of

TLR/NFκB signaling predominating in both data sets. However, closer inspection of the

data revealed that of the 861 genes significantly activated by wild-type *M. tuberculosis*,

162 genes were differentially expressed upon infection with ESX-1 mutant cells (Table

1.1). Genes in this ESX-1-dependent regulon include interferon-stimulated genes (ISGs)

such as *IFIT1*, *IFN-β*, and *Viperin* (*RSAD2*), all of which are hallmarks of the cytosolic

surveillance pathway (CSP) [11] (Figure 1.1A). qPCR experiments monitoring the

expression of several CSP genes over a more detailed time course demonstrated that

activation was evident as early as 1h post-infection, with a peak of expression at 3h

which ultimately leveled off by 7h post-infection (Figure 1.2A).

Comparison of our microarray data with published bacterial response datasets deposited in the NCBI GEO database (ASCN1234) revealed that the ESX-1-dependent transcriptional profile was nearly identical to the response to *L. monocytogenes* infection after it enters into the cytosol via the action of its pore-forming toxin, listeriolysin O (LLO) (Figure 1.1B, [11]). Activation of the CSP by either *L. monocytogenes* or cytoplasmic DNA is controlled by the host transcription factor interferon regulatory factor 3 (IRF3), which is activated via phosphorylation by the kinase TBK1 [11, 27]. The remarkable overlap in the transcriptional response with *L. monocytogenes* infection strongly suggested that *M. tuberculosis* also activated the IRF-3 dependent cytosolic response [11]. Indeed, transcriptional profiling of wild-type and *IRF3*^{-/-} macrophages infected with wild-type *M. tuberculosis* revealed that the majority of ISGs specifically induced by ESX-1^{+} bacteria are also IRF3 dependent (Figure 1.1A, Table 1.1). Likewise, IRF3 was activated and translocated to the nucleus upon infection with wild-type *M. tuberculosis* but not with ESX-1 mutant cells (Figure 1.1C). Quantitative PCR analysis of both IFIT1 and IFN-β mRNA, indicators of CSP activation, revealed that this induction is strictly dependent on IRF3 during *M. tuberculosis* infection (Figure 1.1D). BMDMs lacking TBK1 also failed to induce IFIT1 and IFN-β transcription or IRF3 nuclear translocation in response to *M. tuberculosis* infection, displaying defects similar to *IRF3*^{-/-} cells [6] (Figure 1.1D, 1.4E). Taken together, these results demonstrate that *M. tuberculosis* activates the IRF3-dependent cytosolic response in an ESX-1 dependent manner.

These results, as well as other reports in the literature [11, 28], conflict with a recent article by Pandey *et al.*, which reported that MDP-initiated activation of cytosolic Nod

receptors, led to a RIP2 and IRF5-dependent activation of type I IFN production [26]. This was surprising as we have previously demonstrated that Rip2, a component absolutely required for Nod signaling, is dispensable for activation of IFN-β transcription during *M. tuberculosis* infection of macrophages [6]. To independently test the contribution of the putative novel Nod/IRF5 pathway in CSP activation, we infected macrophages from *NOD1$^{-/-}$ NOD2$^{-/-}$* double knockout mice with *M. tuberculosis*. Upon infection with wild-type *M. tuberculosis*, these macrophages generated robust IRF3 nuclear translocation and produced amounts of IFN-β mRNA that were indistinguishable from wild-type cells (Figures 1.1E and 1.4E). Similarly, macrophages from *IRF5$^{-/-}$* mice were also able to activate IFN-β mRNA transcription nearly to wild-type levels. Although there was a 2-fold decrease in mRNA levels compared to various IRF knockout strains, this was in sharp contrast to *IRF3$^{-/-}$* macrophages that are completely blocked for IFN-β induction (Figure 1.2B). Taken together, our results support the model that, like with *L. monocytogenes* infection [11], initial CSP activation by *M. tuberculosis* critically requires the TBK1/IRF3 pathway. While we cannot account for the discrepancy between the two studies at present, our previous finding that the modulatory effect of Nod2 on IFN-β transcription was only observed in TLR-tolerized macrophages suggests that chronic stimulation of TLR signaling sensitizes the cells to Nod signaling [11]. In this way, Nod signaling may be important for sustained CSP activation during chronic infection rather than initial activation of the pathway.

***M. tuberculosis* permeabilizes the phagosomal membrane early after infection**

The concordance between CSP activation by *L. monocytogenes* and *M. tuberculosis* was unexpected given the seemingly different pathogenic strategies of these two microbes as *M. tuberculosis* has long been thought to reside primarily within membrane-bound phagosomes of host macrophages [29]. However, ESX-1 has recently been reported to allow *M. tuberculosis* to rupture the phagosomal membrane [21]. Importantly, van der Wel *et al.* observed *M. tuberculosis* in the cytosol only after several days of infection, whereas we detected robust CSP activation as early as three hours post-infection. Electron microscopy studies confirmed that all bacteria at this early time point were clearly encircled by phagosomal membranes (Figure 1.3A). Thus, it is likely that early CSP activation represents limited, ESX-1 mediated perforation of the phagosomal membrane early after infection rather than wholesale membrane dissolution.

To begin to test if the requirement for ESX-1 in CSP activation was due to membrane permeabilization, we infected macrophages with ESX-1 mutants expressing an auto-activated form of LLO from *L. monocytogenes* [30]. Previously, LLO expression from BCG was not reported to confer obvious membrane dissolution, but LLO expression did increase MHC1 presentation, suggesting increased delivery of BCG antigens into the cytosol [31]. As shown in Figure 1.3B, LLO expression restored CSP activation to ESX-1 mutant cells, demonstrating that membrane permeabilization, and not substrates secreted by ESX-1 *per se*, is sufficient for CSP activation. To test if ESX-1 functions to permeabilize the phagosomal membrane during infection, we employed a fluorescent β-lactamase assay previously used to measure vacuolar rupture of phagosomes [32, 33]. This provides a direct way to detect mixing of phagosomal contents with the cytosol during the course of infection through the use of the dual-fluorophore probe, CCF4, a

membrane impermeable FRET reporter. CCF4 contains a coumarin and a fluorescein molecule connected by a β-lactam substrate [32]. After loading the cytosol with CCF4, excitation of coumarin leads to efficient FRET and emission of green (520nm) light by fluorescein, as there is no β-lactamase present in eukaryotic cells [34]. If the substrate is cleaved by a β-lactamase introduced into the cytosol, however, FRET is inhibited and coumarin emits blue fluorescence (450nm) upon excitation. Infection of CCF4-loaded BMDMs with wild-type *M. tuberculosis* over-expressing the secreted mycobacterial β-lactamase BlaC led to blue fluorescence by 3 h post infection, indicating mixing of phagosomal contents with the cytosol (Figure 1.3C). Importantly, ESX-1 mutant bacteria over-expressing BlaC led to no cleavage of the CCF4 substrate. Taken together, these results demonstrate that the ESX-1 secretion system leads to rapid permeabilization of the phagosomal membrane upon macrophage infection. Thus, ESX-1-mediated activation of the CSP by *M. tuberculosis* infection requires phagosomal membrane permeabilization, but not its complete dissolution.

M. tuberculosis **activates the STING/TBK1/IRF3 pathway**

We next sought to determine the host pathway activated by *M. tuberculosis* to initiate TBK1 activation and induction of the CSP. TBK1 is activated by a variety of pattern recognition receptors, including Toll-like receptors (TLR), cytosolic RNA receptors, and cytosolic DNA receptors [35]. To determine how *M. tuberculosis* activates the CSP, we measured *IFIT1* and *IFN-β* mRNA levels as well as IRF3 nuclear translocation, as metrics for CSP activation in a variety of mouse knockout cells. Macrophages deficient either for TLR signaling (*MYD88$^{-/-}$ TRIF$^{-/-}$*) or RNA sensing (*MAVS$^{-/-}$*) were

indistinguishable from wild-type cells, producing similar amounts of IFIT1 and IFN-β transcription and IRF3 nuclear translocation in response to *M. tuberculosis* infection (Figures 1.4A, 1.4B and 1.4E). Furthermore, chemical inhibition of the RNA-Polymerase III/Rig-I pathway [36] had no effect on *M. tuberculosis* activation of CSP transcripts in BMDMs (Figure 1.4C).

Sting is an adapter protein specifically required for both DNA and cyclic di-nucleotide mediated activation of IRF3 and IFN-β transcription [18, 25, 37]. To test if *M. tuberculosis* activates the CSP via Sting, we infected *STING^-/-* BMDMs and monitored CSP activation. Surprisingly, macrophages lacking Sting were unable to activate IRF3 translocation and CSP transcription upon infection (Figure 1.4D, 1.4E). Additionally, in wild-type macrophages, Sting translocated from the ER to cytosolic puncta in an ESX-1 dependent manner (data not shown). Thus, Sting is an essential component required for *M. tuberculosis*-activation of IRF3.

We next determined the bacterial ligand necessary for Sting activation during *M. tuberculosis* infection. *L. monocytogenes* produces cyclic di-AMP that elicits the CSP [19], and Sting has recently been found to be a direct sensor of cyclic di-nucleotides [37, 38]. Hence, we explored the possibility that Sting senses *M. tuberculosis* cyclic di-nucleotides during infection to activate the STING-TBK1-IRF3 pathway. c-di-GMP is unlikely to be the trigger of the CSP as the Erdman strain used in our studies contains a genomic deletion, common in several TB clinical isolates, that removes the only identified di-guanylate cyclase, *MT1397* [39]**.** In addition, macrophages infected with an *M. tuberculosis* strain containing *MT1397*, CDC1551, elicited similar levels of IFN-β transcription as the Erdman strain, and over-expression of *MT1397* in the Erdman strain

had no effect on IFN-β induction (Figure 1.5A). Likewise, *M. tuberculosis* infection of macrophages expressing the cyclic-di GMP phosphodiesterase, RocR, had no effect on IFN-beta production (data not shown) [37, 38]. Furthermore, infection of BMDMs with strains of Erdman either lacking or overexpressing the sole di-adenylate cyclase gene in *M. tuberculosis*, *disA* (*Rv3586*), led to equivalent levels of IFN-β production (Figures 1.5B, 1.5C, and 1.5D). Taken together, our data suggests that mycobacterial derived cyclic-di GMP and cyclic di-AMP are not required for *M. tuberculosis*-mediated CSP activation and Sting activation.

The cytosolic DNA sensor IFI204/IFI16 contributes to CSP activation

We next explored the possibility that *M. tuberculosis* DNA is the trigger for activation of Sting and the CSP response. We first tested the role of two reported cytosolic DNA sensors, DAI (ZBP1) and IFI16/IFI204, in *M. tuberculosis* induction of the CSP [15, 16]. Although BMDMs from *DAI*^{-/-} mice responded normally to both DNA transfection and *M. tuberculosis* infection (Figure 1.6A), knockdown of IFI204 expression (the mouse homolog of human IFI16) in immortalized BMDMs significantly reduced IFIT1 and IFN-β induction upon *M. tuberculosis* infection (Figures 1.6B and 1.6C), suggesting that IFI16/IFI204 may serve as the predominant DNA sensor in BMDMs. In addition, wild-type *M. tuberculosis* induced cytosolic translocation of IFI204, consistent with its relocalization upon DNA transfection and IFN stimulation [16] (Figure 1.6D). Taken together, these results demonstrate that the IFI204 cytosolic DNA sensor contributes to the ESX-1-specific response of macrophages.

Extracellular *M. tuberculosis* DNA triggers the CSP

To further explore the link between cytosolic DNA responses and *M. tuberculosis* infection, we determined whether cytosolic DNAses could modulate CSP activation during *M. tuberculosis* infection. Trex1 is a cytosolic DNase that negatively regulates the ISD pathway by decreasing the half-life of cytoplasmic DNA, and mice lacking TREX1 display enhanced IFN-β production in response to cytosolic DNA but not other inducers such as RNA [25, 40]. Importantly, infection of *TREX1^-/-* knockout macrophages with wild-type *M. tuberculosis* led to over three-fold increased induction of *IFN-β* and *IFIT1* as compared to control cells (Figure 1.7A). Conversely, over-expression of *TREX1* significantly reduced *IFIT1* and *IFN-β* transcription during *M. tuberculosis* infection (Figure 1.7B). This data strongly suggests that extracellular *M. tuberculosis* DNA (eDNA) located in the macrophage cytoplasm is the trigger for IRF3 activation.

Although it was curious that DNA would be a ligand during bacterial infection, we reasoned that eDNA, perhaps released as a result of bacterial lysis, may be the ligand that triggers the CSP. To test this idea, we first asked whether *M. tuberculosis* was capable of transferring DNA into infected macrophages. We created an *M. tuberculosis* strain carrying an episomal plasmid encoding a luciferase reporter gene under the control of eukaryotic expression signals, including the CMV promoter [41]. The enzyme also contains a N-terminal signal sequence that directs its secretion from eukaryotic cells. As expected, this bacterial strain produced no luminescence signal when grown in culture, though directly transfecting the plasmid into human and mouse cell lines resulted in robust luminescence activity in cell supernatants (not shown). Infection of macrophages with the luciferase reporter strain gave rise to significant luminescence signal during

infection (Figure 1.7C). Importantly, infection with ESX-1 mutant bacteria carrying the same reporter construct failed to elicit any luminescence signal. These results strongly suggest that mycobacterial DNA is released into the macrophage cytosol during infection in an ESX-1 dependent manner.

To directly detect *M. tuberculosis* eDNA within the macrophage cytosol, we infected macrophages with BrdU-labeled *M. tuberculosis*, gently lysed the cells, and then fractionated via centrifugation to obtain a cleared cytosolic extract (Figure 1.7D). Immunoprecipitation using anti-BrdU antibodies, followed by agarose gel electrophoresis, revealed a significant enrichment of *M. tuberculosis* DNA from macrophages infected with wild-type versus ESX-1 mutant bacteria (Figure 1.7D). Quantification of *M. tuberculosis* DNA from the immunoprecipitate using qPCR primers for the *sigF* gene showed greater than 10-fold enrichment of DNA recovered from wild-type infected cells over mock or ESX-1 mutant infected cells (Figure 1.7E). These results demonstrate that the ESX-1 system exposes *M. tuberculosis* eDNA to the host cytosol, which then triggers the activation of the cytosolic surveillance pathway via activation of the STING-TBK1-IRF3 axis.

Cytosolic signaling is required for virulence of *M. tuberculosis*

A growing body of work indicates that ESX-1 contributes to *M. tuberculosis* virulence by modulating host innate immune responses of macrophages [6]. Thus, activation of the CSP by *M. tuberculosis* may be an important virulence mechanism. To test the functional role of the CSP during *M. tuberculosis* infection, we performed low-dose aerosol infections of *IRF3*$^{-/-}$ mice and congenic C57BL/6 controls. Surprisingly,

while wild-type mice began to succumb at approximately 120 days post infection, all

IRF3$^{-/-}$ mice survived more than one year, suggesting that activation of IRF3 by *M.*

tuberculosis is deleterious to the host (Figure 1.8A). Enumeration of colony forming units

(CFUs) from lungs and spleens of infected mice revealed that though the kinetics of

bacterial replication during the acute phase of infection was identical in *IRF3$^{-/-}$* and wild-

type mice, *M. tuberculosis* viability declined continuously during the chronic stage of

infection in *IRF3$^{-/-}$* mice (Figure 1.8B, 1.8C). Cytokine analysis of mouse serum

demonstrated decreased levels of IFN-β protein in *IRF3$^{-/-}$* mice relative to wild-type mice,

demonstrating that IRF3 controls *M. tuberculosis* induction of type I IFNs and ISGs

during infection (Figure 1.8D). In addition, serum from infected *IRF3$^{-/-}$* mice had reduced

levels of the chemokines RANTES and MCP-1, and increased levels of IL-12p70 and IL-

1β (Figure 1.8D). Collectively, this data demonstrates that IRF3 activation plays a critical

role to promote *M. tuberculosis* virulence, likely driven by DNA mediated activation of

the CSP, and the induction of cytokines including type I IFN.

Discussion

We have identified a mechanism by which virulent *M. tuberculosis*, a vacuolar

pathogen, elicits the same innate immune transcriptional response induced by

cytoplasmic pathogens. The requirement for the mycobacterial ESX-1 secretion system to

elicit interferon stimulatory genes from macrophages has been well documented [6, 7,

42], but how this occurred was unknown. By showing that host molecules required for

sensing of DNA in the cytoplasm (the cytoplasmic DNA receptor IFI204, Sting, and the

DNase Trex1) are also involved in the response to ESX-1$^+$ *M. tuberculosis*, as well as

identifying mycobacterial DNA specifically in the cytoplasm in an ESX-1 specific

fashion, we conclude that *M. tuberculosis* triggers the CSP via exposure of extracellular

mycobacterial DNA to the cytosol of macrophages. Importantly, this response is

independent of TLR/Nod signaling and distinct from cytoplasmic RNA sensing

molecules. Recognition of DNA in the cytoplasm leads to phosphorylation of IRF3 by

TBK1 and, ultimately, the induction of a defined set of approximately 160 genes,

including *IFN-β*, *IFIT1*, and *RSAD2*. Importantly, mice lacking IRF3 are more resistant to

M. tuberculosis infection. While this is consistent with a role of type I IFN playing a

negative role in host resistance, the phenotype of the *IRF3*^{-/-} mouse is likely due to many

factors besides type I IFN, as discussed below. Moreover, cytosolic sensing of *M.*

tuberculosis DNA likely takes place during human tuberculosis, as ESX-1 mediated

DNA sensing is operative in human macrophages and is likely responsible for the robust

type I IFN signature associated specifically with active disease [7, 43].

Although Type I IFN is absolutely critical for resistance to viruses, there is growing

literature about the role of IFN-α/β in bacterial infections [44, 45]. Because type I IFN

inhibits IL-1β, a cytokine that promotes *M. tuberculosis* clearance, it suggests that

differential cytokine responses mediated by IFN-α/β contribute to the phenotype of the

IRF3^{-/-} mouse [7]. It is important to note that while IFN-α/β likely plays a role in this

phenotype, the *IRF3*^{-/-} mouse is much more resistant to *M. tuberculosis* infection than the

IFNAR^{-/-} mouse that is only deficient for type I IFN signaling [6]. These results strongly

suggest that other immune modulators regulated by the CSP contribute significantly to

pro-*M. tuberculosis* inflammatory immune responses. Indeed, our microarray studies of

the global response of host macrophages identified a large number of transcripts

specifically induced by ESX-1/IRF3, some of which may function to promote *M. tuberculosis* infection.

Activation of IRF3 by *M. tuberculosis* is mediated by two bacterial components, the action of the ESX-1 secretion system to permeabilize the phagosomal membrane and subsequent *M. tuberculosis* DNA exposed to the cytosol. Given the growing evidence that ESAT-6 perturbs membranes [4, 23], we propose that *M. tuberculosis* utilizes the ESX-1 system to deliver ESAT-6 to create conduits in phagosomal membranes, allowing bacterial eDNA to contact cytosolic receptors and activate the IRF-3 dependent cytosolic surveillance response. Although the nature of the connection between the phagosomal lumen and cytoplasm is unknown, activation of the CSP does not appear to require entry of the entire bacterium into the cytosol as the transcriptional effects of ESX-1 on macrophages occurs much earlier than *van der Wel et al*. have reported vacuolar escape of *M. tuberculosis* [21]. Likewise, our electron microscopy data indicates that wholesale lysis of the phagosomal membrane does not occur at this time point. Although we are unable to distinguish whether eDNA is recognized in the cytosol or within the permeabilized phagosome, our results suggest that ESX-1 mediates limited perforation of the lipid bilayer. Because the secretion system delivery of pathogenic proteins leads to activation of cytosolic responses in other pathogens [44], we envision that the primary role of ESAT-6-mediated membrane damage is to provide access of secreted virulence factors to enter the host cytosol, and eDNA exposure to cytosolic receptors is an indirect consequence of membrane perforation. Furthermore, the ability of *M. tuberculosis* to perforate the membrane without its dissolution is likely under a delicate balance of factors, including the robustness of ESX-1 secretion and rate of host membrane repair

mechanisms. Indeed, fine control of ESX-1 secretion may serve to limit membrane perforation and cytosolic signaling [46].

Identification of mycobacterial DNA as the ligand raises the question of how eDNA is liberated and exposed during *M. tuberculosis* infection. Although it could be released from bacteria that have lysed due to killing by macrophages after phagocytosis, the fact that CSP activation occurs within hours after infection of naïve macrophages, conditions in which bacterial viability is very high, argues against this idea. Alternatively, eDNA may be naturally occurring on the surface of the bacterium during normal growth, and thus pre-existing prior to infection. Indeed, a strong body of literature supports the notion that eDNA can play important roles in normal bacterial physiology, most notably biofilm formation [47, 48]. Furthermore, eDNA has been identified within outer membrane vesicles secreted by various gram-negative and gram-positive bacterial species [49] and has recently been found to be encapsulated within mycobacterial membrane vesicles [50] (personal communication). Thus, we favor a model in which the mycobacterial eDNA sensed by the macrophage also plays a fundamental role in mycobacterial cell biology that is distinct from CSP triggering, perhaps to promote biofilm formation.

Although our data supports the involvement of eDNA as the ligand that triggers IFN-β, the work of Pandey *et al.* suggests that peptidoglycan fragments detected by cytosolic Nod receptors is responsible for initiating the response [26]. While Nod2 can contribute partially to IFN-β production by modulating NFκB activity in response to *M. tuberculosis* and *L. monocytogenes* infection, Nod signaling does not affect IRF3 activation [11, 51]. Importantly, the effect of Nod activation of NFκB on IFN-β induction was apparent only in cells in which TLR signaling was inhibited by chronic stimulation, suggesting that it

plays only a minor role in the initiation of the CSP. Moreover, the fact that the course of infection in *NOD2*^{-/-} mice is similar to that in wild-type mice demonstrates that this signaling pathway plays only a minor role in *M. tuberculosis* control [52]. We cannot at this time account for the discrepancy between our results and those of Pandey *et al.*, though the fact that we observe strong IRF3 phosphorylation and nuclear translocation provides corroborative independent evidence that this pathway is the major pathway activated by ESX-1^{+} *M. tuberculosis* cells early after infection. Overall, our data supports the conclusion that it is extracellular DNA that is the incipient ligand that is recognized and activates this intracellular pathway.

Since bacterial infection correlates with type I IFN production, it is tempting to speculate that CSP induction is a "strategy" adopted by *M. tuberculosis* to promote infection, and that the ability of the bacteria to expose eDNA arose for the sole purpose of triggering this response [7]. The phenotype of the *IRF3*^{-/-} mouse is certainly consistent with this notion. However, if eDNA provides a fitness advantage *in vivo*, an alternative view is that eDNA exposure to the cytosol is an inevitable consequence of membrane perforation to deliver virulence proteins into the cytosol. In this way, while CSP activation initiates profound inflammatory responses, *M. tuberculosis* may have evolved to require these changes in host tissues to activate virulence mechanisms or produce an environment conducive to growth. Consistent with this idea, recent studies have shown that *Salmonella* promotes inflammatory immune responses which, in turn, enhances persistent infection [53, 54]. Thus, *M. tuberculosis* may have evolved a dependency that requires the effects of robust innate immune signaling triggered by DNA. In either case, it

is likely that excessive host immunopathology triggered by CSP activation contributes to the susceptibility of wild-type mice to *M. tuberculosis* [55].

It is curious that ESX-1 is important for both genetic exchange in *M. smegmatis* as well as for exposure of DNA to eukaryotic cells [56, 57]. Although *M. smegmatis* transfers DNA in a method similar to conjugation, the mechanism by which this occurs is unclear and the focus of active investigation [56]. Given the common requirement of ESX-1 in both DNA transfer between *M. smegmatis* and DNA triggering in eukaryotic cells, we envision the possibility that the mechanism by which DNA is transferred into other bacterial cells is similar to that used for exposure to the cytosol of eukaryotes.

Although CSP activation via detection of nucleic acids is a key mechanism by which cells sense intracellular pathogens, cytosolic DNA sensing is likely to initiate other innate immune responses in addition to the transcriptional changes described here. For example, *Franciscella tularensis*, a cytosolic pathogen, activates the DNA receptor AIM2, leading to Caspase1 inflammasome activation [58]. Likewise, links between nucleic acid sensing and autophagy, an important mediator of bacterial clearance, are also beginning to emerge [59]. Hence, eDNA generation may be common to a wide variety of bacterial species, and its exposure to the cytosol during infection allows host cells to elicit a multifactorial innate response. Furthermore, the placement of DNA receptors in the cytosol allows host cells to specifically elicit these responses only in response to bacteria that access the cytosol (pathogens) verses those that do not (non-pathogens).

Materials and Methods

Electron Microscopy

BMDMs were seeded onto Aclar disks in DME medium within 12-well tissue culture dishes and grown for 48 h prior to infection. Monolayers were infected with *M. tuberculosis* at an MOI of 10 for 4 h and adherent cells were fixed in 3% glutaraldehyde in 0.1M Sodium cacodylate for 2 h. Fixed cells were rinsed in sodium cacodylate buffer, stained with uranyl acetate, embedded and sectioned.

Mice and macrophages

IRF3$^{-/-}$ mice were a gift from T. Taniguchi (University of Tokyo, Tokyo, Japan). Wild-type C57BL/6 mice were purchased from Jackson laboratories. BMDMs were obtained from the following mouse strains: *MYD88$^{-/-}$/TRIF$^{-/-}$* [60], *TREX1$^{-/-}$* [25], *STING$^{-/-}$* [18], *TNFR1-/-* & *TBK1$^{-/-}$/ TNFR1$^{-/-}$* [61], *IRF1$^{-/-}$*, *IRF3$^{-/-}$*, *IRF5$^{-/-}$*, and *IRF7$^{-/-}$* [15]. RAW264.7 cells were obtained from ATCC. C57BL/6 immortalized BMDMs (iBMDMs) were a gift from R. Vance (UC Berkeley).

Cell culture

RAW264.7 cells were cultured in DMEM-H21 containing 10%FBS. Immortalized BMDMs (iBMDMs) were cultured in RPMI-1640 containing 10% FBS. BMDMs were obtained from mouse femurs as previously described [11] and cultured in DMEM H-21 supplemented with 10% MCSF derived from 3T3-MCSF cells.

Bacterial strains

Unless noted, the Erdman strain of *M. tuberculosis* was used as the wild-type strain. The CDC1551 *M. tuberculosis* strain was obtained from the Colorado State TBVTRM contract. The *M. tuberculosis* Erdman mutants Δ*esxA* and Tn*5370*::*EccD₁*($Rv3877$) were previously described [5]. The *M. tuberculosis Rv3676* deletion mutant (Δ*disA*) was constructed by replacing the entire *Rv3676* open reading frame with the hygromycin resistance gene by homologous recombination. The deletion plasmid was delivered into *M. tuberculosis* using specialized phage transduction as described previously [46]. Deletion of *Rv3676* was confirmed by Southern blotting using the DIG nucleic acid detection kit (Roche). All strains were cultured in 7H9 medium supplemented with 10% OADC, 0.5% Glycerol, and 0.05% Tween-80.

Macrophage infection

For infections with *M. tuberculosis*, macrophages were infected as previously described [46], with some modifications. Briefly, *M. tuberculosis* cultures were washed twice with PBS, gently sonicated to disperse clumps, and resuspended in DMEM supplemented with 10% horse serum. Media was removed from cells, monolayers overlaid with the bacterial suspension, and centrifuged for 10 min at 1,000 RPM. Cells were washed twice in PBS and returned to macrophage media.

Cellular fractionation and western blotting

Cytosolic and nuclear protein fractions were obtained from *M. tuberculosis* infected macrophages using the Qproteome Nuclear Protein Kit (Qiagen) according to manufacturer's instructions. Micro BCA protein kit (Pierce) was used to measure protein

levels and equal amounts of protein were run on 4-20% Tris-HCL Criterion gels (Biorad). Proteins were transferred onto nitrocellulose membranes and incubated simultaneously with anti-IRF3 (Invitrogen) and anti-TBP (Abcam) antibodies. Western blots were analyzed using an Odyssey Imager (Licor) according to manufacturer's instructions. Western blot figures are a representative of at least three independent experiments.

RNA isolation and qPCR

RNA was isolated and purified from macrophages using the Trizol micro-midi RNA isolation kit (Invitrogen) per manufacturer's instructions. For qPCR analysis 1□g of RNA was reverse transcribed using the VILO cDNA synthesis kit (Invitrogen) and qPCR analysis was performed in triplicate, as previously described [46] using gene specific primers. Data presented is a representative of at least three independent experiments.

Microarrays

Microarray analysis was performed using total RNA isolated from BMDMs infected with *M. tuberculosis*. Total RNA was amplified and hybridized to MEEBO mouse microarrays as previously described [11]. Acuity software (Molecular probes) was used for microarray data analysis [11]. Statistically significant differences in gene expression were identified using the Statistical Analysis of Microarray (SAM) software tool version 3.1, using a false discovery rate (FDR) of less than 5%. Microarray data shown are from two independent experiments. Datasets will be deposited in the NCBI Geo Database at the time of publication.

Mouse infection

IRF3$^{-/-}$ and wild-type C57BL/6 mice were infected with *M. tuberculosis* (Erdman) via low-dose aerosol infection as previously described [46]. Lungs and spleens were harvested, homogenized, and plated on 7H10 agar plates. Serum from infected mice was harvested via cardiac puncture. For survival experiments, infected mice were sacrificed when they had lost 15% of their maximal body weight.

Trex1 Overexpression:

TREX1 was cloned into the pTracer CMV/BSD vector (Invitrogen) using cDNA generated from RAW264.7 macrophage total RNA. Plasmids were electroporated into RAW264.7 cells using the Amaxa nucleofector kit IV. Twenty-four hours post electroporation, cells were cultured in media containing blasticidin (5ug/mL) for 5 days, followed by FACs sorting for GFP positive cells.

Cytokine measurements:

IFN-β levels in mouse serum was measured using the Verikine mouse Interferon-β ELISA kit (PBL). IL-12p70, MCP-1, RANTES, and IL-1β serum levels were measured using SearchLight Multiplex ELISA Array (Pierce).

Luminescence Assay

Bacterial DNA release was measured as previously described [41], with the following modifications. The CMV promoter, the *Metridia* secreted luciferase, and SV40 early polyA of the pMet plasmid (Clonetech) were subcloned into the mycobacterial plasmid

pMV261-Zeo (PMAN-1). *M. tuberculosis* carrying the luciferase reporter construct was used to infect macrophages and cell supernatants were removed 16 h post infection and analyzed for luciferase activity using the Ready-to-Glow assay kit (Clonetech).

Knockdown cells

The mouse TRC1 lentiviral library [62] was obtained from Sigma and used to knockdown *IFI204* mRNA in immortalized bone marrow derived cells according to manufacturer's protocol.

CCF4-am Beta-lactamase Assay

Prior to infection, macrophages were pre-loaded with CCF4-am, using the Live-BLAzer FRET B/G load kit (Invitrogen) per manufacturer's instructions. After loading, macrophages were than infected with either wild-type *M. tuberculosis* or Δe*sxA M. tuberculosis* strains over-expressing the mycobacterial beta-lactamase gene, *BlaC*. CCF4 cleavage in the cytosol was measured via excitation of cells at 405nm and measuring the emission at 535nm(intact) and 450nm(cleaved).

BrdU Assay

M. tuberculosis strains were grown in 5μM BrdU (Sigma) for 3-4 days in the dark. BrdU labeled cells were used to infect 30 million macrophages at an MOI of 10. 3 h post infection, cells were washed once in K buffer (20 mM HEPES, pH 7.6, 150 mM KCl, 5 mM MgCl2 + protease inhibitors) and then lysed in K buffer containing .0125% digitonin for 10 min on ice. Lysates were centrifuged at 1,500xg for 5 min at 4°C, supernatants

transferred to a fresh tube and then centrifuged at 15,000xg for 5 min at 4°C. The

resulting supernatants were than filtered through a 0.45 micron filter, boiled for 2 mins

and then applied to Protein-G Dynal beads conjugated with anti-BrdU antibody (Sigma).

Beads were incubated overnight, washed twice in PBS .01%Tween-20 and the bound

BrdU labeled DNA was then released via boiling of beads followed by phenol-

chloroform extraction.

References

1. Dye, C. and B.G. Williams, *The population dynamics and control of tuberculosis.* Science, 2010. **328**(5980): p. 856-61.

2. Abdallah, A.M., et al., *Type VII secretion--mycobacteria show the way.* Nat Rev Microbiol, 2007. **5**(11): p. 883-91.

3. Guinn, K.M., et al., *Individual RD1-region genes are required for export of ESAT-6/CFP-10 and for virulence of Mycobacterium tuberculosis.* Mol Microbiol, 2004. **51**(2): p. 359-70.

4. Hsu, T., et al., *The primary mechanism of attenuation of bacillus Calmette-Guerin is a loss of secreted lytic function required for invasion of lung interstitial tissue.* Proc Natl Acad Sci U S A, 2003. **100**(21): p. 12420-5.

5. Stanley, S.A., et al., *Acute infection and macrophage subversion by Mycobacterium tuberculosis require a specialized secretion system.* Proc Natl Acad Sci U S A, 2003. **100**(22): p. 13001-6.

6. Stanley, S.A., et al., *The Type I IFN response to infection with Mycobacterium tuberculosis requires ESX-1-mediated secretion and contributes to pathogenesis.* J Immunol, 2007. **178**(5): p. 3143-52.

7. Novikov, A., et al., *Mycobacterium tuberculosis Triggers Host Type I IFN Signaling To Regulate IL-1β Production in Human Macrophages.* J Immunol, 2011.

8. Manca, C., et al., *Virulence of a Mycobacterium tuberculosis clinical isolate in mice is determined by failure to induce Th1 type immunity and is associated with induction of IFN-alpha /beta.* Proc Natl Acad Sci U S A, 2001. **98**(10): p. 5752-7.

9.   Henry, T. and D.M. Monack, *Activation of the inflammasome upon Francisella tularensis infection: interplay of innate immune pathways and virulence factors.* Cell Microbiol, 2007. **9**(11): p. 2543-51.

10.   McCaffrey, R.L., et al., *A specific gene expression program triggered by Gram-positive bacteria in the cytosol.* Proc Natl Acad Sci U S A, 2004. **101**(31): p. 11386-91.

11.   Leber, J.H., et al., *Distinct TLR- and NLR-mediated transcriptional responses to an intracellular pathogen.* PLoS Pathog, 2008. **4**(1): p. e6.

12.   Vance, R.E., R.R. Isberg, and D.A. Portnoy, *Patterns of pathogenesis: discrimination of pathogenic and nonpathogenic microbes by the innate immune system.* Cell Host Microbe, 2009. **6**(1): p. 10-21.

13.   Decker, T., M. Muller, and S. Stockinger, *The yin and yang of type I interferon activity in bacterial infection.* Nat Rev Immunol, 2005. **5**(9): p. 675-87.

14.   Takeuchi, O. and S. Akira, *Pattern recognition receptors and inflammation.* Cell, 2010. **140**(6): p. 805-20.

15.   Takaoka, A., et al., *DAI (DLM-1/ZBP1) is a cytosolic DNA sensor and an activator of innate immune response.* Nature, 2007. **448**(7152): p. 501-5.

16.   Unterholzner, L., et al., *IFI16 is an innate immune sensor for intracellular DNA.* Nat Immunol, 2010. **11**(11): p. 997-1004.

17.   Wang, Z., et al., *Regulation of innate immune responses by DAI (DLM-1/ZBP1) and other DNA-sensing molecules.* Proc Natl Acad Sci U S A, 2008. **105**(14): p. 5477-82.

18.   Ishikawa, H., Z. Ma, and G.N. Barber, *STING regulates intracellular DNA-mediated, type I interferon-dependent innate immunity.* Nature, 2009. **461**(7265): p. 788-92.

19.   Woodward, J.J., A.T. Iavarone, and D.A. Portnoy, *c-di-AMP secreted by intracellular Listeria monocytogenes activates a host type I interferon response.* Science, 2010. **328**(5986): p. 1703-5.

20.   Armstrong, J.A. and P.D. Hart, *Response of cultured macrophages to mycobacterium tuberculosis, with observations on fusion of lysosomes with phagosomes.* Journal of Experimental Medicine, 1971. **134**(3): p. 713-740.

21.   van der Wel, N., et al., *M. tuberculosis and M. leprae translocate from the phagolysosome to the cytosol in myeloid cells.* Cell, 2007. **129**(7): p. 1287-98.

22.   Smith, J., et al., *Evidence for Pore Formation in Host Cell Membranes by ESX-1-Secreted ESAT-6 and Its Role in Mycobacterium marinum Escape from the Vacuole.* Infection and Immunity, 2008. **76**(12): p. 5478-5487.

23.   de Jonge, M.I., et al., *ESAT-6 from Mycobacterium tuberculosis dissociates from its putative chaperone CFP-10 under acidic conditions and exhibits membrane-lysing activity.* J Bacteriol, 2007.

24.   Fortune, S.M., et al., *Mutually dependent secretion of proteins required for mycobacterial virulence.* Proc Natl Acad Sci U S A, 2005. **102**(30): p. 10676-81.

25.   Stetson, D.B., et al., *Trex1 prevents cell-intrinsic initiation of autoimmunity.* Cell, 2008. **134**(4): p. 587-98.

26.   Pandey, A.K., et al., *NOD2, RIP2 and IRF5 play a critical role in the type I interferon response to Mycobacterium tuberculosis.* PLoS Pathog, 2009. **5**(7): p. e1000500.

27.   Fitzgerald, K.A., et al., *IKKepsilon and TBK1 are essential components of the IRF3 signaling pathway.* Nat Immunol, 2003. **4**(5): p. 491-6.

28.   Stockinger, S., et al., *IFN regulatory factor 3-dependent induction of type I IFNs by intracellular bacteria is mediated by a TLR- and Nod2-independent mechanism.* J Immunol, 2004. **173**(12): p. 7416-25.

29.   Russell, D.G., *Mycobacterium tuberculosis and the intimate discourse of a chronic infection.* Immunol Rev, 2011. **240**(1): p. 252-68.

30.   Singh, R., A. Jamieson, and P. Cresswell, *GILT is a critical host factor for Listeria monocytogenes infection.* Nature, 2008. **455**(7217): p. 1244-7.

31.   Hess, J., et al., *Mycobacterium bovis Bacille Calmette-Guerin strains secreting listeriolysin of Listeria monocytogenes.* Proc Natl Acad Sci U S A, 1998. **95**(9): p. 5299-304.

32.   Ray, K., et al., *Tracking the dynamic interplay between bacterial and host factors during pathogen-induced vacuole rupture in real time.* Cell Microbiol, 2010. **12**(4): p. 545-56.

33.   Kong, Y., et al., *Imaging tuberculosis with endogenous beta-lactamase reporter enzyme fluorescence in live mice.* Proc Natl Acad Sci U S A, 2010. **107**(27): p. 12239-44.

34.   Charpentier, X. and E. Oswald, *Identification of the secretion and translocation domain of the enteropathogenic and enterohemorrhagic Escherichia coli effector*

Cif, using TEM-1 beta-lactamase as a new fluorescence-based reporter. J Bacteriol, 2004. **186**(16): p. 5486-95.

35.   Nakhaei, P., et al., *RIG-I-like receptors: sensing and responding to RNA virus infection.* Semin Immunol, 2009. **21**(4): p. 215-22.

36.   Chiu, Y.H., J.B. Macmillan, and Z.J. Chen, *RNA polymerase III detects cytosolic DNA and induces type I interferons through the RIG-I pathway.* Cell, 2009. **138**(3): p. 576-91.

37.   Burdette, D.L., et al., *STING is a direct innate immune sensor of cyclic di-GMP.* Nature, 2011. **478**(7370): p. 515-8.

38.   McWhirter, S.M., et al., *A host type I interferon response is induced by cytosolic sensing of the bacterial second messenger cyclic-di-GMP.* J Exp Med, 2009. **206**(9): p. 1899-911.

39.   Tsolaki, A.G., et al., *Functional and evolutionary genomics of Mycobacterium tuberculosis: insights from genomic deletions in 100 strains.* Proc Natl Acad Sci U S A, 2004. **101**(14): p. 4865-70.

40.   Yan, N., et al., *The cytosolic exonuclease TREX1 inhibits the innate immune response to human immunodeficiency virus type 1.* Nat Immunol, 2010. **11**(11): p. 1005-13.

41.   Sauer, J.D., et al., *Listeria monocytogenes triggers AIM2-mediated pyroptosis upon infrequent bacteriolysis in the macrophage cytosol.* Cell Host Microbe, 2010. **7**(5): p. 412-9.

42.   Schnappinger, D., et al., *Transcriptional Adaptation of Mycobacterium tuberculosis within Macrophages: Insights into the Phagosomal Environment.* J Exp Med, 2003. **198**(5): p. 693-704.

43.   Berry, M.P., et al., *An interferon-inducible neutrophil-driven blood transcriptional signature in human tuberculosis.* Nature, 2010. **466**(7309): p. 973-7.

44.   Barber, G.N., *Innate immune DNA sensing pathways: STING, AIMII and the regulation of interferon production and inflammatory responses.* Curr Opin Immunol, 2011. **23**(1): p. 10-20.

45.   Monroe, K.M., S.M. McWhirter, and R.E. Vance, *Induction of type I interferons by bacteria.* Cell Microbiol, 2010. **12**(7): p. 881-90.

46.   Ohol, Y.M., et al., *Mycobacterium tuberculosis MycP1 Protease Plays a Dual Role in Regulation of ESX-1 Secretion and Virulence.* Cell Host Microbe, 2010. **7**(3): p. 210-220.

47.   Whitchurch, C.B., et al., *Extracellular DNA required for bacterial biofilm formation.* Science, 2002. **295**(5559): p. 1487.

48.   Kuehn, M.J. and N.C. Kesty, *Bacterial outer membrane vesicles and the host-pathogen interaction.* Genes Dev, 2005. **19**(22): p. 2645-55.

49.   Ellis, T.N. and M.J. Kuehn, *Virulence and immunomodulatory roles of bacterial outer membrane vesicles.* Microbiol Mol Biol Rev, 2010. **74**(1): p. 81-94.

50.   Prados-Rosales, R., et al., *Mycobacteria release active membrane vesicles that modulate immune responses in a TLR2-dependent manner in mice.* J Clin Invest, 2011. **121**(4): p. 1471-83.

51.   Balachandran, S. and A.A. Beg, *Defining emerging roles for NF-kappaB in antivirus responses: revisiting the interferon-beta enhanceosome paradigm.* PLoS Pathog, 2011. **7**(10): p. e1002165.

52.   Divangahi, M., et al., *NOD2-deficient mice have impaired resistance to Mycobacterium tuberculosis infection through defective innate and adaptive immunity.* J Immunol, 2008. **181**(10): p. 7157-65.

53.   Winter, S.E., et al., *Gut inflammation provides a respiratory electron acceptor for Salmonella.* Nature, 2010. **467**(7314): p. 426-9.

54.   Arpaia, N., et al., *TLR signaling is required for Salmonella typhimurium virulence.* Cell, 2011. **144**(5): p. 675-88.

55.   Philips, J.A. and J.D. Ernst, *Tuberculosis pathogenesis and immunity.* Annu Rev Pathol, 2012. **7**: p. 353-84.

56.   Coros, A., et al., *The specialized secretory apparatus ESX-1 is essential for DNA transfer in Mycobacterium smegmatis.* Mol Microbiol, 2008. **69**(4): p. 794-808.

57.   Nguyen, K.T., et al., *Mycobacterial biofilms facilitate horizontal DNA transfer between strains of Mycobacterium smegmatis.* J Bacteriol, 2010. **192**(19): p. 5134-42.

58.   Fernandes-Alnemri, T., et al., *The AIM2 inflammasome is critical for innate immunity to Francisella tularensis.* Nat Immunol, 2010. **11**(5): p. 385-93.

59.   Saitoh, T., et al., *Atg9a controls dsDNA-driven dynamic translocation of STING and the innate immune response.* Proc Natl Acad Sci U S A, 2009. **106**(49): p. 20842-6.

60.   Barbalat, R., et al., *Toll-like receptor 2 on inflammatory monocytes induces type I interferon in response to viral but not bacterial ligands.* Nat Immunol, 2009. **10**(11): p. 1200-7.

61.   Ishii, K.J., et al., *TANK-binding kinase-1 delineates innate and adaptive immune responses to DNA vaccines.* Nature, 2008. **451**(7179): p. 725-9.

62.   Moffat, J., et al., *A lentiviral RNAi library for human and mouse genes applied to an arrayed viral high-content screen.* Cell, 2006. **124**(6): p. 1283-98.

Figure 1.1 *M. tuberculosis* **elicits the CSP via ESX-1 secretion.** (A) Microarray analysis of CSP-regulated genes in wild-type and *IRF3$^{-/-}$* BMDMs infected with the indicated *M. tuberculosis* strains. Log$_2$ fold induction versus uninfected macrophages is shown. (B) Cluster analysis of BMDM genes induced during infection with wild-type (WT) or Δ*hly L. monocytogenes* (*hly$^-$*), and with wild-type or ESX-1 mutant (Esx1$^-$) *M. tuberculosis*. (C) Nuclear translocation of IRF3 in BMDMs 3 h post-infection was assessed by western blotting of nuclear fractions using IRF3 and TATA-binding protein (TBP)-specific antibodies. (D and E) IFIT1 and IFN-β mRNA levels were assessed by qRT-PCR 3 h post-infection in BMDMs (MΦ) and normalized to actin. *TBK1$^{-/-}$* mice are viable only when TNFα signaling is abrogated, thus BMDMs from *TNFR1$^{-/-}$* mice serve as the control for this strain. Data shown is the mean ± SD, (N=3 per group). *P<0.001 as determined by Student's t-test comparing gene expression in each mutant macrophage and its corresponding control.
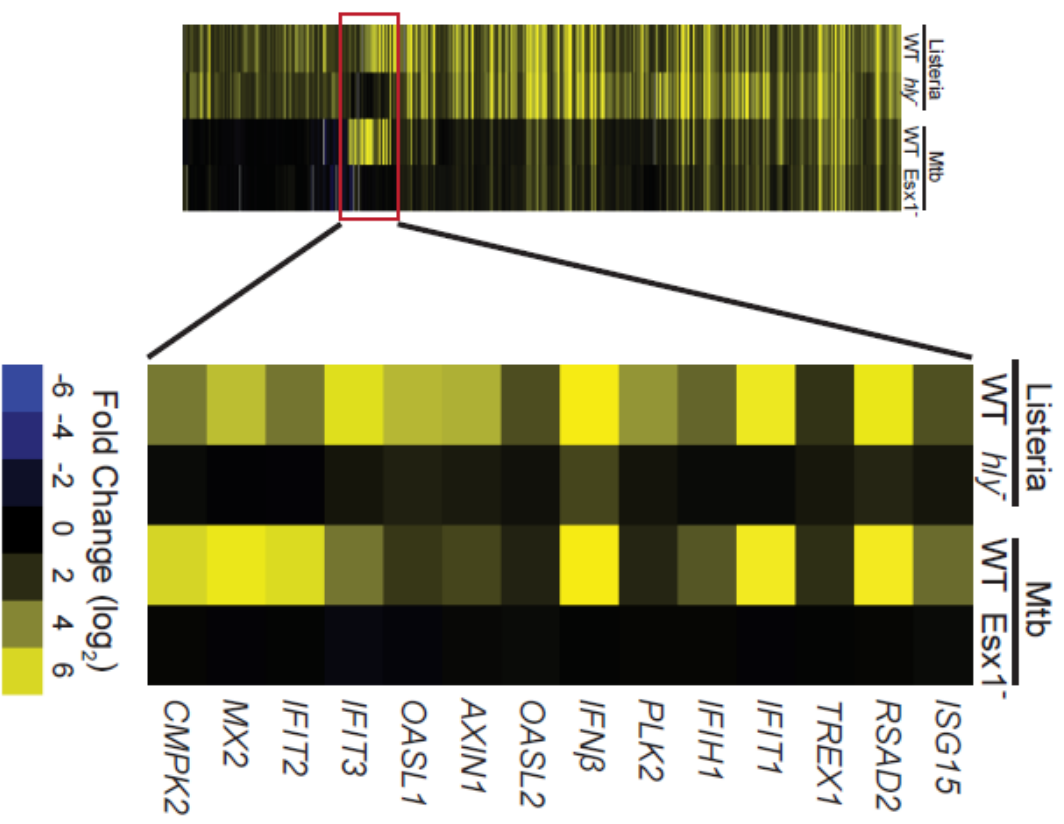
Figure 1.1

32

Figure 1.1

c

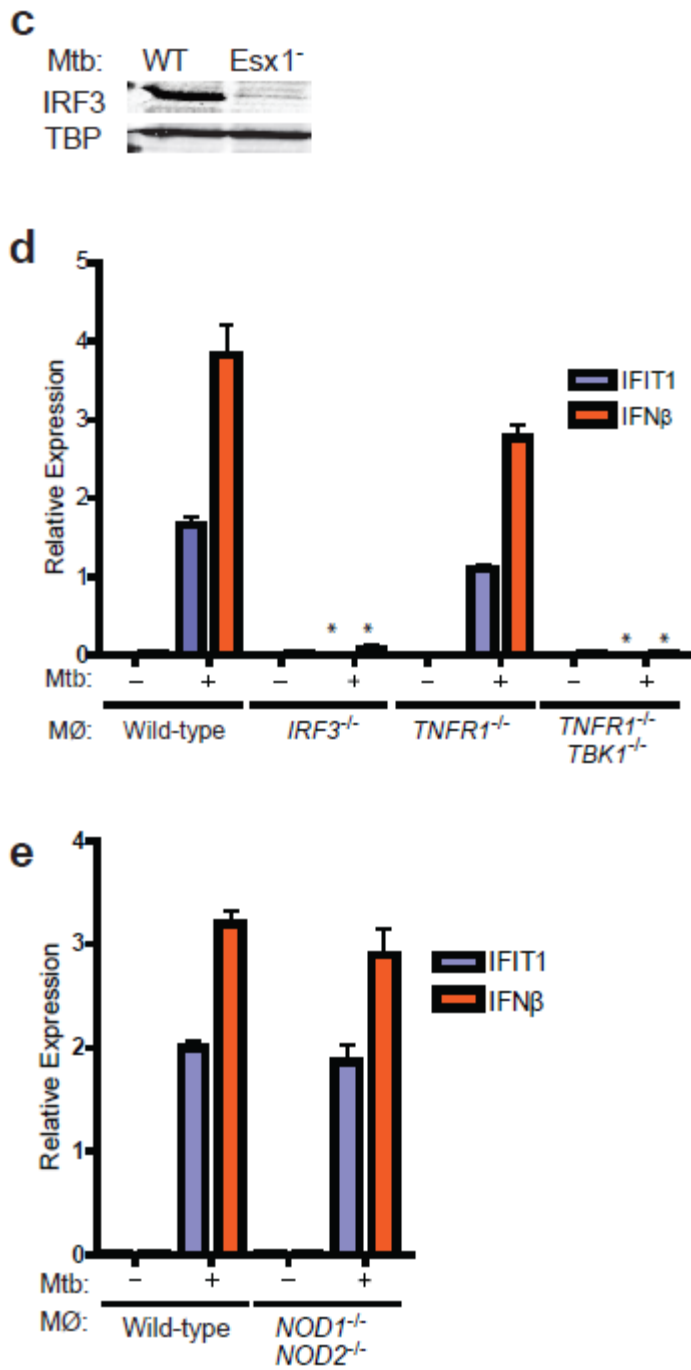Mtb: WT   Esx1‾

IRF3

TBP

d

e
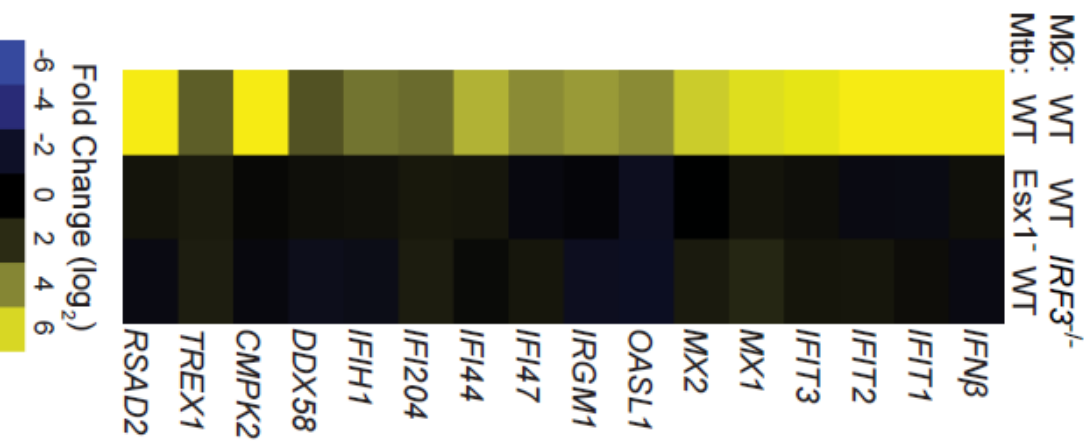
Figure 1.2 The role of *IRF3* in Mtb CSP activation.

(A) *RSAD2*, *IFIT1*, and *IFN*-β mRNA levels were assessed by qRT-PCR in BMDMs

(MΦ) from wild-type and *IRF3*$^{-/-}$ knockout mice infected with wild-type *M. tuberculosis*

at the indicated time points. (B) IFN-β mRNA levels assessed by qRT-PCR in BMDMs

from *IRF1*$^{-/-}$, *IRF3*$^{-/-}$, *IRF5*$^{-/-}$, and *IRF7*$^{-/-}$ mice infected with wild-type *M. tuberculosis*

for 3 h. Gene expression was normalized to expression of actin. Data shown is the mean

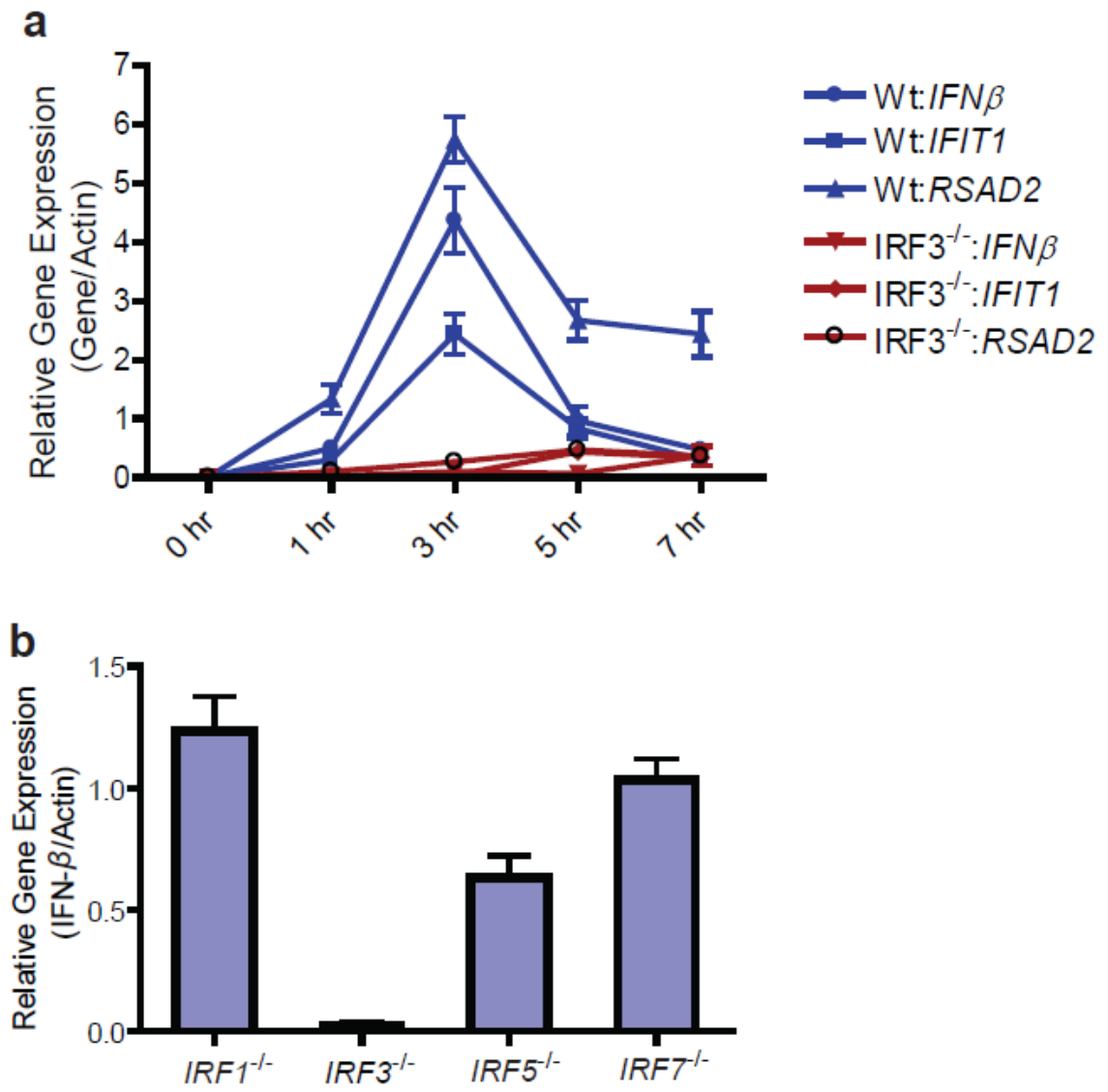± SD, (N=3 per group).

Figure 1.2

Figure 1.3 *M. tuberculosis* permeabilizes the phagosomal membrane early after infection. (A) Electron microscopy of C57/B6 BMDMs infected with wild-type *M. tuberculosis* 3 h post-infection. Macrophage cytosol (MΦ), *M. tuberculosis* cell (tb) and intact phagosomal membrane (arrows) are indicated. (B) IFIT1 and IFN-β mRNA levels were assessed by qRT-PCR (actin normalized) in BMDMs infected with Δ*esxA M. tuberculosis* cells containing an LLO expression plasmid or empty vector. Data shown is the mean ± SD, (N=3 per group). *P<0.001 as determined by Student's t-test comparing gene expression in each mutant macrophage and its corresponding control. (C) Macrophages were preloaded with CCF4-am substrate and infected with wild-type or Δ*esxA M. tuberculosis* strains, both of which over-expressed the *blaC* gene. 3 h post infection, cells were excited with a 405nm laser, and percent CCF4 cleavage was measured as the ratio of 450nm:535nm emission by fluorescence microscopy of infected cells (D). Data shown is the mean ± SD, (N=3 per group).

Figure 1.3

a

b

LLO: − +

Esx1⁻

IFIT1
IFNβ

c

Wt   Esx1⁻

520nm

450nm

d

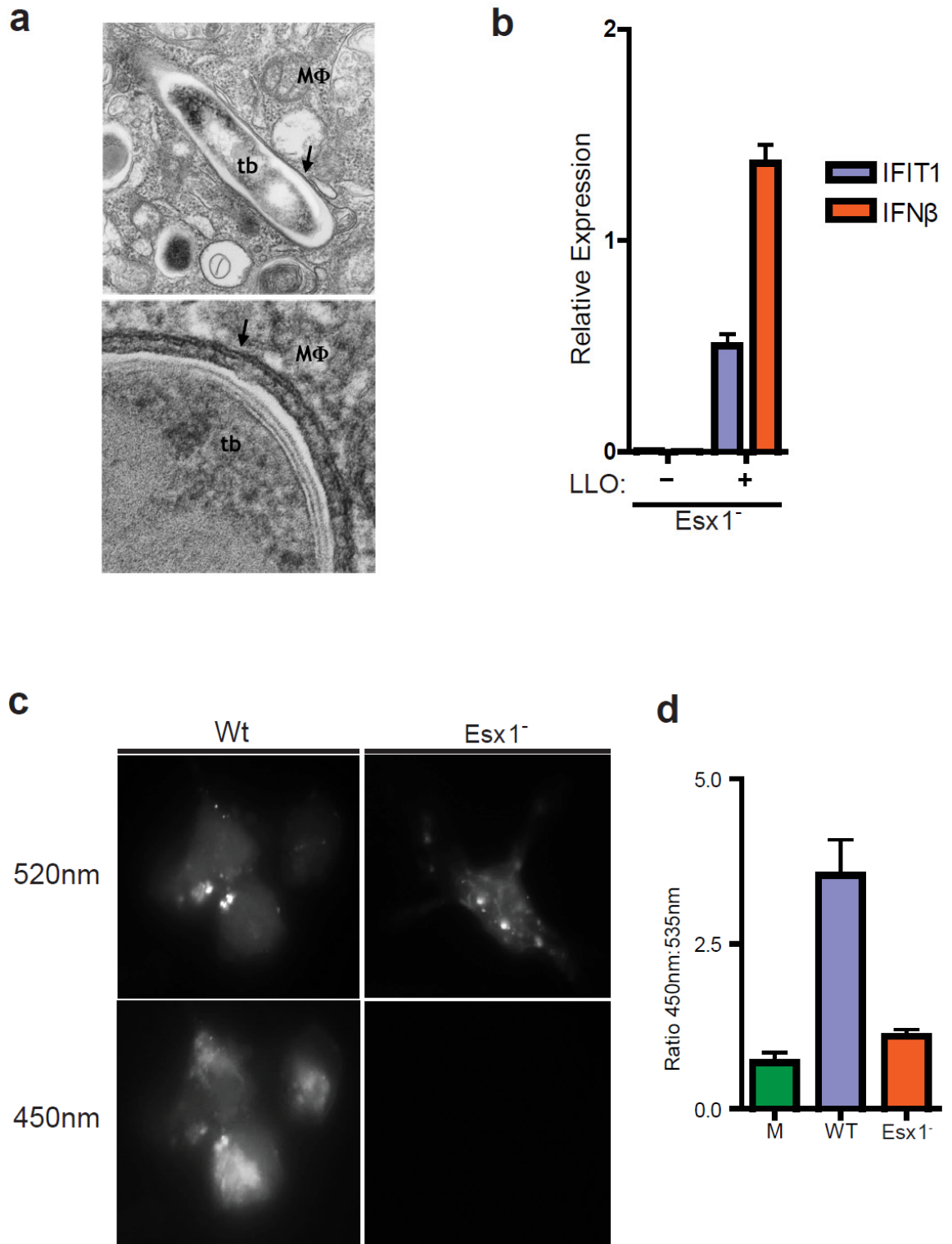

Ratio 450nm:535nm

M   WT   Esx1⁻

Figure 1.4 *M. tuberculosis* activates the STING/TBK1/IRF3 pathway. (A, B) IFIT1 and IFN-β mRNA levels were assessed by qRT-PCR in BMDMs (MΦ) as in Figure 1. Data shown is the mean ± SD, (N≥3 per group). (C) Wild-type C57L/B6 BMDMs were pre-treated for two-hours with the RNA polymerase III inhibitor ML-60218 and infected with wild-type *M. tuberculosis* for 3 hours prior to RNA extraction. Data shown is the mean ± SD, (N=3 per group). (D) IFIT1 and IFN-β mRNA levels were assessed 3 h post-infection of *STING*$^{-/-}$ macrophages wild-type *M. tuberculosis*. Data shown is the mean ± SD, (N=3 per group). *P<0.001 as determined by Student's t-test. (E) Nuclear translocation of IRF3 in BMDMs was determined as described in Figure 1C.

Figure 1.4

Figure 1.4

c

d

e

40
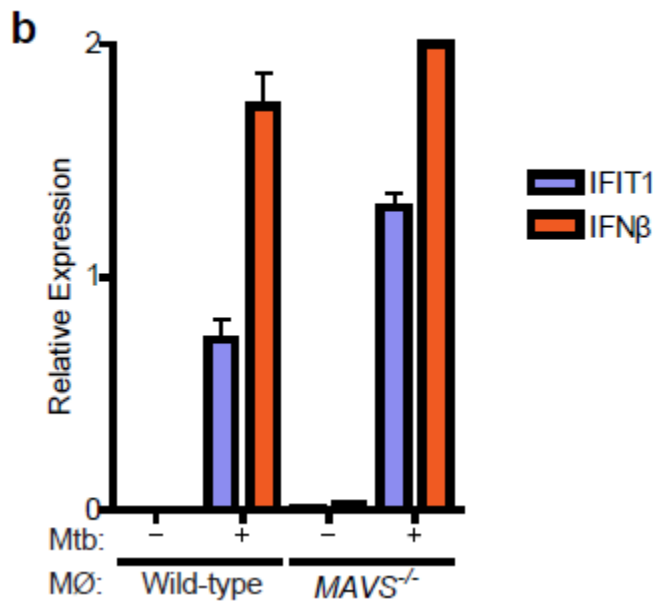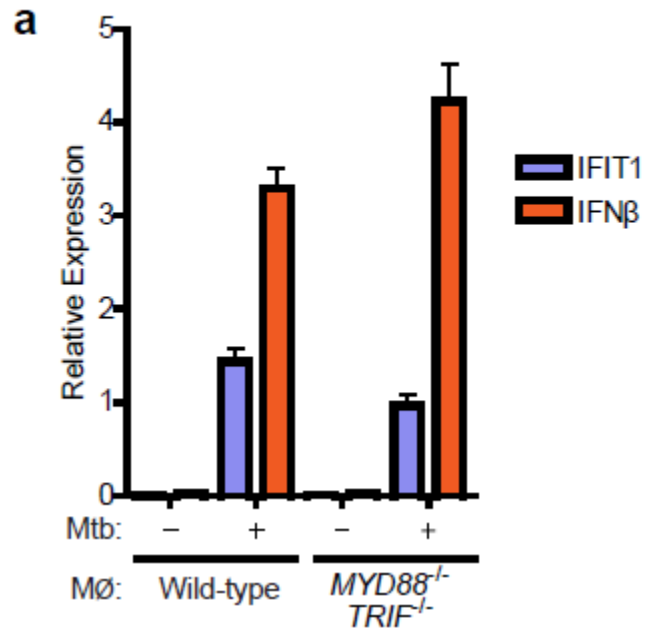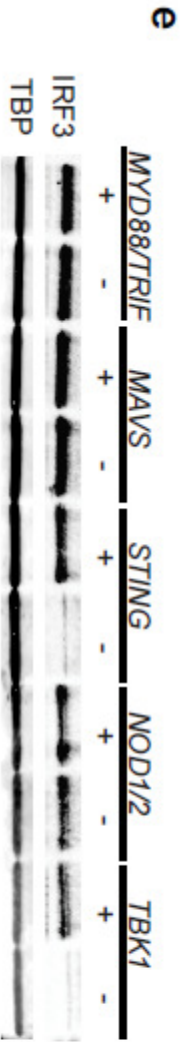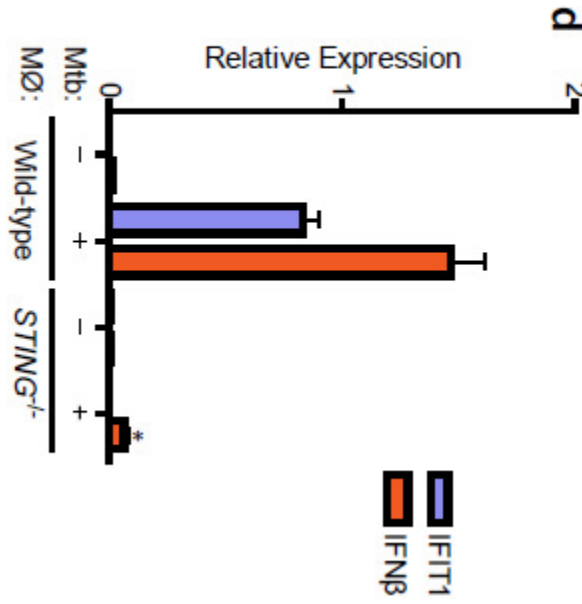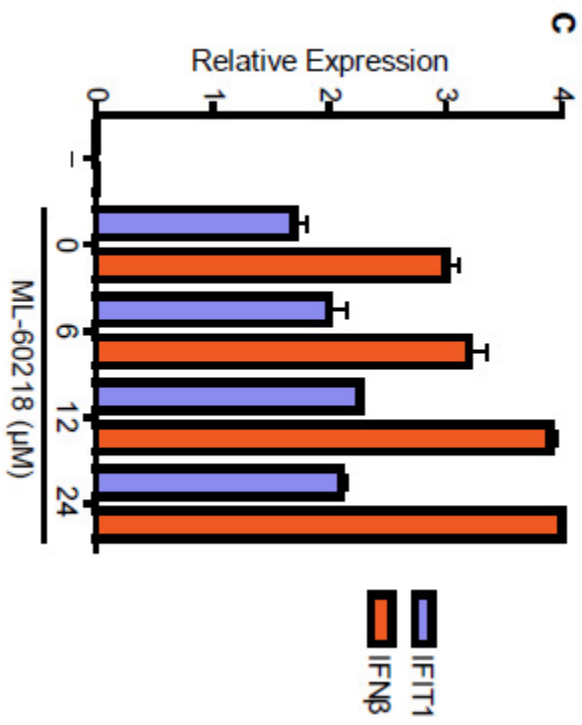
Figure 1.5 Mycobacterial di-adenylate and di-guanylate cyclases are not required for production of IFN-β. (A) IFN-β transcript levels determined by qRTPCR in mouse BMDMs infected with wild type or *MT1397* overexpression strains of Erdman and CDC1551 *M. tuberculosis*. (B) Genomic map of *disA* (*Rv3586*) region in wild type *M. tuberculosis* and in the Δ*disA* knockout, restriction sites and probe location used for Southern blot analysis. (C) Southern analysis of genomic DNA derived from wildtype and Δ*disA* strains. (D) IFN-β transcript levels determined by qRT-PCR in mouse BMDMs infected with wild type Erdman (Wt), Δ*esxA*, Δ*disA*, or wild type Erdman overexpressing the *disA* gene (Wt p*disA*).

Figure 1.5

a

c

b

d

42
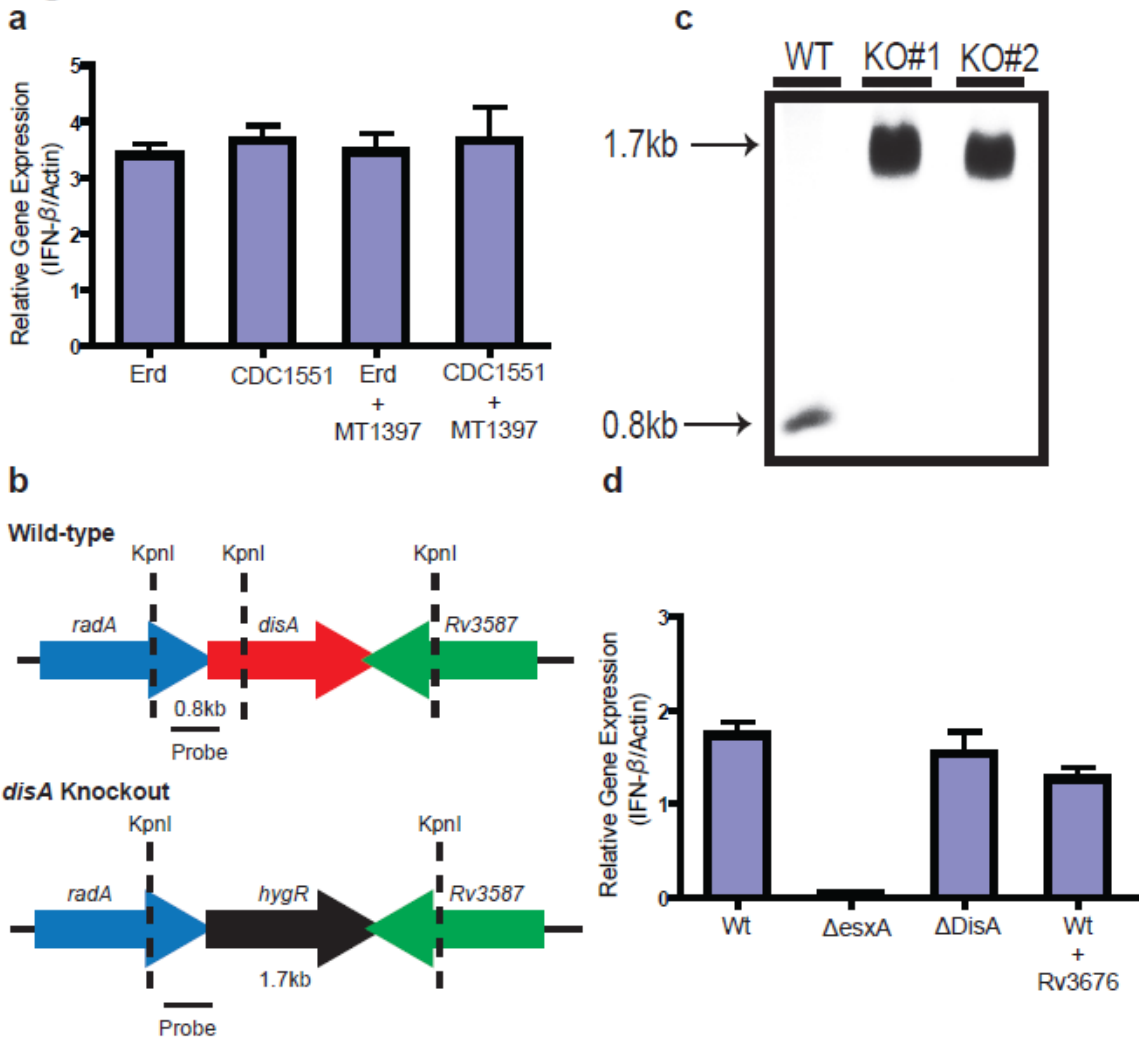
Figure 1.6 The cytosolic DNA sensor IFI204/IFI16 contributes to CSP activation.

(A) IFIT1 and IFN-β mRNA levels were assessed by qRT-PCR in BMDMs (MΦ) from wild-type and DAI knockout mice infected with wild-type *M. tuberculosis* for 3 h. Data shown is the mean ± SD, (N=3 per group). (B) IFIT1 and IFN-β mRNA levels were assessed by qRT-PCR after *M. tuberculosis* infection of immortalized BMDMs (iBMDMs) transduced with lentiviral constructs expressing one of two different shRNAs targeting *IFI204* (*IFI204-1* and *IFI204-2*) or a scrambled shRNA control. Data shown is the mean ± SD, (N=3 per group). *P<0.005 by Student's T-test. (C) *IFI204* mRNA levels were assessed by qRT-PCR in the transduced iBMDMs described in (B). *P<0.005 by Student's T-test. (D) Wild-type C57L/B6 BMDMs were infected with either wild-type or Δ*esxA M. tuberculosis* for 3 hours and cellular localization of IFI204 as assessed via immunofluorescence.

Figure 1.6

a

b

Figure 1.6

c
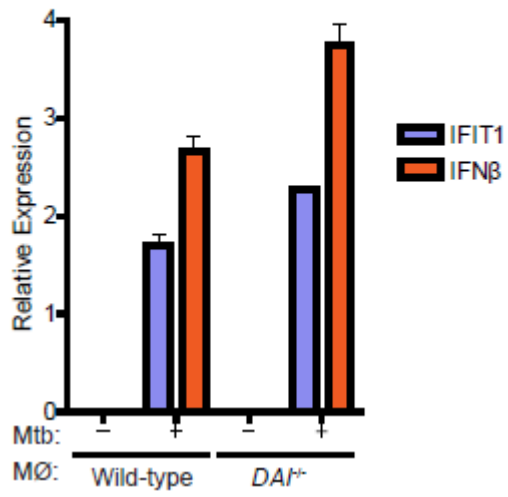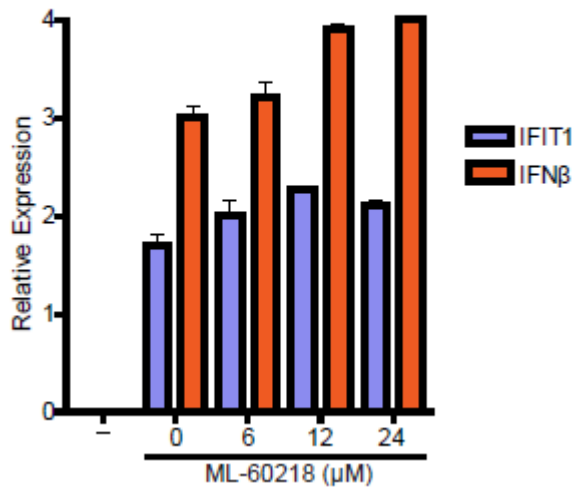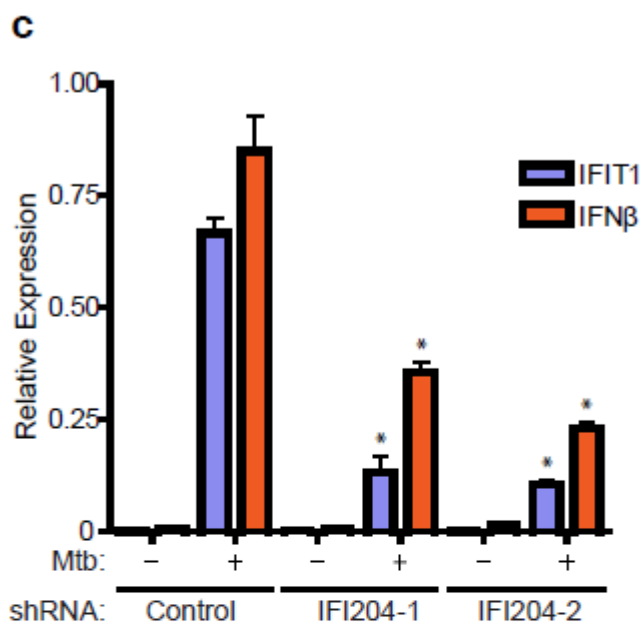
d
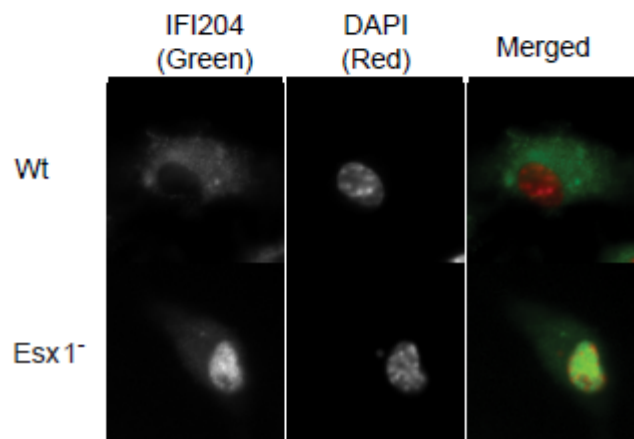
Figure 1.7 Extracellular *M. tuberculosis* DNA triggers the CSP. (A) IFIT1 and IFN-β
mRNA levels were assessed by qRT-PCR in infected BMDMs (MΦ) as described in
Figure 1. (B) RAW264.7 cells were stably transfected with a plasmid over-expressing
either Trex1 or LacZ and infected with wild-type *M. tuberculosis* for 4 h. *IFIT1* and *IFN-
β* gene expression was analyzed by qRT-PCR. (C) Luminescence readings from BMDMs
infected with either wild-type (Wt), ESX-1 mutant (Esx1⁻), or complemented ESX-1
mutant (Comp) *M. tuberculosis* carrying either empty vector or a plasmid encoding a
secreted form of *Metridia* luciferase under the control of the eukaryotic-specific CMV
promoter (pMAN4). Luminescence readings were taken at 16 h post infection. (D) *M.
tuberculosis* cells were labeled with BrdU prior to macrophage infection. After 3 h,
macrophage cytosolic fractions were isolated and BrdU-labeled bacterial DNA was
recovered by immunoprecipitation using anti-BrdU antibodies, and separated by agarose
gel electrophoresis. (E) Lysates from (D) were used as templates for qPCR quantification
of *M. tuberculosis* DNA. Data shown for (A) (B) and (D) is the mean ± SD, (N=3 per
group). *P<0.01 by Student's T-test, comparing mutant and overexpression strains to
their corresponding controls.

Figure 1.7

Figure 1.7

e

Relative DNA Levels

Mtb: — Esx1⁻ WT

d

BrdU → Infect → Cytoplasm → BrdU IP

Mtb: — Esx1⁻ WT
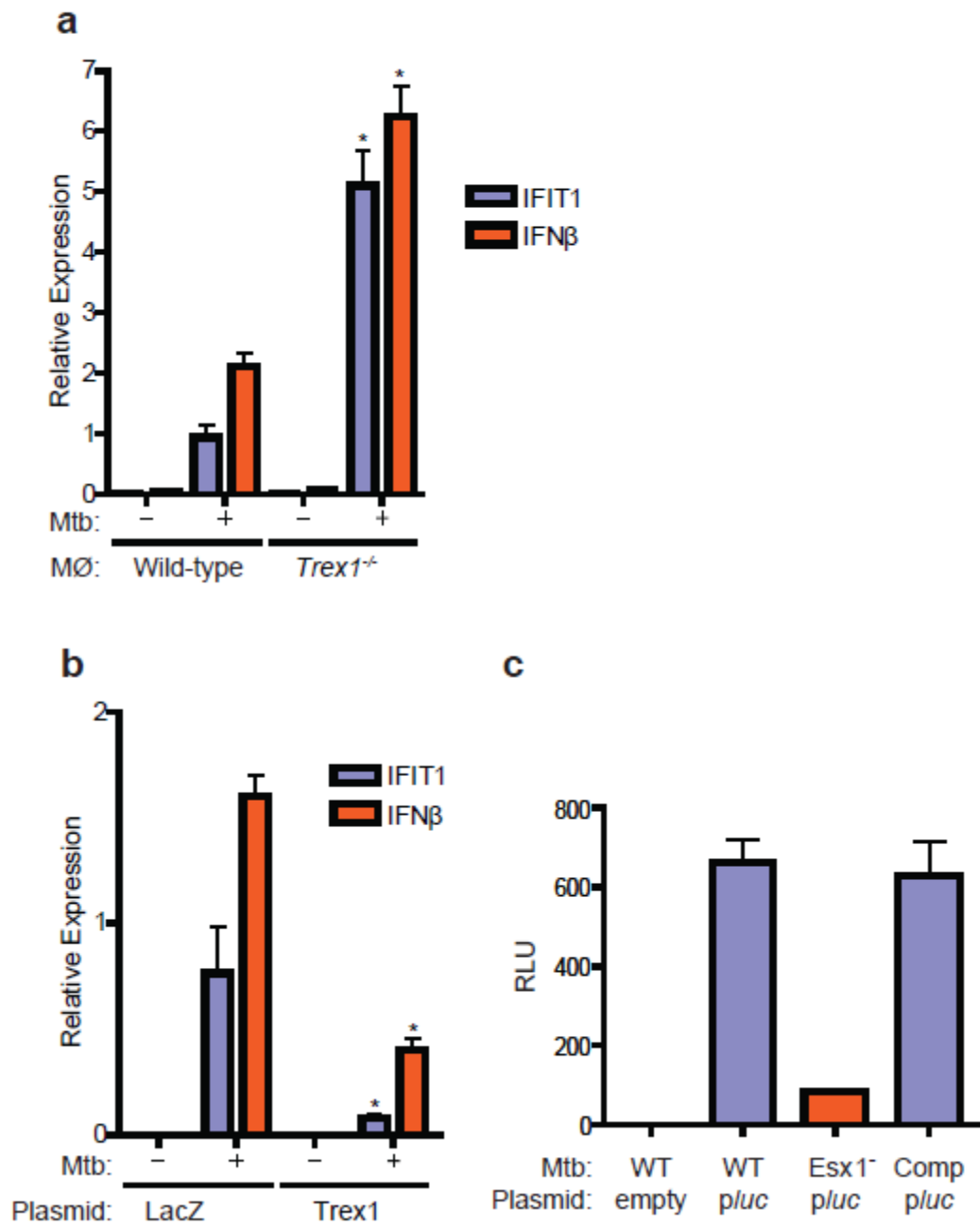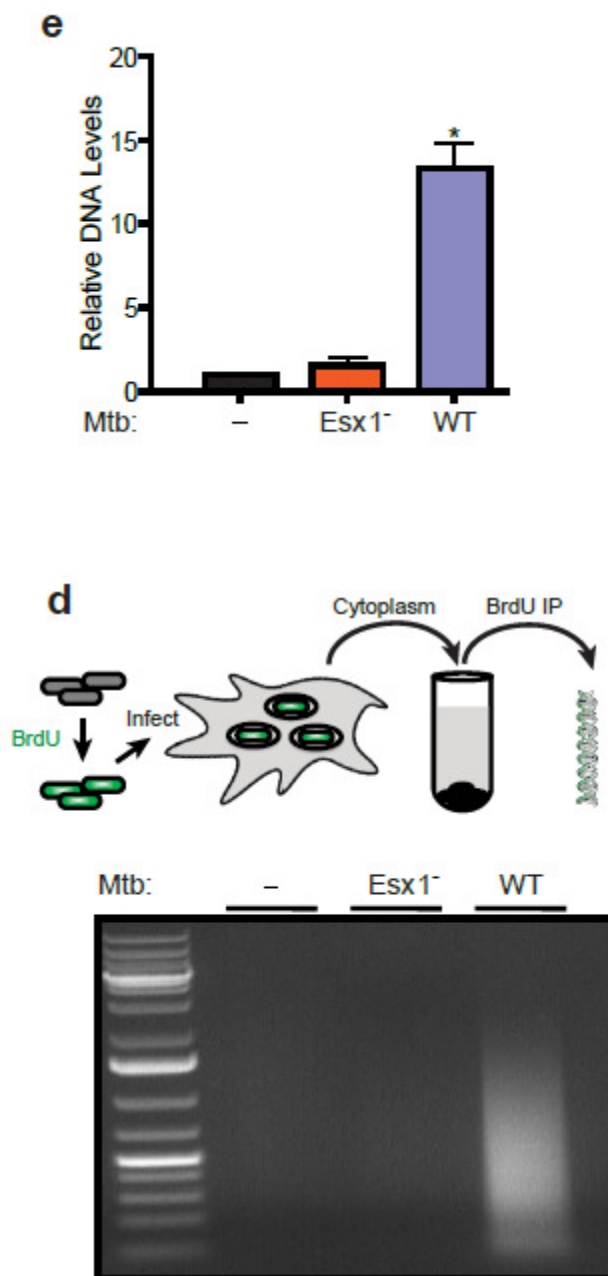
Figure 1.8 Cytosolic signaling is required for virulence of *M. tuberculosis*. (A) Kaplan-Meier survival analysis of *IRF3^-/-^* and C57BL/6 control mice infected with 10^2 CFU wild-type *M. tuberculosis* via the aerosol route (n = 10 per group). *IRF3^-/-^* mice showed significantly improved survival compared to wild-type (WT) mice as calculated by log-rank test (**P < 0.001). (B, C) Bacterial burdens as measured by colony forming units (CFU) in the lungs (B) and spleen (C) of *IRF3^-/-^* and wild-type mice infected as described in (A) (n = 5 per time point) at the indicated time points. Data shown are the mean ± SD. *P < 0.02 and **P <0.005 comparing C57BL/6 and *IRF3^-/-^* mice by Kruskal Wallis. (D) IFN-β, Rantes, MCP1, IL-12 and IL-1β levels were measured by ELISA in serum from *IRF3^-/-^* and C57BL/6 control mice 21 days post infection (n = 4 per group). Data shown is the mean ± SD. *P < 0.005 comparing C57BL/6 and *IRF3^-/-^* mice as determined by Student's T-test.

Figure 1.8

Table 1.1 ESX-1 dependent gene transcription. MEEBO Microarray analysis of RNA obtained from BMDMs infected with either wild-type Erdman Mtb or ESX-1 mutant Mtb. Data shown are genes statistically significant between infection with Wild-type Mtb and ESX-1 mutant Mtb.

Table 1.1

Log2 fold induction versus uninfected macrophages

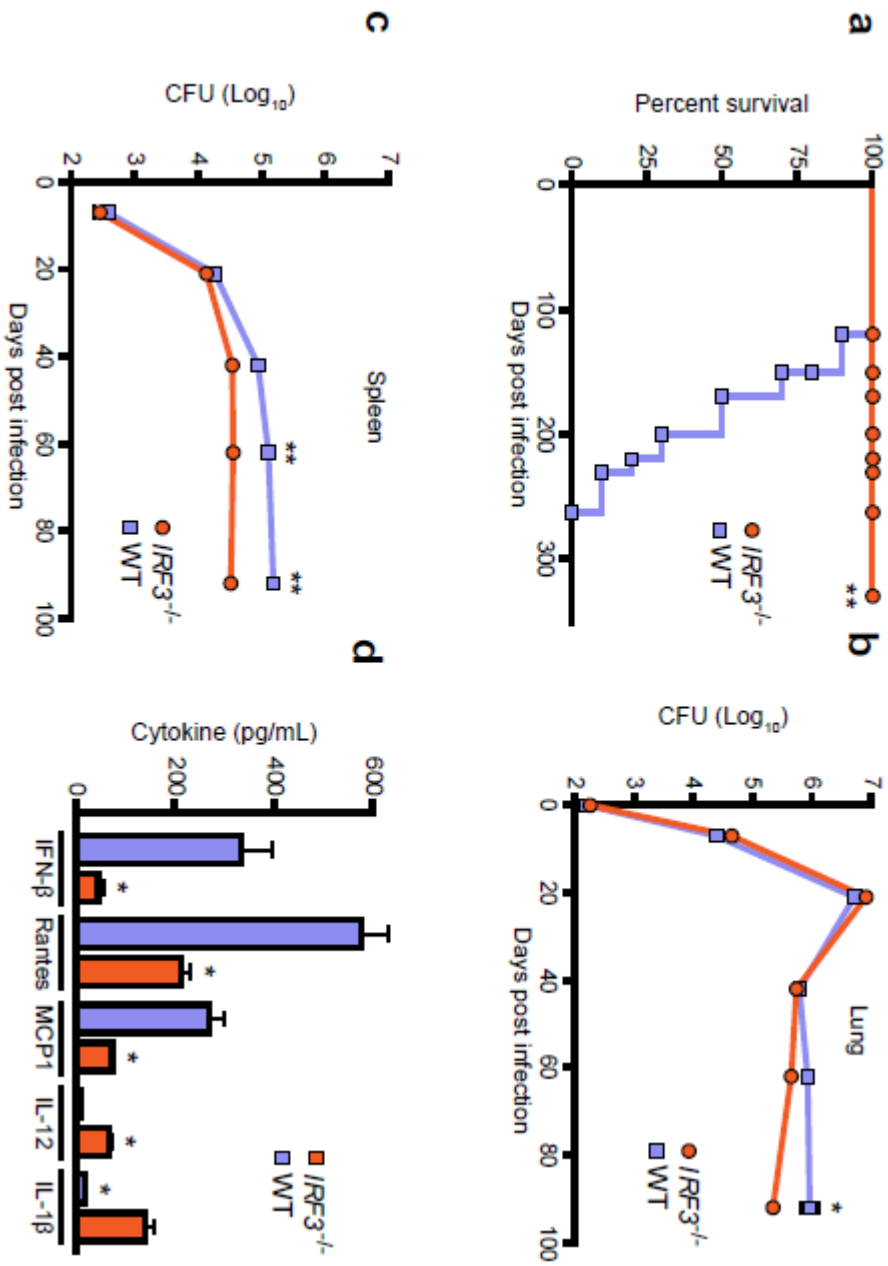| Oligo ID	Gene symbol	Mtb: BMDM:	Wt Erd Wt	Wt Erd Wt	ESX-Wt	ESX-Wt	Wt Erd IRF3-/-	Wt Erd IRF3-/-
mMC012417	IFIT2		3.469	3.528	-0.187	-0.187	0.374	0.055
mMC011595	IL6		6.26	6.34	3.225	3.225	2.844	2.813
mMC013715	CXCL10		3.23	3.259	0.157	0.157	0.327	0.519
mMC013848	IFIT1		3.866	4.025	-0.15	-0.15	0.116	0.079
mMR028612	Iigp1		4.618	4.573	0.118	0.118	0.818	1.481
mMC013727	SPRY4		3.186	3.359	0.21	0.21	0.376	0.513
mMC016397	IFNB1		4.658	4.659	-0.045	-0.045	-0.271	-0.12
mMR030594	GBP5		4.447	4.554	2.167	2.167	0.982	0.889
mMC005508	CMPK2		4.117	4.425	0.107	0.107	-0.343	0.045
mMR026603	GVIN1		1.924	1.98	-0.053	-0.053	-0.238	-0.216
mMR028932	CXCL9		1.711	1.912	-1.123	-1.123	-0.892	null
mMC025695	MX1		2.821	3.007	0.1	0.1	0.234	0.707
mMA035547	Ifi205		3.652	3.755	1.813	1.813	0.98	1.094
mMC007031	IFI44		2.322	2.324	0.152	0.152	0.187	-0.04
mMR026583	PPM1K		1.501	1.568	-0.047	-0.047	-0.651	-0.355
mMC024032	IFIT3		2.694	2.859	-0.482	-0.482	0.26	0.422
mMC025349	Igtp		1.722	1.824	-0.371	-0.371	0.02	0.154
mMC013932	C130051F05Rik		3.465	3.718	0.029	0.029	-0.094	-0.087
mMC011370	CXCL11		2.994	2.925	0.225	0.225	0.196	0.787
mMR026842	IFIT3		2.566	2.856	-0.249	-0.249	0.384	-0.048
mMC003495	GBP4		2.419	2.546	0.556	0.556	0.695	0.797
mMA031689	RBBP6		15.161	15.114	0.59	0.59	null	null
mMC017265	MDK		1.621	1.727	-0.159	-0.159	0.116	0.287
mMC010618	SLFN5		1.686	1.768	0.41	0.41	-0.368	-0.228
mMC019705	Ms4a4c		2.231	2.233	0.474	0.474	0.601	0.536
mMR028602	SOCS1		2.693	2.836	0.455	0.455	0.256	0.293
mMC021419	CD69		3.043	3.164	1.59	1.59	1.563	1.741
mMC001969	RSAD2		3.876	4.191	-0.099	-0.099	-0.444	0.058
mMR027574	MAGI1		2.571	2.568	0.998	0.998	0.903	0.901
mMC019312	IFI205		2.913	3.109	1.181	1.181	0.342	0.754
mMC007217	FAM26F		2.109	2.098	0.478	0.478	0.34	0.48
mMC006438	PPM1K		2.016	1.991	0.105	0.105	-0.7	-0.616
mMC005082	CH25H		1.846	1.91	0.662	0.662	0.397	0.45
mMA034042	OASL1		1.72	1.906	-0.347	-0.347	null	-0.484
mMC100286	Gm5431		1.134	1.301	-0.332	-0.332	-0.05	0.251
mMC000953	OAS2		0.854	0.925	-0.238	-0.238	-0.793	-0.332
mMC026028	Ifi47		1.936	2.101	-0.007	-0.007	-0.483	-0.366
mMR027562	IFI205		2.82	3.02	1.283	1.283	1.396	1.445
mMC024415	HERC6		0.967	1.06	-0.167	-0.167	-0.408	-0.302
mMC100436	Gm4951		2.565	3.186	-1.47	-1.47	null	null
mMC012328	IFI16		1.373	1.427	0.188	0.188	0.332	0.279

Table 1.1   Continued

Oligo ID	Gene symbol	Mtb: BMDM:	Wt Erd Wt	Wt Erd Wt	ESX- Wt	ESX- Wt	Wt Erd IRF3-/-	Wt Erd IRF3-/-
mMC001981	LOC100044768		1.568	1.707	-0.19	-0.19	0.781	0.271
mMC001042	PPM1K		1.449	1.642	-0.064	-0.064	-0.098	-0.105
mMC004924	TNFSF10		3.33	3.336	0.685	0.685	-0.272	0.267
mMC025310	Phf11		1.08	1.228	-0.059	-0.059	-0.019	0.072
mMC024853	BC094916		2.514	2.766	0.095	0.095	-0.225	0.854
mMC011522	EDN1		3.003	3.032	1.533	1.533	2.078	1.911
mMC009824	IRGM		1.654	1.835	-0.258	-0.258	-0.197	-0.394
mMA032762	`		1.987	2.126	0.916	0.916	0.899	0.985
mMR029377	-		2.685	2.888	0.811	0.811	1.049	1.028
mMC100640	Ccl12		1.265	1.377	0.191	0.191	0.925	1.099
mMC007427	Ccl12		1.625	1.877	0.218	0.218	0.979	1.136
mMC003286	FAM46A		0.627	0.758	-0.374	-0.374	-0.294	-0.128
mMC010986	EGR1		0.566	0.483	-0.885	-0.885	-0.193	-0.02
mMC006762	MX2		2.562	2.82	0.188	0.188	0.242	0.283
mMC004797	CCNJ		1.481	1.532	0.071	0.071	0.018	1.2
mMR028592	RGS1		0.058	0.109	-0.908	-0.908	-0.254	-0.113
mMC020606	IRF1		2.209	2.432	0.949	0.949	0.456	0.7
mMC024746	GBP1		2.432	2.706	0.889	0.889	0.314	0.705
mMC021101	IFIT3		2.973	3.086	-0.229	-0.229	0.413	-0.031
mMC012881	RTP4		0.973	1.074	0.072	0.072	-0.018	0.202
mMR030116	SLFN13		0.714	0.713	-0.376	-0.376	-0.143	0.35
mMC025225	IRGM2		2.093	2.348	-0.235	-0.235	-0.377	0.227
mMC019577	CD274		2.195	2.35	0.857	0.857	0.551	0.529
mMC014328	FGL2		0.748	0.835	-0.162	-0.162	-0.384	-0.344
mMC100662	Ccl5		2.029	2.107	1.04	1.04	1.169	1.766
mMC005250	B230207M22		1.473	1.605	0.407	0.407	1.082	1.206
mMC018948	Gdap10		2.328	2.252	0.985	0.985	0.383	null
mMA033942	PELI1		0.73	0.834	-0.238	-0.238	0.059	0.285
mMC015219	LOC268537		2.578	2.705	1.676	1.676	0.788	0.744
mMC005166	ARL13B		1.269	1.381	0.412	0.412	0.331	0.382
mMC017279	Slfn4		2.416	2.985	0.253	0.253	-0.167	-0.597
mMC010553	IFIH1		1.47	1.553	0.01	0.01	-0.283	-0.311
mMC021626	ISG15		1.573	1.859	0.174	0.174	0.753	0.843
mMR027334	HIST3H2BB		0.286	0.196	-1.277	-1.277	-0.861	0.092
mMC012412	4930551O13Rik		1.37	1.349	0.091	0.091	0.34	0.291
mMC006436	ZUFSP		1.437	1.456	0.11	0.11	-0.066	-0.074
mMC008739	CSRNP1		1.272	1.397	0.108	0.108	0.735	0.617
mMC024156	CCRL2		2.063	2.189	1.038	1.038	1.993	1.975
mMC025156	DDX60		1.172	1.307	0.233	0.233	-0.392	-0.119
mMR031089	IFI203		2.008	2.146	1.186	1.186	0.871	1.104
mMC006992	TNFSF10		0.864	0.874	-0.575	-0.575	-0.304	-0.05
mMC018907	USP18		1.735	1.965	-0.245	-0.245	-0.002	0.019
mMC020260	DDX60		0.94	1.066	-0.01	-0.01	0.482	0.418

Table 1.1   Continued

Oligo ID	Gene symbol	Mtb: BMDM:	Wt Erd Wt	Wt Erd Wt	ESX-Wt	ESX-Wt	Wt Erd IRF3-/-	Wt Erd IRF3-/-
mMC024449	TMEM69		1.179	1.217	0.348	0.348	0.648	0.586
mMC013357	Clec2d		2.618	2.946	1.344	1.344	1.532	1.934
mMC013685	Rnf213		0.846	0.99	0.008	0.008	0.188	0.145
mMC024437	Mndal		1.547	1.71	0.603	0.603	0.768	0.683
mMC017163	TNFSF8		0.304	0.404	-0.485	-0.485	-0.576	-0.788
mMC006707	SOCS1		0.817	1.053	-0.241	-0.241	-0.28	-0.195
mMC004888	F830004M19Rik		1.826	1.88	0.955	0.955	0.939	1.284
mMC021173	GVIN1		1.073	1.245	0.085	0.085	-0.357	-0.22
mMC007052	GBP5		2.862	2.97	1.762	1.762	0.154	0.688
mMC013106	Slfn8		1.515	1.545	0.391	0.391	0.22	-0.135
mMC009242	GCA		2.049	1.962	0.882	0.882	0.803	0.469
mMA035267	RGS1		0.206	0.293	-0.814	-0.814	-0.108	-0.303
mMR030098	STAT1		0.72	0.836	-0.002	-0.002	-0.333	-0.287
mMC018731	1500012F01Rik		1.019	1.224	0.1	0.1	0.459	1.176
mMC100430	Tnfaip8l3		1.153	1.248	0.3	0.3	-0.222	-0.323
mMC012433	GBP7		2.026	2.157	0.822	0.822	-0.167	-0.1
mMC010351	IL10		2.027	2.166	1.147	1.147	1.588	1.691
mMC011607	IL12A		9.418	9.71	7.687	7.687	null	null
mMC023252	PAPD7		0.853	1.048	-0.048	-0.048	0.138	0.193
mMC001992	OASL1		1.041	1.298	-0.201	-0.201	null	null
mMR028686	BCAT1		-0.1	0.186	-1.318	-1.318	0.736	null
mMC025712	SLFN12		0.87	0.87	-0.184	-0.184	-0.857	-1.007
mMC015136	EIF2AK2		0.931	1.016	-0.055	-0.055	0.542	0.607
mMA035331	IRGM		1.687	1.936	-0.451	-0.451	0.189	0.219
mMR030729	ZUFSP		1.939	1.773	0.574	0.574	-0.329	null
mMC022884	FEM1C		0.354	0.438	-0.224	-0.224	-0.517	-0.554
mMR100103	IFI203		0.868	1.033	0.091	0.091	0.256	0.333
mMA035279	NPHS2		-0.385	-0.071	-1.48	-1.48	-0.205	-0.246
mMC002496	DDX58		1.679	1.834	0.89	0.89	0.872	1.003
mMC020652	RAB9A		0.132	0.195	-0.448	-0.448	-0.086	-0.106
mMR031060	PNP		2.436	2.833	1.22	1.22	null	null
mMC100919	-		0.832	0.947	0.201	0.201	0.189	0.214
mMC003011	MAFK		0.368	0.539	-0.415	-0.415	-0.234	-0.048
mMC007860	FNDC3A		0.424	0.436	-0.287	-0.287	-0.647	-0.672
mMC017218	TRIM21		1.142	1.326	0.083	0.083	0.196	0.159
mMC013426	E130102H24Rik		0.462	0.472	-0.557	-0.557	-0.583	-0.412
mMC004493	ISG20		2.065	2.264	1.136	1.136	0.387	0.747
mMA032453	IRF1		1.25	1.513	0.327	0.327	0.136	0.512
mMC016279	NT5C3		1.015	1.098	0.17	0.17	-0.04	0.065
mMR030976	-		4.078	4.094	3.362	3.362	4.135	3.954
mMR030000	H2-T9		0.662	0.847	-0.068	-0.068	-0.249	-0.094
mMC017168	TIPARP		0.2	0.254	-0.62	-0.62	-0.929	-0.561
mMC016938	Serpina3f		0.38	0.198	-0.833	-0.833	-0.742	1.095

Table 1.1	Continued							
Oligo ID	**Gene symbol**	**Mtb: BMDM:**	**Wt Erd Wt**	**Wt Erd Wt**	**ESX- Wt**	**ESX- Wt**	**Wt Erd IRF3-/-**	**Wt Erd IRF3-/-**
mMC009139	Oasl2		0.478	0.649	-0.196	-0.196	0.133	0.128
mMC025187	TREX1		1.108	1.33	0.302	0.302	0.228	0.426
mMC003285	OTUD1		0.484	0.644	-0.242	-0.242	-0.024	-0.091
mMC022258	TPST1		0.43	0.55	-0.234	-0.234	null	-0.719
mMC004056	PNPT1		0.443	0.489	-0.208	-0.208	-0.539	-0.656
mMC023634	CXCL1		3.187	3.325	2.382	2.382	3.625	3.422
mMC006843	EGR3		1.31	1.307	0.478	0.478	2.515	2.332
mMR029558	RGS2		-0.322	-0.347	-1.098	-1.098	-1.107	-0.751
mMA033612	DCLRE1C		0.35	0.449	-0.379	-0.379	-0.242	null
mMC022593	CXCL2		3.18	3.143	2.412	2.412	2.875	3.131
mMC015088	MXD1		0.818	1.006	0.056	0.056	0.193	0.313
mMR026409	FLRT2		0.562	0.599	-0.217	-0.217	-0.151	-0.122
mMC015527	RGS17		-0.588	-0.537	-1.417	-1.417	-0.102	0.477
mMC020628	-		1.983	2.641	0.499	0.499	0.761	1.075
mMC024533	1600002D24Rik		0.506	0.603	-0.058	-0.058	0.174	0.456
mMC007335	DDX4		2.234	1.698	-0.981	-0.981	null	null
mMC023123	PELI1		0.297	0.397	-0.252	-0.252	-0.376	-0.396
mMC008851	ZC3HAV1		0.602	0.753	-0.055	-0.055	0.591	0.564
mMC017740	SAMD9L		1.05	1.043	0.064	0.064	-0.408	-0.423
mMC017626	TOR3A		0.874	1.051	0.194	0.194	0.31	0.371
mMC019497	A630072M18Rik		0.419	0.569	-0.245	-0.245	0.231	0.333
mMC022703	H2-T10		0.615	0.778	-0.038	-0.038	-0.268	-0.131
mMC012006	MAP3K8		1.957	2.082	0.95	0.95	1.011	0.992
mMC018719	STAT2		0.506	0.65	-0.443	-0.443	-0.252	0.015
mMC003611	Gm8995		1.427	1.337	-1.028	-1.028	-0.95	-0.646
mMC005764	CCL7		0.922	1.171	0.152	0.152	1.368	1.23
mMA034116	CCL6		2.06	2.406	1.129	1.129	1.091	0.679
mMC020765	DTX3L		1.064	1.255	0.419	0.419	0.221	0.583
mMR026790	GBP9		0.938	0.816	-0.018	-0.018	-0.424	-0.513
mMR029096	4930428B01Rik		0.291	0.394	-0.213	-0.213	0.523	0.743
mMC019511	Ubxn7		-0.356	-0.184	-1.426	-1.426	-0.135	null
mMC012291	GLRX3		3.112	2.65	1.138	1.138	3.087	2.997
mMC100490	Xaf1		0.908	1.26	0.021	0.021	0.042	0.539
mMC023053	C10orf18		0.983	1.037	0.211	0.211	-0.247	-0.468
mMA035185	IFI203		1.344	1.552	0.614	0.614	0.397	0.755

Table 1.2

Plasmid/Strain	Description	Reference
Plasmids		
PMV260-Kan	Mtb epsiomal plasmid containing GroEL promoter and KanR	W. R. Jacobs, Jr.
PMAN-1	pmv260-kan,in which the Kanamycin resistance marker was replaced with Zeo resistance marker	This study
PMAN-2	pman-1 plasmid expressing the Mtb Rv13540 gene	This study
PMAN-3	pman-1 plasmid expressing the Mtb disA gene	This study
PMAN-4	pman-1 plasmid in which the groEL promoter was excised and replaced with the CMV, Matridia luciferase, and SV40 polyA tail of the pMET plasmid (clontech)	This study
PMAN-5	pTracer-BSD vector expressing mouse Trex1	This Study
PMAN-6	pTracer-BSD vector expressing LacZ	This Study
PMAN-7	pman-1 plasmid expressing the BlaC (Rv2068c)	This Study
PMAN-8	pBluescript plasmid containg HLY gene from L. monocytogenes 10403S containing C430A mutation	This Study
PMAN-9	pman-1 plasmid expressing fusion protein containing the sec signal sequence of Rv1886c (fbpB) fused to the pro-domain of HLY from pman-8	
PMAN-10	pman-1 plasmid expressing MT1397 gene from CDC1551	
M.tuberculosis Strains		
Erdman RV3877::Tn5370	Erdman strain RV3877 transposooon mutant	Stanley et al.
Erdman ΔESXA	Erdman strain Esat-6 KO	Stanley et al.
Erdman ΔESXA : Compelemented	Erdman strain Esat-6 KO complemented strain	Stanley et al.
Erdman ΔRv3586	Erdman strain Rv3586 KO	This study
Erdman Strain		W. R. Jacobs, Jr.
CDC1551 Strain		Colorado State TBVTRM

Chapter 2.

Detection of mycobacterial DNA activates autophagy and is essential for control of

***Mycobacterium tuberculosis* infection.**

Abstract

Eukaryotic cells sterilize the cytosol by using autophagy to route invading bacterial pathogens to the lysosome. During macrophage infection with *Mycobacterium tuberculosis*, a vacuolar pathogen, exogenous induction of autophagy can limit replication but the mechanism of autophagy targeting and its role in natural infection remain unclear. Here we show that phagosomal permeabilization mediated by the bacterial ESX-1 secretion system allows cytosolic components of the ubiquitin-mediated autophagy pathway access to phagosomal *M. tuberculosis*. Recognition of extracellular bacterial DNA by host cytosolic components is required for marking bacteria with ubiquitin, and delivery of bacilli to autophagosomes.

Introduction

Autophagy is an evolutionarily conserved process in eukaryotes whereby cytoplasmic components are enveloped and sequestered by membranous structures that subsequently fuse to lysosomes for degradation. In response to nutrient limiting conditions, general autophagy serves a catabolic function by mediating non-selective consumption of organelles and other cellular components to generate substrates for both energy metabolism and vital protein synthesis [1]. In contrast, selective autophagy functions to specifically renovate the cell by targeting protein aggregates and specific organelles for removal through the use of ubiquitin-mediated targeting [2]. For example, damaged mitochondria are designated for destruction by targeting only the non-functional organelles to the lysosome via the autophagy pathway, a process termed mitophagy.

58

Ubiquitin-tagged mitochondria are directed into the general autophagy pathway via the action of the adaptor protein p62, which binds both ubiquitin and the autophagosome-associated protein, LC3, although other factors are likely required. Once LC3 is targeted to the cargo, other components of the general autophagy pathway, including ATG proteins such as ATG5, function to form autophagosomes and deliver the organelle to the lysosome [2].

In addition to eliminating endogenous organelles, autophagy also plays an important role in innate defense against invading intracellular pathogens. A number of studies have shown that many viruses and intracellular bacteria are eliminated by selective autophagy [1]. The prevailing view is that autophagy functions to eliminate intracellular microbes that enter into the cytosol by sequestering invading pathogens in autophagosomes and delivering them to the lysosome. Furthermore, some pathogens, most notably herpesviruses and lentiviruses, employ autophagy evasion mechanisms that are critical for long-term, persistent infection [3]. Previous studies of *Salmonella enterica* serovar Typhimurium (*S.* Typhimurium) and Listeria monocytogenes infection of cultured epithelial cells have shown that bacteria which exit the endosomal pathway and enter into the cytosol are ubiquitinated and delivered to autophagosomes via recognition by the cytosolic autophagy receptors p62 and NDP52 [4, 5]. Yet how cytosolic bacteria are recognized and targeted for ubiquitination is currently unknown.

Much of the groundbreaking work on the role of autophagy in mycobacterial clearance was performed using *Mycobacterium bovis* Bacille Calmette-Guérin (BCG), the attenuated vaccine strain [6, 7]. Curiously, in these studies, targeting of LC3 to BCG-containing vacuoles required exogenous stimulation of autophagy. Although this vaccine

strain has been extremely helpful in modeling many basic functions of *M. tuberculosis*, it lacks several virulence factors, including the Type VII secretion system, ESX-1 [8-11]. This is a key difference between *M. tuberculosis* and BCG, as mutants lacking ESX-1 are defective for replication within macrophages, are severely attenuated in animal models of infection, and fail to activate innate immune signaling responses of macrophages [8, 12-14]. Furthermore, BCG does not undergo selective autophagy and recruitment of LC3 to the phagosomal membrane unless autophagy is experimentally induced [6, 7, 15]. During infection with *Mycobacterium marinum*, an ectothermic pathogen related to *M. tuberculosis*, ESX-1 secretion is required for vacuolar escape [16] and for subsequent localization of ubiquitin [17] and LC3 [18] to the bacterial surface. However, unlike *M. marinum*, *M. tuberculosis* remains membrane bound, although eventual escape has been observed late in infection [19]. Although inducing autophagy exogenously via starvation, treatment with rapamycin, interferon gamma (IFN-γ), vitamin D3, or genetic depletion of autophagy inhibitors can lead to decreased bacterial replication in macrophages [6, 7, 20, 21], how *M. tuberculosis* interfaces with the selective autophagy pathway from within the phagosome, and the contribution of autophagic targeting by macrophages to host resistance, is unknown.

Here we report that wild-type *M. tuberculosis* cells elicit ubiquitin-mediated autophagy targeting in resting macrophages, resulting in the delivery of bacilli to lysosomes. Targeting requires both the bacterial ESX-1 system and the host cytosolic DNA sensing pathway, revealing a novel link between nucleic acid sensing and selective autophagy of intracellular pathogens. Remarkably, we show for the first time that autophagy is a major mechanism of host control during *M. tuberculosis* infection *in vivo*.

Results

Autophagic targeting of *M. tuberculosis*

To determine if *M. tuberculosis* is specifically targeted by selective autophagy, we first examined the dynamics of the autophagosome-specific marker, LC3, over the course of wild-type *M. tuberculosis* infection of naïve macrophages. Primary murine bone marrow-derived macrophages (BMDMs) derived from GFP-LC3 transgenic mice were infected with *M. tuberculosis* expressing mCherry, and localization of GFP-LC3 was analyzed via microscopy at defined times after infection. Two hours after infection, ~15% of intracellular bacteria colocalized with GFP-LC3, and by 4 hours this increased to ~30% of the bacterial population (Figure 2.1A top panels, and Figure 2.1B). Although the number of small GFP-LC3 puncta increased during the infection, targeting of LC3 to larger structures in the cell occurred exclusively at the *M. tuberculosis* phagosome. Three-dimensional confocal imaging of these cells revealed that GFP-LC3 envelops the entire *M. tuberculosis* phagosome (data not shown). Similar results were observed during infection of the macrophage-like cell line RAW 264.7 stably expressing GFP-LC3 (Figure 8.1A and 8.1B), as well as BMDMs immunostained using an antibody specific for endogenous LC3 (Figure 2.8C and 2.8D). *M. tuberculosis* also colocalized with another autophagy protein, ATG12, in both BMDMs (Figure 2.1C and 2.1D) and RAW 264.7 cells (Figure 2.8G and2.8H). Western blot analysis of endogenous LC3 during *M. tuberculosis* infection revealed an increase in conversion of LC3-I to LC3-II, consistent with autophagy activation (Figure 2.1E). In addition, we tested whether LC3 recruitment required the canonical autophagy protein, ATG5. Indeed, BMDMs from *Atg5^{flox/flox}*-Lyz-

Cre mice [15], which contain a genomic deletion of *Atg5* within monocytes/macrophages (hereafter referred to as *Atg5⁻* mice), were unable to recruit LC3 to phagosomes containing *M. tuberculosis* (Figure 2.9). Thus, wild-type *M. tuberculosis* is specifically recognized and targeted by the autophagy pathway in the absence of autophagy inducers.

Because BCG lacks genes encoding ESX-1 [11, 22] and previous work by Lerena and Columbo showed that ESX-1 is required for autophagy targeting of *M. marinum* [18], we tested whether this secretion system was required for native LC3 targeting to *M. tuberculosis* during infection. While infection with BCG induced no LC3 recruitment, restoration of ESX-1 secretion via complementation with the RD1 locus of *M. tuberculosis* led to a partial yet significant increase in targeting during infection of GFP-LC3 RAW 264.7 cells (Figure 2.1F and 2.1G). Likewise an *M. tuberculosis* mutant defective in ESX-1 secretion, *Δesat-6*, failed to recruit LC3 (Figure 2.1A bottom panels, and 2.1B) and did not induce LC3 processing (Figure 2.1C). Consistent with previous studies, wild-type *M. marinum* also colocalized with GFP-LC3 in an ESX-1-dependent manner (Figure 2.8E and 2.8F) [18]. These data indicate that the ESX-1 secretion system is required for targeting mycobacteria to autophagosomes during infection.

Mounting evidence strongly suggests that ESAT-6, the major ESX-1 secreted substrate, has membrane damaging activity [12, 16, 23-25] that functions to permeabilize the phagosomal membrane, allowing access of the bacterium to the cytosol [19, 26]**.** Because pore-forming toxins such as listeriolysin-O (LLO) are required for cytosolic access and to induce autophagy during *L. monocytogenes* infection [27, 28], we hypothesized that ESX-1 mediated autophagy was due to ESAT-6 pore formation. To test this, we created an ESX-1 mutant strain that expressed and secreted an auto-activated

form of the heterologous pore-forming toxin LLO [29]. Expression of LLO in either *M. tuberculosis* or *M. marinum* partially restored targeting of GFP-LC3 to ESX-1 mutants (Figure 2.1H, 2.1I, and 2.1J), suggesting that the requirement of ESX-1 secretion in autophagy targeting is pore formation of the phagosomal membrane.

During macrophage infection, the majority of *M. tuberculosis* cells block phagosomal maturation into lysosomes [30], a process that requires a functional ESX-1 secretion system [31, 32], and the bacilli reside and grow in an endosome-like compartment,[33]. Therefore, we considered the possibility that wild-type bacteria colocalized with LC3 due to this block in intracellular trafficking, perhaps by trapping and stabilizing an intermediate LC3+ compartment that is short-lived during infection with ESX-1 mutants. To test this, we infected GFP-LC3 RAW macrophages with *M. tuberculosis* mutants that have functional ESX-1 secretion systems but fail to inhibit phagolysosome fusion. MoaB1 and Rv1506c are involved in molybdopterin and acytrehalose-containing glycolipid biosynthesis, respectively, and have been identified in separate screens to traffic to lysosomes [32, 34]. We observed that both *Rv1506c::Tn* and *moeB1::Tn* mutant cells colocalized with GFP-LC3 to a similar extent as wild-type *M. tuberculosis*, while the Δ*esat-6* mutant failed to recruit GFP-LC3 (Figure 2.1K and 2.1L). Triple-labeling experiments demonstrated that these GFP-LC3+ bacteria also colocalized with ubiquitin (Figure 2.1O). Collectively, these results further demonstrate that the ESX-1 Type VII secretion system serves to expose phagosome-bound *M. tuberculosis* to the cytosol, where the bacilli are recognized and targeted to autophagic compartments.

Role of LC3 and ubiquitin adaptors in *M. tuberculosis* targeting to the autophagy pathway

To understand the mechanism by which LC3 is recruited to ESX-1^{+} *M. tuberculosis*, we tested whether p62 and NDP52 are required for targeting bacilli to autophagosomes. As shown in Figure 2.2A-2.2D, approximately 20-25% of the *M. tuberculosis* population recruited both p62 and NDP52 to phagosomes in an ESX-1-dependent fashion. Triple-labeling experiments showed that ~70% of the LC3+ population also localized with both p62 and NDP52 (Figure 2.2E and 2.2F). Knockdown of either p62 or NDP52 expression in GFP-LC3 RAW 264.7 cells (Figure S4) resulted in a dramatic decrease in LC3 colocalization (Figure 2.2G). Thus, as with *S.typhimurium* , both adaptors are required for autophagy targeting of *M. tuberculosis* [35].

NDP52, in addition to binding LC3, interacts with NAP1 and SINTBAD to recruit Tank binding kinase (TBK1) [36]. TBK1 is necessary for transcriptional induction of type I interferon (IFN) during wild-type *M. tuberculosis* infection [8], but is also required for selective targeting of salmonella to autophagy [37]. To determine if TBK1 is also important in autophagy targeting of *M. tuberculosis*, we stained infected BMDMs using antibodies specific for the activated, phosphorylated form of TBK1. As shown in Figure 2.2H and 2.2I, activated TBK1 colocalized to wild-type *M. tuberculosis* but not to ESX-1 mutants, and dual labeling experiments showed that the majority of the TBK1+ bacteria colocalized with LC3 (Figure 2.2J and 2.2K). Importantly, BMDMs from *TBK1*^{-/-} mice had a 60% reduction in their ability to target LC3 to *M. tuberculosis* during infection (Figure 2.2L), demonstrating that the kinase plays an important role in both transcriptional and autophagic innate immune responses to virulent *M. tuberculosis*.

LC3 positive *M. tuberculosis* cells are ubiquitinated

Because both p62 and NDP52 are recruited to ubiquitinated substrates, we tested if *M. tuberculosis* colocalized with host ubiquitin by immunostaining using anti-ubiquitin antibodies that recognize conjugated mono- and poly-ubiquitin. As shown in Figures 2.3A and 2.3B, approximately 30% of wild-type *M. tuberculosis* colocalized with ubiquitin at 4 h post-infection, while ESX-1 mutant bacteria did not colocalize with ubiquitin. Coimmunostaining for both ubiquitin and LC3 revealed that approximately 70% of all wild-type *M. tuberculosis* that were coated with ubiquitin also recruited LC3 (Figure 2.3C and 2.3D). Using antibodies that recognize specific linkages of polyubiquitin chains, we found that approximately 20% of the total *M. tuberculosis* population was associated with K63-linked ubiquitin, while approximately 7% was K48-linked (Figure 2.3E and 2.3F). Importantly, ubiquitin recruitment was unaffected in *Atg5*⁻ macrophages, indicating that ubiquitin acquisition precedes the recruitment of LC3 and that the observed LC3 colocalization is specific to the ubiquitin-mediated autophagy pathway (Figure 2.9A and 2.9B).

Cytosolic DNA activates selective autophagy

Next, we sought to determine the microbial signal(s) necessary for host recognition and targeting of ubiquitin-mediated selective autophagy to *M. tuberculosis*. We found previously that *M. tuberculosis* extracellular DNA (eDNA) is exposed to the host cytosol during macrophage infection, activating TBK1 to elicit the production of type I IFNs [38]. Although how eDNA is liberated and exposed during *M. tuberculosis*

infection is unknown, a strong body of literature supports the notion that eDNA plays important roles in normal bacterial physiology, most notably biofilm formation [39, 40]. Given the necessity of TBK1 in both autophagic targeting of *M. tuberculosis* and activation of type I IFNs in response to *M. tuberculosis* DNA [41], we sought to test if DNA sensing is necessary and sufficient to mediate autophagy recruitment during infection of macrophages.

We first explored whether transfection of purified double-stranded DNA (dsDNA) into the cytosol could trigger ubiquitin-mediated selective autophagy. Indeed, transfection of plasmid DNA into LC3-GFP BMDMs resulted in production of autophagic puncta to an extent similar to rapamycin treatment (Figure 2.4A), and induced processing of LC3 in an ATG5-dependent manner (Figure 4B). This is in agreement with recent studies showing that dsDNA viruses (HSV-1, HCMV) can induce robust LC3 lipidation [42, 43] and suggests that cytosolic dsDNA, in addition to activating transcriptional responses, is a potent inducer of autophagy.

Previous work showed that transfected dsDNA is not distributed heterogeneously within the cell, but instead mostly exists in discrete cytoplasmic foci [44]. We took advantage of this phenomenon to determine whether dsDNA induced a general, non-specific autophagic response in cells or whether the nucleic acid itself it was targeted for selective autophagy. We transfected Cy3-labeled dsDNA into GFP-LC3 RAW 264.7 cells and monitored DNA-LC3 colocalization. As seen in Figure 4C and 4D, Cy3-dsDNA appeared within LC3 positive vesicles during lipofection or electroporation of cells, but not in cells incubated with DNA in the absence of transfection reagents. Immunopreciptation experiments using biotinylated DNA resulted in the recovery of an

LC3-DNA protein complex (Figure 2.4E), suggesting that cytosolic DNA recruits LC3-positive autophagic vesicles after transfection. Furthermore, DNA also appeared within ATG12 and LAMP-1 positive vesicles (Figure 2.4F), suggesting that cytosolic DNA is targeted to autophagosomes that subsequently fuse with the lysosome. Transfection of either dsDNA species such as poly dG:dC, poly dA:dT, *E. coli* genomic DNA, and plasmid DNA resulted in robust induction of autophagy as well as targeting to autophagosomes, while ssDNA was not targeted (Figure 4C and S5A). These requirements for autophagy induction by DNA are identical to the immunostimulatory properties of cytosolic DNA [45]. Furthermore, dsRNA and ssRNA did not result in autophagic autophagosome formation or targeting (Figure 2.4C and Figure 2.12A), despite their ability to activate a similar immune response in host cells [46], showing that the induction of autophagy is specific to dsDNA.

Cytosolic DNA is directly targeted for autophagy via ubiquitin-mediated selective autophagy and STING

Because TBK1 kinase activity is stimulated by cytosolic DNA and the protein physically interacts with NDP52, we hypothesized that cytosolic DNA also activates ubiquitin-mediated selective autophagy. As shown in Figure 4F, ubiquitin, TBK1, and NDP52 all colocalized to DNA puncta by 4 h after transfection. GFP-LC3-positive dsDNA puncta also colocalized with ubiquitin, and both K48 and K63 linkages were observed (Figures 2.13A-D). Furthermore, knockdown of NDP52 resulted in reduced targeting of DNA into LC3 autophagosomes (Figure 2.4G), further suggesting that DNA is targeted to LC3 positive vesicles via ubiquitin-mediated selective autophagy.

STING is an essential adaptor protein that functions upstream of TBK1 in the interferon stimulatory DNA pathway [47]. STING colocalizes with LC3 during DNA stimulation [48] and is required for LC3 lipidiation in response to herpes virus DNA [43]. Thus, we next sought to determine if STING directly mediates ubiquitin–selective autophagy in response to cytosolic DNA. In contrast to wild-type BMDMs, *Sting*^{-/-} macrophages were unable to recruit ubiquitin, LC3, and NDP52 to transfected dsDNA (Figure 2.4H and 2.4I). Furthermore, direct activation of STING using either cyclic di-AMP and cyclic di-GMP [49] activated GFP-LC3 puncta formation to a similar extent to cytosolic DNA stimulation and rapamycin treatment (Figure 2.4A), suggesting that direct activation of STING is sufficient to induce autophagsome formation. Taken together, we conclude that activation of STING serves a critical role during the initial steps of ubiquitin-mediated autophagy of DNA.

Cytosolic DNA sensing mediates targeting of *M. tuberculosis* to autophagosomes

Because STING is activated within macrophages by *M. tuberculosis* [38], we hypothesized that mycobacterial DNA is the ligand that triggers ubiquitin-mediated selective autophagy of *M. tuberculosis* during infection. As shown in Figure 2.5A and 2.5B, *Sting*^{-/-} BMDMs displayed reduced ubiquitin-*M. tuberculosis* colocalization and were severely defective in targeting LC3 to bacteria. In addition, *M. tuberculosis* colocalization with NDP52 and phospho-TBK1 was undetectable during infection of *Sting*^{-/-} BMDMs (Figure 2.5C). Ubiquitin and LC3 localization to *M. tuberculosis* was normal in macrophages deficient for inflammasomes (*Asc1*^{-/-} and *Nalp3*^{-/-}, [50]), TLR signaling (*Myd88*^{-/-} *Trif*^{-/-}), or type I IFN signaling (*Irf3*^{-/-} *Irf7*^{-/-}, *Ifnar1*^{-/-}), indicating that

targeting is independent of other pathways activated by cytosolic nucleic acid (Figure 2.13). Taken together, our data suggest that STING is necessary for directing the formation of the ubiquitin signals that route *M. tuberculosis* to the ubiquitin-mediated selective autophagy pathway.

Host DNases affect autophagic targeting of *M. tuberculosis*

To further demonstrate the role of DNA in targeting *M. tuberculosis* to autophagosomes, we determined whether host DNases could modulate autophagic targeting of bacilli during infection. DNases such as TREX1 and DNASE IIb, have been shown to negatively regulate the innate immune response to cytosolic DNA [51, 52], and TREX1 negatively regulates the induction of type I IFN during *M. tuberculosis* infection [38]. Overexpression of TREX1 or DNASE IIb within macrophages greatly reduced co-localization of *M. tuberculosis* with ubiquitin (Figure 2.5D) and LC3 (Figure 2.5E) during infection. Furthermore, *M. tuberculosis* infection of *Trex1*^{-/-} BMDMs resulted in an increase in targeting of *M. tuberculosis* to these markers (Figures 2.5F and 2.5G). These data reveal an unprecedented role of host DNases in modulating selective autophagy and provides corroborative evidence that *M. tuberculosis* DNA serves as a molecular signal for selective autophagy.

Ubiquitin-mediated autophagy targets *M. tuberculosis* to the lysosome

Since autophagy has been implicated in acute *M. tuberculosis* restriction by macrophages [6], we sought to determine the fate of ubiquitinated bacteria marked for autophagy early after infection. We first asked whether ubiquitin and LC3-positive

bacteria are targeted to lysosomes by staining *M. tuberculosis*-infected macrophages with antibodies that recognize the lysosomal marker LAMP-1. During *M. tuberculosis* infection of *Atg5$^+$* BMDMs, approximately 30% of bacilli were positive for LAMP-1 at 6 h post-infection (Figures 2.6A and 2. 6B). In contrast, only 2-5% of bacilli colocalized with LAMP-1 during *M. tuberculosis* infection of *Atg5$^-$* macrophages. Importantly, macrophages deficient for TBK1 or STING also had severe defects in LAMP-1 colocalization to bacteria, indicating that DNA/ubiquitin-mediated targeting leads to delivery of *M. tuberculosis* to the lysosome (Figures 2.6A and 2.6B).

To test whether the differences in lysosomal targeting correlated with changes in bacterial survival, we infected BMDMs with wild-type *M. tuberculosis* and determined bacterial viability by enumerating colony forming units at 6 and 24 hours post-infection. Infection of BMDMs deficient for ATG5, STING, or TBK1 resulted in a 2- to 3-fold increase in bacterial survival relative to wild-type or control BMDMs (Figure 2.6C), and shRNA knockdown of NDP52 expression had similar effects (Figure 2.6D) on bacterial numbers. These data demonstrate that targeting of *M. tuberculosis* to the autophagy pathway is required for the cell-autonomous control of *M. tuberculosis* replication within macrophages. Moreover, since *M. tuberculosis* grows extremely slowly and very little replication occurs during the first 24 h of infection, this data suggests that the population of bacteria targeted by the ubiquitin-mediated autophagy pathway is specifically killed in the lysosome, whereas the non-targeted bacteria remain viable.

Autophagy is essential *in vivo* for control of *M. tuberculosis*

Because previous studies on the role of autophagy during *M. tuberculosis* infection have been performed using cultured macrophage cells [53], we sought to determine the contribution of autophagy in macrophages to host resistance *in vivo* using a mouse model of tuberculosis infection. To this end, we performed low-dose aerosol infections of $Atg5^-$ mice ($Atg5^{flox/flox}$-Lyz-*Cre*) and monitored both mouse survival and bacterial burdens within infected tissues. Surprisingly, $Atg5^-$ mice were extremely sensitive to *M. tuberculosis*, as all mutant mice succumbed to infection by four weeks post-infection, in contrast to $Atg5^+$ mice that displayed no overt signs of distress at this early time point (Figure 2.7A). In addition, the rate of *M. tuberculosis* replication was unchecked within $Atg5^-$ mice, which resulted in nearly a 1,000-fold increase in bacilli within the lungs and a 10-20 fold increase of bacilli within the spleen and liver at 21 days post-infection, relative to control mice (Figure 2.7B and 2.7C). The increased bacterial burden in $Atg5^-$ mice was accompanied by massive pulmonary abscesses that were obvious both by gross morphology of entire lungs and by staining of tissue sections (Figure 2.7D and 2.7E). Furthermore, lungs from $Atg5^-$ mice contained 5- to 10-fold higher levels of pro-inflammatory cytokines TNFα, IL-1α, IL-1β, and IL-6 within infected lung tissues (Figure 2.7F). In contrast, production of IFN-γ was unchanged between $Atg5^-$ and $Atg5^+$ infected mice (Figure 2.7F) suggesting that the defect in $Atg5^-$ mice was not simply due to a failure of T cells to produce this important cytokine. Collectively, this data demonstrates that ATG5-mediated autophagy in monocytes plays a major role in eliciting an effective innate immune response to *M. tuberculosis* infection *in vivo*.

Discussion

We have identified four critical steps in the pathway by which *M. tuberculosis* cells are recognized by host macrophages and targeted to autophagosomes. First, the bacterial ESX-1 secretion system initiates the interaction by permeabilizing the phagosomal membrane early after phagocytosis. Second, permeabilization exposes DNA on the surface of the bacteria that is recognized by components of the cytosolic DNA pathway, including STING, to initiate autophagy targeting. Third, a population of the engulfed bacteria become associated with, and surrounded by, host ubiquitin chains. Most of the labeled bacteria are associated with K63-linked chains but some K48 linkages are also detectable on a lower percentage of bacteria. Our finding that STING is necessary for ubiquitin colocalization of a subpopulation of bacteria suggests that distinct recognition events underlie *M. tuberculosis* targeting. Fourth, the ubiquitin LC3 binding autophagy adaptors, p62 and NDP52, are required to recruit autophagy components to create a phagophore surrounding the bacilli, a process that also requires the TBK1 kinase and ATG5. Once targeted to the ubiquitin-mediated autophagy pathway, bacilli-containing autophagosomes are matured via fusion with lysosomes to create autophagolysosomes. Delivery of this population of bacteria to the lysosome is responsible for limited bacterial killing by macrophages *ex vivo*, but the entire autophagy pathway in macrophages is a major determinant of host resistance to *M. tuberculosis* infection *in vivo*.

Given the modest effect of ATG5 on *M. tuberculosis* survival in macrophages, it may be surprising that the *Atg5⁻* mice are so profoundly susceptible to infection. Indeed, *Atg5⁻* mice succumb to infection with kinetics nearly identical to that of mice that completely lack an adaptive immune system or are missing key activators of macrophage

activation, such as IFN-γ [54]. However, it is becoming clear that autophagy plays a broader role in innate and adaptive immune responses than simply leading to direct killing of microbes in the lysosome. For example, autophagy enhances antigen presentation in dendritic cells [55] and negatively regulates inflammasome activation [15, 56, 57]. Indeed, the pronounced increase in inflammatory cytokines during infection of *Atg5⁻* mice, such as IL-1β , suggests that inflammasome signaling is augmented in the *Atg5⁻* mice during *M. tuberculosis* infection [50]. Therefore, while delivery of bacteria to the lysosome plays a direct role in acute bacterial restriction, autophagy may play a more pronounced role in overall control via non-cell autonomous effects on innate and specific immune responses.

In contrast to the major role of ATG5 in controlling *M. tuberculosis* infection, previous studies demonstrated that macrophages from *Atg5⁻* mice are capable of controlling BCG infection [15]. Our results suggest that the reason for the apparent dispensability of ATG5 during BCG infection is because the vaccine strain does not naturally induce the ubiquitin-mediated pathway due to a lack of ESX-1 secretion and the concomitant lack of membrane permeabilization. Importantly, reintroduction of ESX-1 secretion to BCG [22], or induction of general autophagy by administering rapamycin [55], increased the potency of vaccination, suggesting that incorporation of autophagy inducing elements may uniquely benefit vaccination strategies to prevent human tuberculosis. Similarly, mice lacking ATG5 in monocytes had a relatively minor defect in protection from infection with *L. monocytogenes* [15], especially compared to the dramatic effects with *M. tuberculosis*. In this case, it is probable that the ability of *L. monocytogenes* to evade autophagy by nucleating actin renders the bacteria insensitive to

the absence of autophagic machinery [58]. Moreover, it is likely that the ubiquitin-mediated autophagy pathway acts as an inducible mechanism to traffic intracellular pathogens that permeabilize membranes into lysosomes, whereas non-pathogens that do not perturb membranes traffic to lysosomes via the constitutive endosomal-lysosomal maturation pathway.

Ubiquitin appears to play multiple roles in innate immune defense. In addition to targeting intracellular bacteria to autophagy, recent results have demonstrated that peptides derived from the proteolysis of ubiquitin in the lysosome have anti-microbial properties [59, 60]. This raises the possibility that the ubiquitin on the surface of *M. tuberculosis* used to deliver bacteria to autophagy may also directly participate in bacterial killing once the complexes reach the lysosome.

It is curious that only one-third of intracellular bacteria are targeted by the ubiquitin pathway and colocalize with LC3. This observation is consistent, however, with classic EM studies of *M. tuberculosis* trafficking in macrophages which showed that although live *M. tuberculosis* bacilli were able to profoundly inhibit phagosome maturation to lysosomes, approximately a third of bacilli still trafficked to lysosomes [30]. It is likely that the fate of those lysosomal bacteria was mediated by autophagic targeting. Although we do not yet understand the mechanistic basis for the heterogeneous response, one possibility is that *M. tuberculosis* may employ an autophagy evasion strategy that prevents ubiquitination but is only partially effective. Similarly, though perhaps more appealing, is the possibility that cell-to-cell variations in ESX-1 secretion, and thus variations in membrane permeability from phagosome-to-phagosome, could account for the heterogeneity in autophagy targeting [61]. In either case,

heterogeneity of autophagic targeting may be important for successful infection by *M. tuberculosis*. For example, although bacilli that become targeted to lysosomes may be killed, the resultant increase in pro-inflammatory responses and elicitation of adaptive immune responses may promote and favor the persistence strategy of the bulk of the bacterial population. Alternatively, it is possible that the heterogeneity is due to host processes, for example there may be an exclusive interplay between bacterial targeting and membrane repair.

The findings that DNA is a bacterial-derived molecule recognized by host cells to target *M. tuberculosis* to autophagy, and that STING and TBK1 are required for this process, reveals a surprisingly broad connection between cytosolic DNA detection and innate immune responses to pathogens. Indeed, introduction of exogenous DNA into the cytosol of cells triggers three distinct yet interrelated responses: autophagy, cytokine signaling, and inflammasome activation [62, 63]. STING is a required factor for both autophagy and cytokine signaling and, either directly [49] or indirectly (via interactions with cytosolic DNA receptors) recognizes DNA and leads to ubiquitination and recruitment of both TBK1 and NDP52. It will be interesting to determine if other ubiquitin binding adaptors implicated in autophagy, including NBR1 and optineurin, are also important for this pathway [64, 65]. Although the molecular connections between DNA and ubiquitination remains unknown, STING itself is a plausible ubiquitinated target as it colocalizes to bacteria and is ubiquitinated during DNA stimulation [66].

It is likely that cytoplasmic DNA detection also targets other pathogens that access the cytosol to the autophagy pathway. Although it remains to be seen if autophagy targeting of other bacterial pathogens depends on DNA sensing and STING, it is

becoming clear that this same pathway is also operational to limit dsDNA virus infection which expose their genome during virion assembly in the cytoplasm [42, 43]. Furthermore, given the eubacterial origin of the mitochondrion, it is tempting to speculate that a signal for mitophagy may also be exposure of mitochondrial DNA on the surface of damaged organelles.

A common requirement of intracellular pathogens is the ability to penetrate host cell membranes in order to gain access to the cytosol. The mechanisms described here illustrate that it is the combination of pathogen molecule and spatial distribution of pattern recognition receptors that allow host cells to detect membrane puncture and discriminate pathogens from non-pathogens. It is thus a combination of ESX-1 secretion and DNA exposure that constitutes the "pattern of pathogenesis" recognized by host cells to mount innate responses against *M. tuberculosis* [67]. In addition to detection of microbial products, cells are also able to target autophagy to intracellular pathogens by directly detecting membrane permeabilization [68]. Such overlapping systems may be beneficial for different host cell types and as well to allow cells to detect virulent pathogens that do not expose stimulatory eDNA.

Materials and Methods

Mice and BMDMs

ATG5$^{flox/flox}$ mice were from N. Mizushima (Tokyo Medical and Dental University, Japan) [69] and *ATG5$^{flox/flox}$*-Lyz-*Cre* were a gift from H. Virgin (University of Washington) [15, 70]. Bone marrow-derived macrophages (BMDMs) were obtained from mouse femurs as previously described [61] and cultured in DMEM H-21

supplemented with 10% MCSF derived from 3T3-MCSF cells. BMDMs were obtained

from the following mouse strains: $MYD88^{-/-}/TRIF^{-/-}$ [71], $TREX1^{-/-}$ [52], $STING^{-/-}$ [72],

$TNFR1^{-/-}$ & $TBK1^{-/-}/TNFR1^{-/-}$ [73], $IFNAR1^{-/-}$ [74], $IRF3^{-/-}/IRF7^{-/-}$(G. Barton). BMDMs

from $ASC1^{-/-}$ and $NLRP3^{-/-}$ mice were a gift from D. Monack (Stanford U.),

Cell lines

RAW264.7 cells were purchased from ATCC (TIB-71) and cultured in DMEM-H21

containing 10% FBS. RAW264.7 cells stably expressing GFP-LC3 were generated by

electroporating the pROW2 plasmid (encoding CMV-GFP-LC3) into RAW264.7 cells

via the Amaxa nucleofactor kit V. Electroporated cells were selected on neomycin for 3

weeks and stable clones were isolated via FACS sorting for GFP positive cells.

Bacterial strains

The Erdman strain of *M. tuberculosis* was used as the wild-type strain and mutant

background strain for all *M. tuberculosis* experiments. The *M. tuberculosis* Δ*esat-6*,

Rv1506c::Tn, and *moeB1::Tn* strains were previously described [8, 32, 34]. BCG Pasteur

was a gift from W.R. Jacobs and was transformed with the cJSC49 cosmid, containing

the Erdman RD1 genomic locus. For generation of mCherry-expressing mycobacteria,

strains were transformed with the pMAN12 plasmid encoding mCherry under the control

of the *groEL1* promoter. LLO-expressing mycobacterium was previously described

(Manzanillo et al.). All strains were cultured in 7H9 media supplemented with 10%

OADC, 0.5% Glycerol, and 0.05% Tween-80.

Macrophage infection

For infections with mycobacteria, macrophages were infected as previously described [61] with some modifications. Briefly, mycobacteria cultures were washed twice with PBS, gently sonicated to disperse clumps, and resuspended in DMEM supplemented with 10% horse serum. Media was removed from cells, monolayers overlaid with the bacterial suspension, and centrifuged for 10 min at 1,000 RPM. Cells were washed twice in PBS and returned to macrophage media. For determination of CFUs, macrophage monolayers were lysed in 0.1% Triton-X 100 and plated on 7H10 agar plates.

Immunofluorescence microscopy

Indicated cells were infected as described above, and at the designated time points, cells were washed three times in PBS and fixed in 4% paraformaldehyde (PFA) for 20 min at room temperature (RT). The fixed cells were washed three times in PBS and permeabilized by incubating them in PBS containing 5% non-fat milk and 0.05% saponin (PBS-MS) (Calbiochem). Cover slips were incubated in primary antibody diluted in PBS-MS for 1 hour. The cover slips were then washed three times in PBS and incubated in secondary antibody. After two washes in PBS and two washes in deionized water, the cover slips were mounted onto glass slides using Prolong Gold antifade reagent (Molecular Probes). Images were acquired on a Zeiss Axiovert200M inverted microscope fitted with a Hamamatsu C4742-80-12AG digital camera controlled by the Axiovision software package version 4.6 (Carl Ziess MicroImaging, Inc.).

Antibodies

The following primary antibodies were used: mouse monocolonal antibodies against poly- and mono-conjugated-ubiquitin (Enzo Life Sciences), K63 and K48 ubiquitin (Milipore), Lamp-1 (BD Biosciences), Sting (Sigma), NDP52 (Novus Biologicals), and Rabbit polyclonal antibodies against phospho-TBK1 (Cell Signaling), Atg12 (Cell Signaling), and LC3B (Invitrogen). Secondary antibodies used were: Alexa 488-conjugated goat anti-rabbit and Alexa 488- and Alexa 350-conjugated goat anti-mouse IgG antiserium (Molecular Probes).

Colocalization of markers with mycobacteria and cytosolic DNA

To quantify the percentage of mycobacterium phagosomes or cytoslic DNA containing different cellular markers, infected cells were visualized directly by fluorescence microscopy. Using the Axiovision software package version 4.6, a series of images were captured including internalized bacteria and the cellular marker. Overlayed fluorescent images were analyzed by determining the number of mycobacterium phagosomes or cytosolic DNA that contained the corresponding marker. A minimum of one hundred phagosomes or DNA puncta were analyzed per cover slip for each treatment and designated post-infection time. Each experiment was completed in triplicate cover slips and expressed as an average. Mycobacterium phagosomes or cytosolic DNA was considered positive for the presence of a marker when they contained detectable amounts of the antibody/fluorescence signal.

Mouse infection

ATG5$^{flox/flox}$-Lyz-*Cre* and *ATG5$^{flox/flox}$* control mice were infected with *M. tuberculosis* (Erdman) via low-dose aerosol infection (~200 CFUs) as previously described [61]. Lungs, spleens, and liver were harvested, homogenized, and plated on 7H10 agar plates. In addition, lungs were sectioned and stained with hematoxylin/eosin or acid-fast staining at the Histology Core Laboratory of the Gladstone Institute. For survival experiments, infected mice were euthanized when they had lost 15% of their maximal body weight.

Cytokine measurements

Lungs were harvested from *M. tuberculosis* infected mice and homogenized in 3ml of PBS containing 0.005% Triton X-100 and protease inhibitor cocktail (Roche). Cytokines were measured using a Q-Plex Mouse Cytokine 16-Plex IR ELISA (Quansys Biosciences) and Quantikine Mouse IL-1β ELISA kit (R&D systems) per manufacturer's instructions.

Lentiviral cell lines

The mouse TRC1 lentiviral library [75], was obtained from Sigma and used to knockdown *p62* (*SQSTM1)* and *NDP52 (Calcoco2)* mRNA in RAW264.7 macrophage cells stably expressing GFP-LC3. RAW264.7-LC3 GFP cells expressing DNAses TREX1 and DNAse2 were generated by via lentiviral transduction using the pCMV-Lenti-puro system as previously described [76]. Knockdown efficiency was validated by RT-qPCR using gene specific-primers.

RNA isolation and qPCR

RNA was isolated and purified from macrophages using the Trizol micro-midi RNA isolation kit (Invitrogen) per manufacturer's instructions. For qPCR analysis, 1μg of RNA was reverse transcribed using the VILO cDNA synthesis kit (Invitrogen) and qPCR analysis was performed in triplicate, as previously described [61] using gene-specific primers.

Nucleic acid transfections

Poly(dA:dT), poly(dG:dC), poly(dA), poly(dT), and poly(I:C) were purchased from Sigma. c-di-AMP was purchased from Biolog. 5'ppp-dsRNA and dsRNA were purchased from Invivogen. Nucleic acids were labeled with Cy3 using the Label-It Cy3 kit (Mirius inc). Cells were transfected using Lipofectamine 2000 (Invitrogen) or were electroporated as previously described [49]. For microscopy analysis, 150,000 macrophages were transfected with 100ng of the indicated nucleic acids.

Biotin-DNA immunopreciptation

DNA was labeled with biotin using the Label-IT kit from Mirius biologicals. 20 million macrophages were transfected with either 20ug of dsDNA or 20ug of biotinylated dsDNA for 3 h and lysed in RIPA buffer. Biotintylated DNA was immunopreciptated using Strep-dynal beads (Invitrogen) according to manufacturer's instructions.

Statistics

Statistical analysis of data was performed using GraphPad Prism software (Graphpad; San Diego, CA). Two-tailed unpaired Student's t tests were used for analysis of

microscopy images and mycobacterium survival assays. The Kaplan-Meir method was

used to analyze mouse survival. Unless otherwise indicated, all experiments were

performed at least three times and presented as the mean ±SEM.

References

1.   Deretic, V. and B. Levine, *Autophagy, immunity, and microbial adaptations.* Cell
        Host Microbe, 2009. **5**(6): p. 527-49.

2.   Youle, R.J. and D.P. Narendra, *Mechanisms of mitophagy.* Nat Rev Mol Cell
        Biol, 2011. **12**(1): p. 9-14.

3.   Kudchodkar, S.B. and B. Levine, *Viruses and autophagy.* Rev Med Virol, 2009.
        19(6): p. 359-78.

4.   Thurston, T.L., et al., *The TBK1 adaptor and autophagy receptor NDP52 restricts
        the proliferation of ubiquitin-coated bacteria.* Nat Immunol, 2009. **10**(11): p.
        1215-21.

5.   Zheng, Y.T., et al., *The adaptor protein p62/SQSTM1 targets invading bacteria to
        the autophagy pathway.* J Immunol, 2009. **183**(9): p. 5909-16.

6.   Gutierrez, M.G., et al., *Autophagy is a defense mechanism inhibiting BCG and
        Mycobacterium tuberculosis survival in infected macrophages.* Cell, 2004.
        119(6): p. 753-66.

7.   Singh, S.B., et al., *Human IRGM induces autophagy to eliminate intracellular
        mycobacteria.* Science, 2006. **313**(5792): p. 1438-41.

8.   Stanley, S.A., et al., *Acute infection and macrophage subversion by
        Mycobacterium tuberculosis require a specialized secretion system.* Proc Natl
        Acad Sci U S A, 2003. **100**(22): p. 13001-6.

9.   Cole, S.T., et al., *Deciphering the biology of Mycobacterium tuberculosis from
        the complete genome sequence.* Nature, 1998. **393**(6685): p. 537-44.

10.   Pym, A.S., et al., *Loss of RD1 contributed to the attenuation of the live
        tuberculosis vaccines Mycobacterium bovis BCG and Mycobacterium microti.*
        Mol Microbiol, 2002. **46**(3): p. 709-17.

11.   Mahairas, G.G., et al., *Molecular analysis of genetic differences between
        Mycobacterium bovis BCG and virulent M. bovis.* J Bacteriol, 1996. **178**(5): p.
        1274-82.

12. Hsu, T., et al., *The primary mechanism of attenuation of bacillus Calmette-Guerin is a loss of secreted lytic function required for invasion of lung interstitial tissue.* Proc Natl Acad Sci U S A, 2003. **100**(21): p. 12420-5.

13. Guinn, K.M., et al., *Individual RD1-region genes are required for export of ESAT-6/CFP-10 and for virulence of Mycobacterium tuberculosis.* Mol Microbiol, 2004. **51**(2): p. 359-70.

14. Wong, K.W. and W.R. Jacobs, Jr., *Critical role for NLRP3 in necrotic death triggered by Mycobacterium tuberculosis.* Cell Microbiol, 2011. **13**(9): p. 1371-84.

15. Zhao, Z., et al., *Autophagosome-independent essential function for the autophagy protein Atg5 in cellular immunity to intracellular pathogens.* Cell Host Microbe, 2008. **4**(5): p. 458-69.

16. Smith, J., et al., *Evidence for pore formation in host cell membranes by ESX-1-secreted ESAT-6 and its role in Mycobacterium marinum escape from the vacuole.* Infect Immun, 2008. **76**(12): p. 5478-87.

17. Collins, C.A., et al., *Atg5-independent sequestration of ubiquitinated mycobacteria.* PLoS Pathog, 2009. **5**(5): p. e1000430.

18. Lerena, M.C. and M.I. Colombo, *Mycobacterium marinum induces a marked LC3 recruitment to its containing phagosome that depends on a functional ESX-1 secretion system.* Cell Microbiol, 2011.

19. van der Wel, N., et al., *M. tuberculosis and M. leprae translocate from the phagolysosome to the cytosol in myeloid cells.* Cell, 2007. **129**(7): p. 1287-98.

20. Yuk, J.M., et al., *Vitamin D3 induces autophagy in human monocytes/macrophages via cathelicidin.* Cell Host Microbe, 2009. **6**(3): p. 231-43.

21. Kumar, D., et al., *Genome-wide analysis of the host intracellular network that regulates survival of Mycobacterium tuberculosis.* Cell, 2010. **140**(5): p. 731-43.

22. Pym, A.S., et al., *Recombinant BCG exporting ESAT-6 confers enhanced protection against tuberculosis.* Nat Med, 2003. **9**(5): p. 533-9.

23. de Jonge, M.I., et al., *ESAT-6 from Mycobacterium tuberculosis dissociates from its putative chaperone CFP-10 under acidic conditions and exhibits membrane-lysing activity.* J Bacteriol, 2007.

24. Kinhikar, A.G., et al., *Potential role for ESAT6 in dissemination of M. tuberculosis via human lung epithelial cells.* Mol Microbiol, 2010. **75**(1): p. 92-106.

25.   Bermudez, L.E., et al., *The efficiency of the translocation of Mycobacterium tuberculosis across a bilayer of epithelial and endothelial cells as a model of the alveolar wall is a consequence of transport within mononuclear phagocytes and invasion of alveolar epithelial cells.* Infect Immun, 2002. **70**(1): p. 140-6.

26.   Stamm, L.M., et al., *Mycobacterium marinum escapes from phagosomes and is propelled by actin-based motility.* J Exp Med, 2003. **198**(9): p. 1361-8.

27.   Py, B.F., M.M. Lipinski, and J. Yuan, *Autophagy limits Listeria monocytogenes intracellular growth in the early phase of primary infection.* Autophagy, 2007. **3**(2): p. 117-25.

28.   Birmingham, C.L., et al., *Listeria monocytogenes evades killing by autophagy during colonization of host cells.* Autophagy, 2007. **3**(5): p. 442-51.

29.   Singh, R., A. Jamieson, and P. Cresswell, *GILT is a critical host factor for Listeria monocytogenes infection.* Nature, 2008. **455**(7217): p. 1244-7.

30.   Armstrong, J.A. and P.D. Hart, *Response of cultured macrophages to mycobacterium tuberculosis, with observations on fusion of lysosomes with phagosomes.* Journal of Experimental Medicine, 1971. **134**(3): p. 713-740.

31.   Tan, T., et al., *The ESAT-6/CFP-10 secretion system of Mycobacterium marinum modulates phagosome maturation.* Cellular Microbiology, 2006. **8**(9): p. 1417-1429.

32.   MacGurn, J.A. and J.S. Cox, *A genetic screen for Mycobacterium tuberculosis mutants defective for phagosome maturation arrest identifies components of the ESX-1 secretion system.* Infect Immun, 2007. **75**(6): p. 2668-78.

33.   Sturgill-Koszycki, S., U.E. Schaible, and D.G. Russell, *Mycobacterium-containing phagosomes are accessible to early endosomes and reflect a transitional state in normal phagosome biogenesis.* EMBO Journal, 1996. **15**(24): p. 6960-8.

34.   Brodin, P., et al., *High content phenotypic cell-based visual screen identifies Mycobacterium tuberculosis acyltrehalose-containing glycolipids involved in phagosome remodeling.* PLoS Pathog, 2010. **6**(9): p. e1001100.

35.   Cemma, M., P.K. Kim, and J.H. Brumell, *The ubiquitin-binding adaptor proteins p62/SQSTM1 and NDP52 are recruited independently to bacteria-associated microdomains to target Salmonella to the autophagy pathway.* Autophagy, 2011. **7**(3): p. 22-26.

36.   Ryzhakov, G. and F. Randow, *SINTBAD, a novel component of innate antiviral immunity, shares a TBK1-binding domain with NAP1 and TANK.* EMBO J, 2007. **26**(13): p. 3180-90.

37.   Wild, P., et al., *Phosphorylation of the Autophagy Receptor Optineurin Restricts Salmonella Growth.* Science, 2011.

38.   Manzanillo, P., et al., *Mycobacterium tuberculosis activates the DNA-dependent cytosolic surveillance pathway within macrophages.* Cell Host & Microbe, 2011. **In Press**.

39.   Whitchurch, C.B., et al., *Extracellular DNA required for bacterial biofilm formation.* Science, 2002. **295**(5559): p. 1487.

40.   Kuehn, M.J. and N.C. Kesty, *Bacterial outer membrane vesicles and the host-pathogen interaction.* Genes Dev, 2005. **19**(22): p. 2645-55.

41.   Stanley, S.A., et al., *The Type I IFN response to infection with Mycobacterium tuberculosis requires ESX-1-mediated secretion and contributes to pathogenesis.* J Immunol, 2007. **178**(5): p. 3143-52.

42.   McFarlane, S., et al., *Early induction of autophagy in human fibroblasts after infection with human cytomegalovirus or herpes simplex virus 1.* J Virol, 2011. **85**(9): p. 4212-21.

43.   Rasmussen, S.B., et al., *Activation of autophagy by alpha-herpesviruses in myeloid cells is mediated by cytoplasmic viral DNA through a mechanism dependent on stimulator of IFN genes.* J Immunol, 2011. **187**(10): p. 5268-76.

44.   Hagstrom, J.E., et al., *Nuclear import of DNA in digitonin-permeabilized cells.* J Cell Sci, 1997. **110 (Pt 18)**: p. 2323-31.

45.   Stetson, D.B. and R. Medzhitov, *Recognition of cytosolic DNA activates an IRF3-dependent innate immune response.* Immunity, 2006. **24**(1): p. 93-103.

46.   Takeuchi, O. and S. Akira, *Pattern recognition receptors and inflammation.* Cell, 2010. **140**(6): p. 805-20.

47.   Barber, G.N., *STING-dependent signaling.* Nat Immunol, 2011. **12**(10): p. 929-30.

48.   Saitoh, T., et al., *Atg9a controls dsDNA-driven dynamic translocation of STING and the innate immune response.* Proc Natl Acad Sci U S A, 2009. **106**(49): p. 20842-6.

49.   Burdette, D.L., et al., *STING is a direct innate immune sensor of cyclic di-GMP.* Nature, 2011. **478**(7370): p. 515-8.

50.   Shi, C.S., et al., *Activation of autophagy by inflammatory signals limits IL-1beta production by targeting ubiquitinated inflammasomes for destruction.* Nat Immunol, 2012. **13**(3): p. 255-63.

51.   Okabe, Y., T. Sano, and S. Nagata, *Regulation of the innate immune response by threonine-phosphatase of Eyes absent.* Nature, 2009. **460**(7254): p. 520-4.

52.   Stetson, D.B., et al., *Trex1 prevents cell-intrinsic initiation of autoimmunity.* Cell, 2008. **134**(4): p. 587-98.

53.   Deretic, V., et al., *Autophagy in immunity against mycobacterium tuberculosis: a model system to dissect immunological roles of autophagy.* Curr Top Microbiol Immunol, 2009. **335**: p. 169-88.

54.   MacMicking, J.D., G.A. Taylor, and J.D. McKinney, *Immune control of tuberculosis by IFN-gamma-inducible LRG-47.* Science, 2003. **302**(5645): p. 654-9.

55.   Jagannath, C., et al., *Autophagy enhances the efficacy of BCG vaccine by increasing peptide presentation in mouse dendritic cells.* Nat Med, 2009. **15**(3): p. 267-76.

56.   Nakahira, K., et al., *Autophagy proteins regulate innate immune responses by inhibiting the release of mitochondrial DNA mediated by the NALP3 inflammasome.* Nat Immunol, 2011. **12**(3): p. 222-30.

57.   Saitoh, T., et al., *Loss of the autophagy protein Atg16L1 enhances endotoxin-induced IL-1beta production.* Nature, 2008. **456**(7219): p. 264-8.

58.   Yoshikawa, Y., et al., *Listeria monocytogenes ActA-mediated escape from autophagic recognition.* Nat Cell Biol, 2009. **11**(10): p. 1233-40.

59.   Ponpuak, M., et al., *Delivery of cytosolic components by autophagic adaptor protein p62 endows autophagosomes with unique antimicrobial properties.* Immunity, 2010. **32**(3): p. 329-41.

60.   Alonso, S., et al., *Lysosomal killing of Mycobacterium mediated by ubiquitin-derived peptides is enhanced by autophagy.* Proc Natl Acad Sci U S A, 2007. **104**(14): p. 6031-6.

61.   Ohol, Y.M., et al., *Mycobacterium tuberculosis MycP1 Protease Plays a Dual Role in Regulation of ESX-1 Secretion and Virulence.* Cell Host Microbe, 2010. **7**(3): p. 210-220.

62.   Hornung, V., et al., *AIM2 recognizes cytosolic dsDNA and forms a caspase-1-activating inflammasome with ASC.* Nature, 2009. **458**(7237): p. 514-8.

63.   Roberts, T.L., et al., *HIN-200 proteins regulate caspase activation in response to foreign cytoplasmic DNA.* Science, 2009. **323**(5917): p. 1057-60.

64.   Wild, P., et al., *Phosphorylation of the autophagy receptor optineurin restricts Salmonella growth.* Science, 2011. **333**(6039): p. 228-33.

65.   Kirkin, V., et al., *A role for NBR1 in autophagosomal degradation of ubiquitinated substrates.* Mol Cell, 2009. **33**(4): p. 505-16.

66.   Tsuchida, T., et al., *The ubiquitin ligase TRIM56 regulates innate immune responses to intracellular double-stranded DNA.* Immunity, 2010. **33**(5): p. 765-76.

67.   Vance, R.E., R.R. Isberg, and D.A. Portnoy, *Patterns of pathogenesis: discrimination of pathogenic and nonpathogenic microbes by the innate immune system.* Cell Host Microbe, 2009. **6**(1): p. 10-21.

68.   Thurston, T.L., et al., *Galectin 8 targets damaged vesicles for autophagy to defend cells against bacterial invasion.* Nature, 2012.

69.   Kuma, A., et al., *The role of autophagy during the early neonatal starvation period.* Nature, 2004. **432**(7020): p. 1032-6.

70.   Hara, T., et al., *Suppression of basal autophagy in neural cells causes neurodegenerative disease in mice.* Nature, 2006. **441**(7095): p. 885-9.

71.   Barbalat, R., et al., *Toll-like receptor 2 on inflammatory monocytes induces type I interferon in response to viral but not bacterial ligands.* Nat Immunol, 2009. **10**(11): p. 1200-7.

72.   Ishikawa, H., Z. Ma, and G.N. Barber, *STING regulates intracellular DNA-mediated, type I interferon-dependent innate immunity.* Nature, 2009. **461**(7265): p. 788-92.

73.   Ishii, K.J., et al., *TANK-binding kinase-1 delineates innate and adaptive immune responses to DNA vaccines.* Nature, 2008. **451**(7179): p. 725-9.

74.   Takaoka, A., et al., *DAI (DLM-1/ZBP1) is a cytosolic DNA sensor and an activator of innate immune response.* Nature, 2007. **448**(7152): p. 501-5.

75.   Moffat, J., et al., *A lentiviral RNAi library for human and mouse genes applied to an arrayed viral high-content screen.* Cell, 2006. **124**(6): p. 1283-98.

76.   Campeau, E., et al., *A versatile viral system for expression and depletion of proteins in mammalian cells.* PLoS One, 2009. **4**(8): p. e6529.

Figure 2.1 *M. tuberculosis* **targeting to autophagosomes requires phagosomal permeabilization via ESX-1.**

(A) Fluorescence images of GFP-LC3 BMDMs (green) infected for 4 hours with mCherry-expressing wild-type or Δ*esat-6 M. tuberculosis* (red).

(B) Quantitative analysis of GFP-LC3 colocalization with wild-type and Δesat-6 *M. tuberculosis* at indicated times after infection. Results are the means ± SEM of three independent experiments.

(C) Western blot analysis of LC3 and actin (loading control) of BMDMs infected for 4 hours with wild-type *M. tuberculosis*.

(D) Fluorescence images of BMDMs infected for 4 hours with mCherry-expressing wild-type or Δesat-6 M. tuberculosis (red) and immunostained with anti-ATG12 (green).

(E) Quantitative analysis of colocalization with ATG12 at 4 hours post-infection. Results are the means ± SEM of three independent experiments.

(F) Fluorescence images of RAW 264.7 cells stably expressing GFP-LC3 (green) infected for 6 hours with either mCherry-expressing BCG or BCG complemented with RD1 (red).

(G) Quantitative analysis of GFP-LC3 colocalization with wild-type *M. tuberculosis*, BCG or BCG complemented with RD1 at 6 hours post-infection. Results are the means ± SEM of three independent experiments. (n=3 per group, *P < 0.005)

(H) Fluorescence images of GFP-LC3 RAW 264.7 cells (green) infected with the Δ*esat-6 M. tuberculosis* (red) or Δ*esat-6 M. tuberculosis* expressing listeriolysin-O (LLO) (red). (n=3 per group, *P < 0.005)

(I) Quantitative analysis of GFP-LC3 colocalization with wild-type *M. tuberculosis*, Δ*esat-6 M. tuberculosis*, and Δ*esat*-6 *M. tuberculosis* expressing LLO. Results are the means ± SEM of three independent experiments. (n=3 per group, *P < 0.005)

(J) Quantitative analysis of GFP-LC3 colocalization with wild-type *M. marinum*, ΔRD1 *M. marinum*, and ΔRD1 *M. marinum* expressing LLO. Results are the means ± SEM of three independent experiments. (n=3 per group, *P < 0.005)

(K) Fluorescence images of GFP-LC3 RAW 264.7 cells (green) infected for 6 hours with *Rv1596::Tn*, *moaB::Tn*, and Δ*esat-6 M. tuberculosis* (red).

(L) Quantitative analysis of GFP-LC3 colocalization with wild-type, Δ*esat-6*, Rv1596*::Tn*, and moaB*::Tn M. tuberculosis.* Results are the means ± SEM of three independent experiments.

Figure 2.1

Figure 2.1

G

H

I

M. tuberculosis

J

M. marinum

K

L
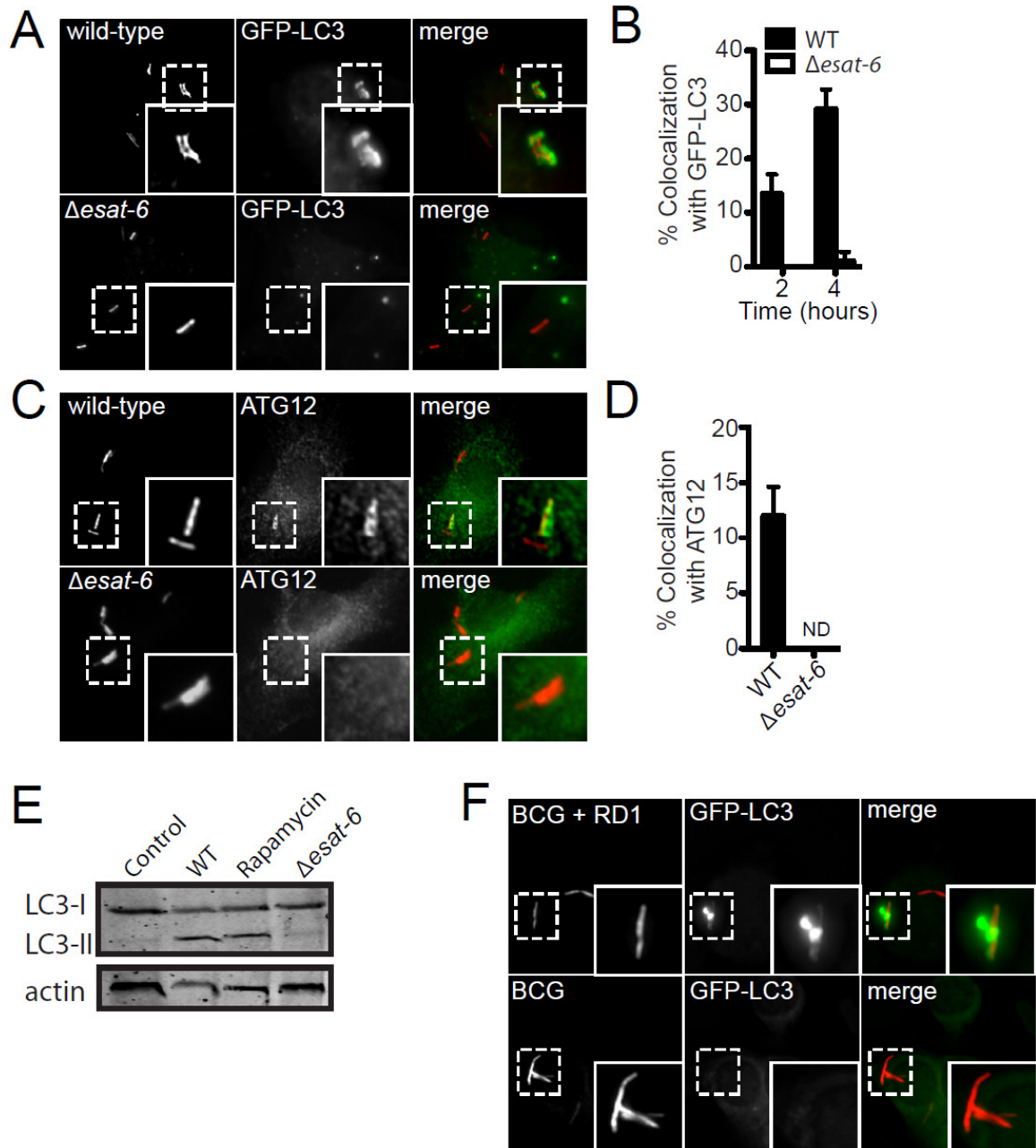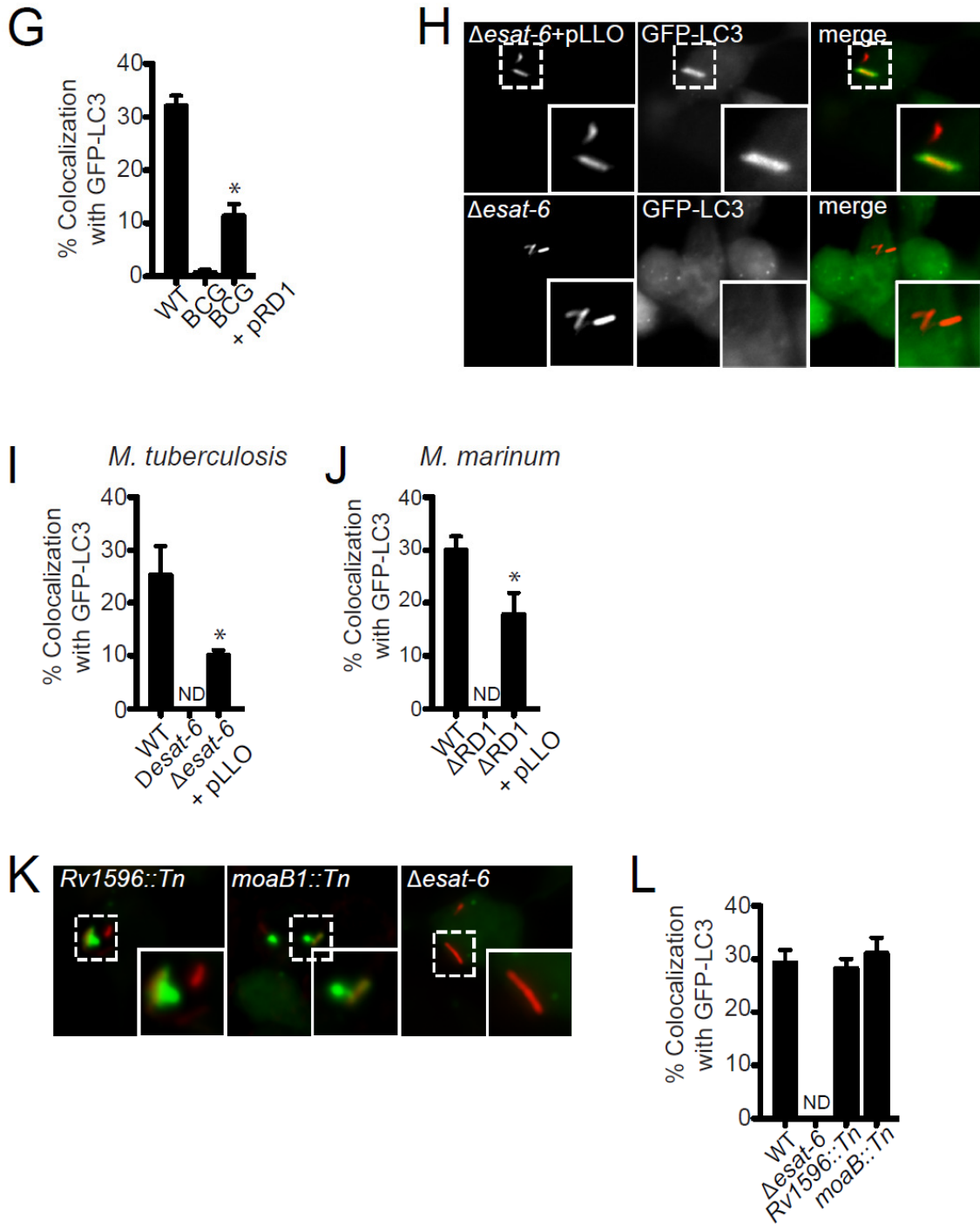
Figure 2.2 The autophagy receptors p62 and NDP52 and the kinase TBK1 are required for efficient delivery of *M. tuberculosis* to autophagosomes.

(A) Fluorescence images of BMDMs infected for 4 hours with mCherry-expressing wild-type or Δesat-6 M. tuberculosis (red) and immunostained with anti-p62 (green).

(B) Quantitative analysis of colocalization with p62 at 4 hours post-infection. Results are the means ± SEM of three independent experiments.

(C) Fluorescence images of BMDMs infected for 4 hours with mCherry-expressing wild-type or Δesat-6 M. tuberculosis (red) and immunostained with anti-NDP52 (green).

(D) Quantitative analysis of colocalization with NDP52 at 4 hours post-infection. Results are the means ± SEM of three independent experiments.

(E) Fluorescence images of BMDMs infected with wild-type M. tuberculosis (blue) for 4 hours and immunostained with anti-LC3 (green), anti-p62 (red) or anti-NDP52 (red).

(F) Quantitative analysis of M. tuberculosis colocalization with p62/NDP52 and LC3 at 4 hours post-infection. Results are the means ± SEM of three independent experiments.

(G) Quantitative analysis of GFP-LC3 colocalization with wild-type M. tuberculosis after shRNA knockdown of p62 or NDP52 in GFP-LC3 RAW 264.7 cells. Results are the means ± SEM of three independent experiments. Data is expressed as a percentage relative to control (scrambled shRNA) knockdown cells. (n=3 per group, $*P < 0.006$)

(H) Fluorescence images of BMDMs infected with either mCherry-expressing wild-type or Δesat-6 M. tuberculosis (red) for 4 hours and immunostained with anti-phospho-TBK1 (red).

(I) Quantitative analysis of M. tuberculosis colocalization with phospho-TBK1 and LC3 at 4 hours post-infection. Results are the means ± SEM of three independent experiments.

(J) Fluorescence images of BMDMs infected for 4 hours with mCherry-expressing wild-type M. tuberculosis (blue) and immunostained with anti-LC3 (green), and anti-phospho-TBK1 (red). (n=3 per group, *P < 0.01)

(K) Quantitative analysis of M. tuberculosis colocalization with TBK1 and LC3 at 4 hours post-infection. Results are the means ± SEM of three independent experiments.

(L) Quantitative analysis of BMDMs from $Tbk1^{+/+}$ and $Tbk1^{-/-}$ mice infected with wild-type M. tuberculosis for 4 hours and immunostained with anti-LC3 antibodies. Results are the means ± SEM of three independent experiments.

Figure 2.2
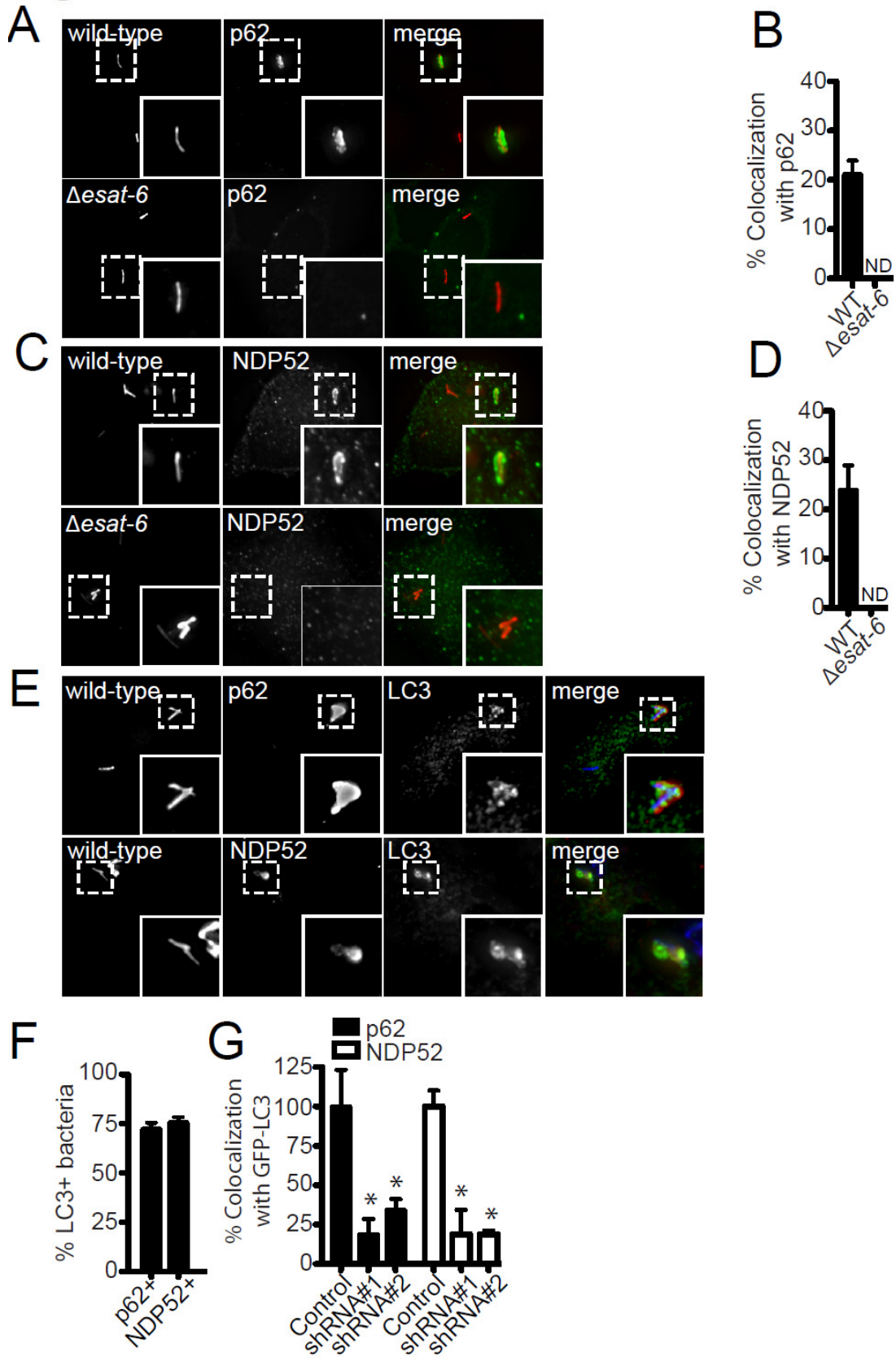
Figure 2.2
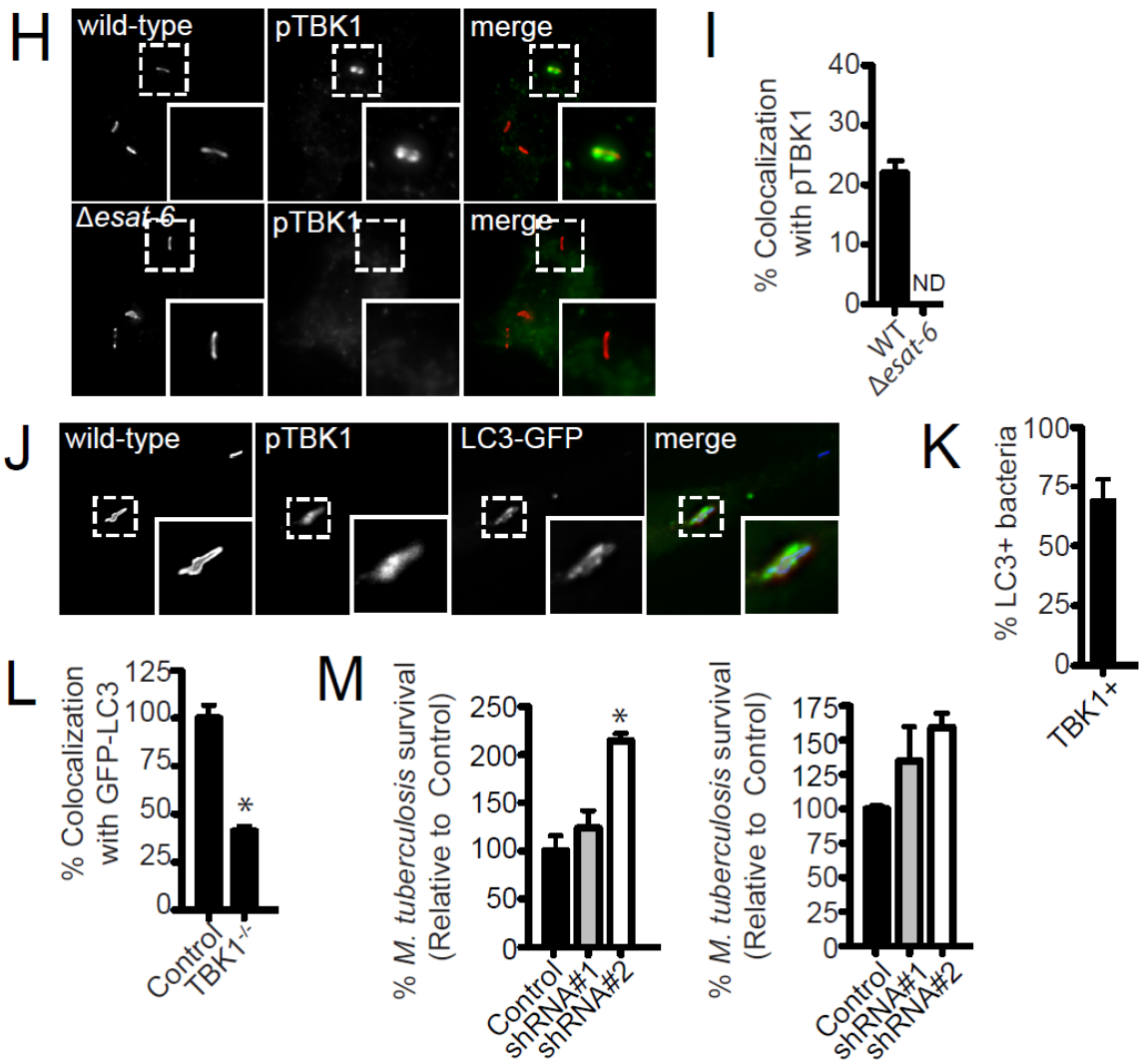
Figure 2.3 Mycobacterial ESX-1 system is required for ubiquitin colocalization.

(A) Fluorescence images of BMDMs infected for 4 hours with mCherry-expressing wild-type or Δesat-6 M. tuberculosis (red) and immunostained with anti-ubiquitin (green).

(B) Quantitative analysis of ubiquitin and LC3 colocalization with wild-type or Δesat-6 M. tuberculosis at indicated times post-infection. Results are the means ± SEM of three independent experiments.

(C) Fluorescence images of BMDMs infected for 4 hours with mCherry-expressing wild-type M. tuberculosis (blue) and immunostained with anti-LC3 (green), and anti-ubiquitin (red).

(D) Quantitative analysis of M. tuberculosis colocalization with ubiquitin and LC3 at 4 hours post-infection. Results are the means ± SEM of three independent experiments.

(E) Fluorescence images of BMDMs infected with mCherry-expressing wild-type *M. tuberculosis* and immunostained with anti-K63 and anti-K48 ubiquitin (green).

(F) Quantitative analysis of K63 and K48 ubiquitin colocalization in BMDMs infected with wild-type M. tuberculosis at 4 hours post-infection. Results are the means ± SEM of three independent experiments.

Figure 2.3

E wild-type | K63 ubiquitin | merge

wild-type | K48 ubiquitin | merge

F

% Colocalization with marker

25
20
15
10
5
0

K63   K48

Ubiquitin linkage
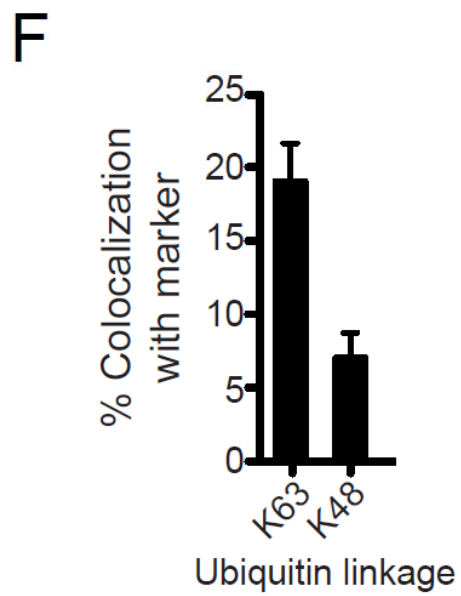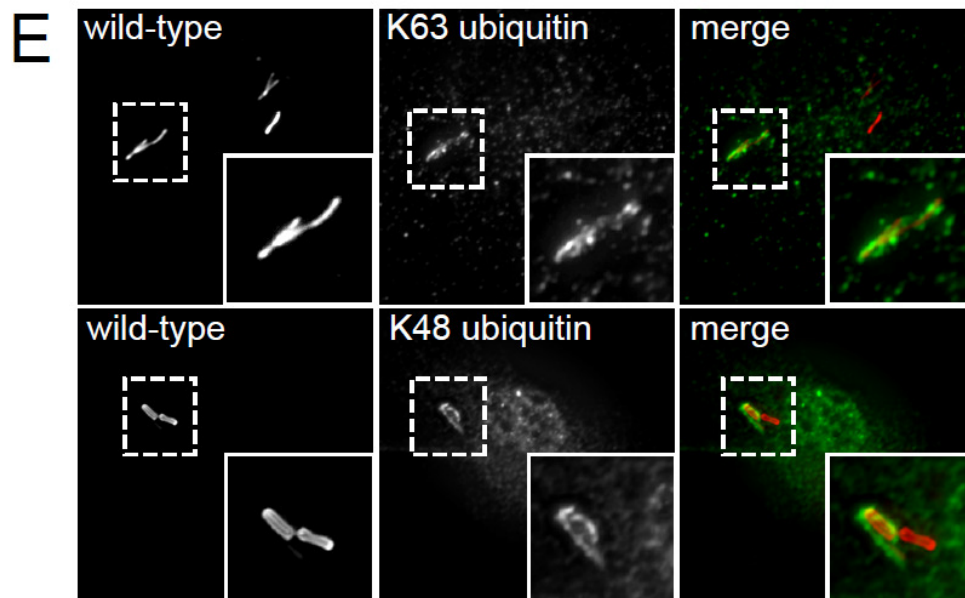
Figure 2.4 Cytosolic DNA is targeted by ubiquitin-mediated selective autophagy requires NDP52 and STING.

(A) Fluorescence images of GFP-LC3 RAW 264.7 cells (green) at 4 hours post-transfection with lipofectamine alone (control), plasmid DNA, cyclic di-AMP, cyclic di-GMP, or treated with rapamycin.

(B) Western blot analysis of LC3 in *Atg5*$^+$ and *Atg5*$^-$ BMDMs transfected with DNA for 3 hours.

(C) Fluorescence images of GFP-LC3 RAW 264.7 cells at 4 hours post-transfection with Cy3-labelled nucleic acid. Plasmid DNA was introduced by either lipofection (Plasmid-lipo) or by electroporation (Plasmid-electro), and all the other nucleic acid species were introduced by lipofection. Cells were also treated with lipofectamine reagent alone (Lipo) or DNA without transfection reagent (DNA only).

(D) Quantitative analysis of Cy3-labelled plasmid DNA with GFP-LC3 RAW 264.7 at 4 hours post-transfection. Results are the means ± SEM of three independent experiments.

(E) Western blot analysis of LC3 after streptavidin immunoprecipitation of cell lysates 4 hours post-transfection of dsDNA or biotintylated dsDNA.

(F) Fluorescence images of BMDMs transfected with Cy3-labelled plasmid DNA (red) and immunostained with anti-ATG12, anti-ubiquitin, anti-LAMP-1, anti-NDP52, or anti-phospho-TBK1 (green).

(G) Quantitative analysis of GFP-LC3 colocalization with Cy3-labelled plasmid DNA at 4 hours post-transfection after shRNA knockdown NDP52 in GFP-LC3 RAW 264.7 cells. Results are the means ± SEM of three independent experiments. Data is expressed as a percentage relative to control knockdown cells. (n=3 per group, *P < 0.005)

(H) Fluorescence images of wild-type and STING-deficient BMDMs at 4 hours post-transfection with Cy3-labelled plasmid DNA (red) and immunostained with anti-ubiquitin or anti-LC3.

(I) Quantitative analysis of ubiquitin, NDP52, and LC3 colocalization with Cy3-labelled plasmid DNA at 4 hours post-transfection in wild-type and STING-deficient BMDMs. Results are the means ± SEM of three independent experiments. Data is expressed as a percentage relative to control knockdown cells. (n=3 per group, $*P < 0.005$)

Figure 2.4
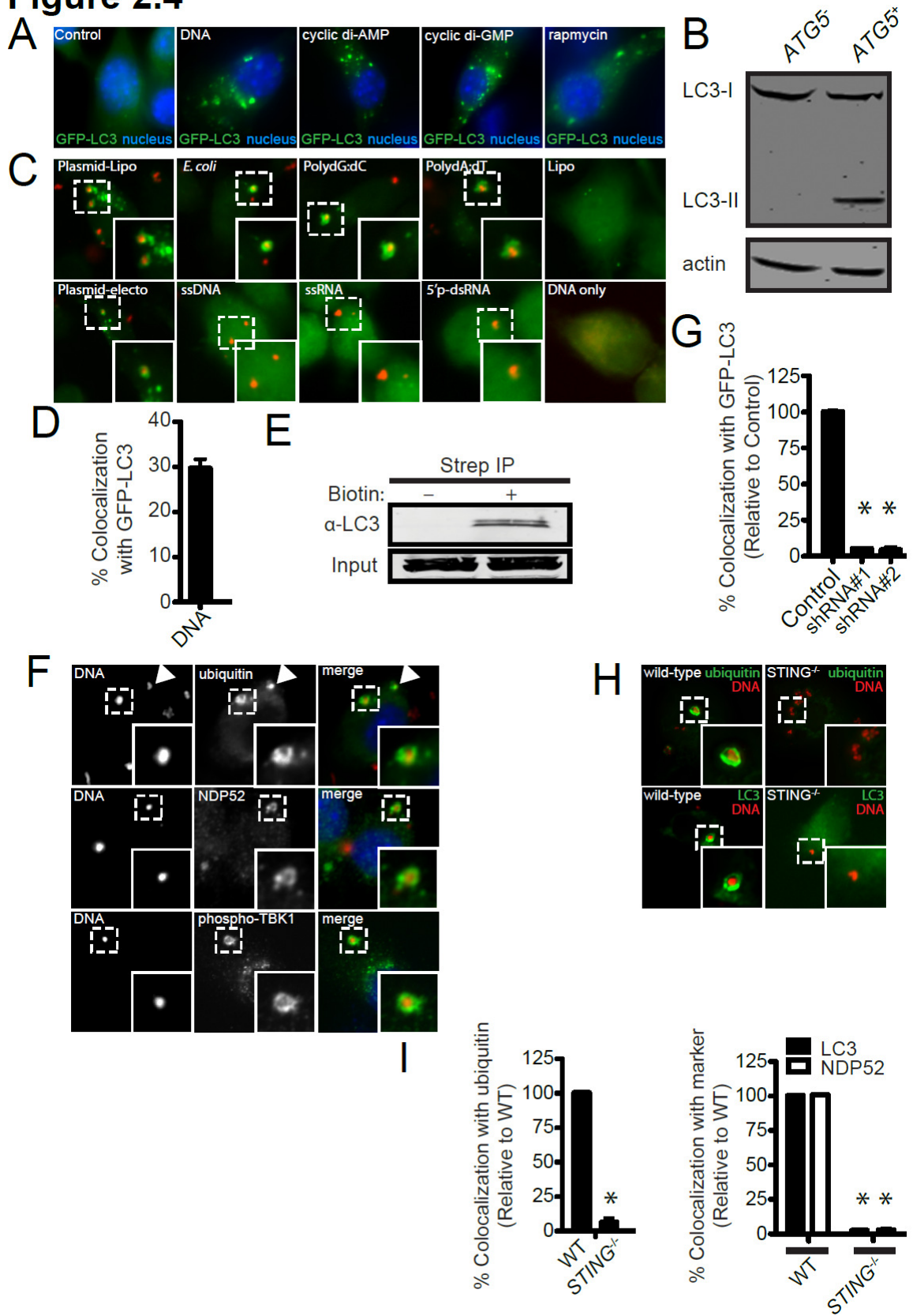
Figure 2.5 STING and cytosolic DNases modulate autophagic targeting of *M.*

tuberculosis

(A) Quantitative analysis of ubiquitin colocalization with wild-type M. tuberculosis at 4

hours post-infection in wild-type or STING-deficient BMDMs. Results are the means ±

SEM of three independent experiments. Data is expressed as the percentage of ubiquitin

positive cells relative to wild-type BMDMs. (n=3 per group, *P < 0.003)

(B) Quantitative analysis of LC3 colocalization with wild-type M. tuberculosis at 4 hours

post-infection in wild-type or STING-deficient BMDMs. Results are the means ± SEM of

three independent experiments. Data is expressed as the percentage of LC3 positive cells
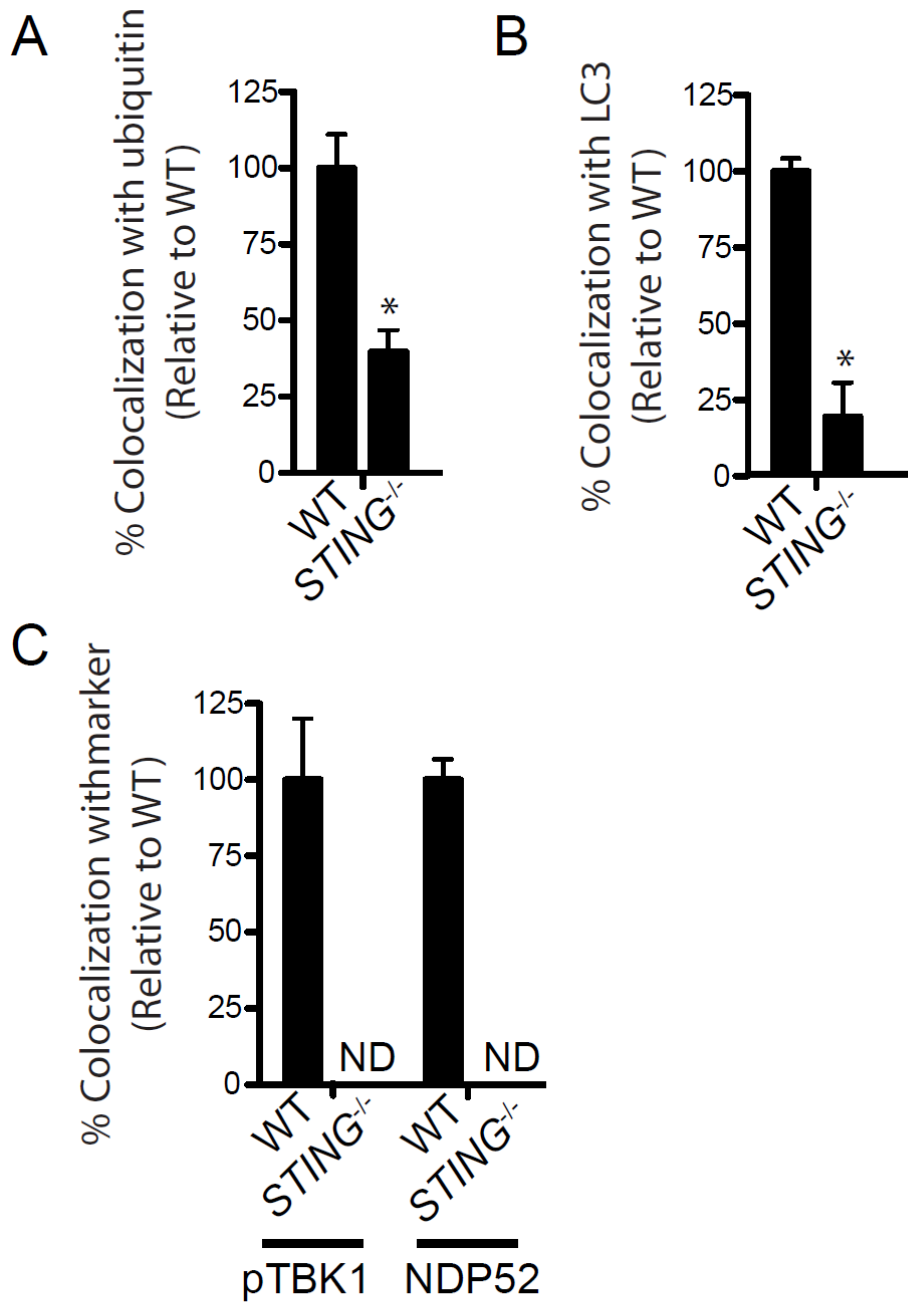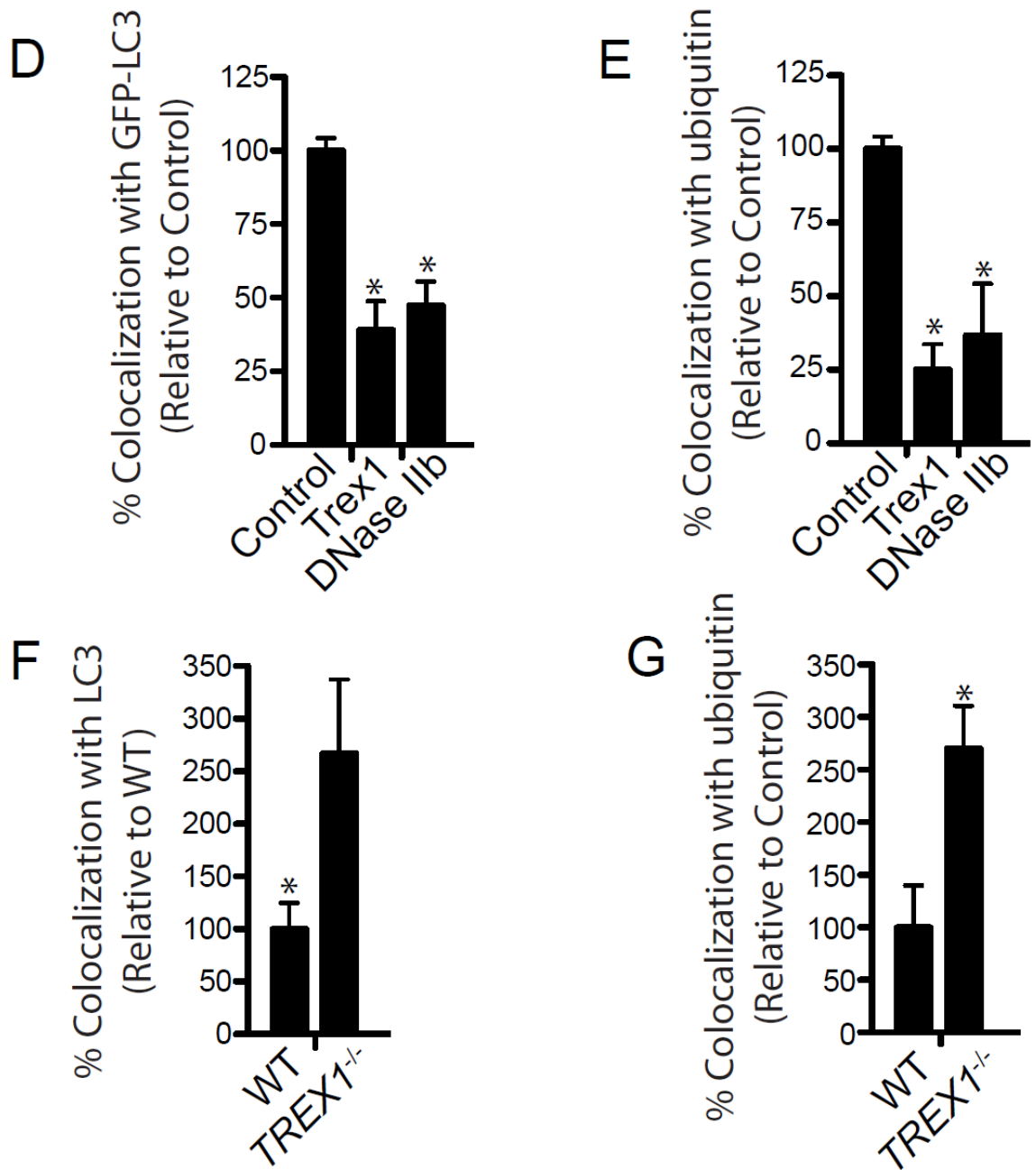
relative to wild-type BMDMs. (n=3 per group, *P < 0.003)

(C) Quantitative analysis of phospho-TBK1 and NDP52 colocalization with wild-type M.

tuberculosis at 4 hours post-infection in wild-type or STING-deficient BMDMs. Results

are the means ± SEM of three independent experiments. Data is expressed as the

percentage of marker positive cells relative to wild-type BMDMs.

(D) Quantitative analysis of ubiquitin colocalization with wild-type M. tuberculosis at 4

hours post-infection in RAW cells 264.7 stably overexpressing TREX1 and DNASE IIb.

Results are the means ± SEM of three independent experiments. Data is expressed as the

percentage of ubiquitin positive cells relative to control (vector only) cells. (n=3 per

group, *P < 0.019)

(E) Quantitative analysis of GFP-LC3 colocalization with wild-type M. tuberculosis at 4

hours post-infection in GFP-LC3 RAW cells 264.7 stably overexpressing TREX1 and

DNASE IIb. Results are the means ± SEM of three independent experiments. Data is

expressed as the percentage of GFP-LC3 positive cells relative to control (vector only) cells. (n=3 per group, *P < 0.003)

 (**F**) Quantitative analysis of ubiquitin colocalization with wild-type M. tuberculosis at 4 hours post-infection in wild-type or Trex1-deficient BMDMs. Results are the means ± SEM of three independent experiments. Data is expressed as the percentage of ubiquitin positive cells relative to wild-type BMDMs. (n=3 per group, *P < 0.005)

(**G**) Quantitative analysis of LC3 colocalization with wild-type M. tuberculosis at 4 hours post-infection in wild-type or Trex1-deficient BMDMs. Results are the means ± SEM of three independent experiments. Data is expressed as the percentage of GFP-LC3 positive cells relative to wild-type BMDMs. (n=3 per group, *P < 0.02)

Figure 2.5

Figure 2.5

Figure 2.6 STING, TBK1, and ATG5-dependent delivery of *M. tuberculosis* to lysosomes limits bacterial replication.

(A) Fluorescence images of indicated BMDMs genotypes infected for 4 hours with mCherry-expressing wild-type M. tuberculosis (red) and immunostained with anti-LAMP-1 (green).

(B) Quantitative analysis of LAMP-1 colocalization with wild-type M. tuberculosis at 4 hours post-infection in indicated BMDMs genotypes. Results are the means ± SEM of three independent experiments. Data is expressed as the percentage of Lamp-1 positive cells relative control BMDMs. (n=3 per group, *P < 0.012)

(C) BMDMs of the indicated genoytpes were infected with wild-type M. tuberculosis (MOI 1) for 0, 6, and 24 hours. Bacterial viability was assessed by colony forming units (CFU). Results are the means ± SEM of three independent experiments. Data is expressed as the percentage of bacterial survival compared to time zero relative to control macrophages. (n=3 per group, *P < 0.025)

(D) RAW 264.7 cells were infected with wild-type M. tuberculosis (MOI 1) for 0, 6 and 24 hours after shRNA knockdown of NDP52. Bacterial viability was assessed by colony forming units (CFU). Results are the means ± SEM of three independent experiments. Data is expressed as the percentage of bacterial survival compared to time zero relative to scambled shRNA (control). (n=3 per group, *P < 0.046)

Figure 2.6

A

M. tuberculosis   Lamp-1   merge   ATG5+

M. tuberculosis   Lamp-1   merge   ATG5-

B

% Colocalization with Lamp-1
(Relative to ATG5+)

*

ATG5+   ATG5-

C

% M. tuberculosis survival
(Relative to ATG5+)

*

ATG5+   ATG5-

D

M. tuberculosis   Lamp-1   merge   wild-type

M. tuberculosis   Lamp-1   merge   STING-/-

E

% Colocalization with Lamp-1
(Relative to WT)

*

WT   STING-/-

106
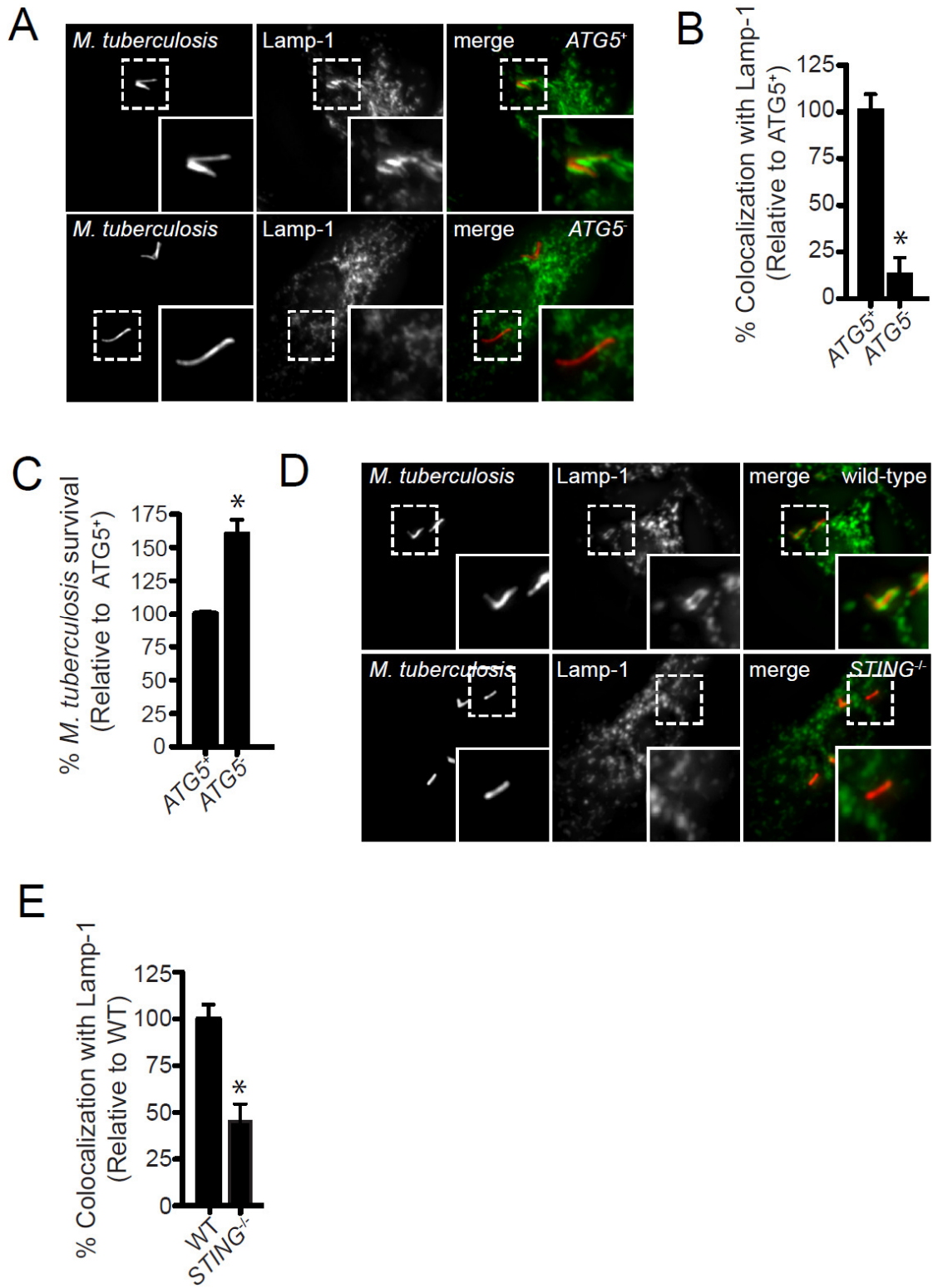
Figure 2.7 ATG5 is required *in vivo* for control of *M. tuberculosis*. $Atg5^{fl/fl}$ $(Atg5^+)$

and Lyz-Cre-$Atg5^{fl/fl}$ $(Atg5^-)$ from a single cohort, were infected with 200 CFUs of wild-

type *M. tuberculosis* via the aerosol route (n = 30 per group).

(A) $Atg5^+$ mice showed significantly improved survival compared to $Atg5^-$ mice as

calculated by log-rank test (**P < 0.001).

(B-C) Bacterial burdens as measured by CFUs in the lungs 0, 7, 21 days post-infection

(B) and the spleen & liver 21 days post-infection **(C)** (n=5 per time point, *P < 0.005,

**P<0.001)

(D) Lungs from $Atg5^+$ and $Atg5^-$ mice 21 days post-infection.

(E) H&E staining of lung sections from $Atg5^+$ and $Atg5^-$ mice 21 days post-infection.

Arrows indicate large pulmonary abcesses not observed in wild-type mice.

(F) Multiplex ELISA analysis of cytokines from lungs of control and $Atg5^-$ mice 21 days

post-infection (n=4 per group).

Figure 2.7

A

D

B

E

C

F
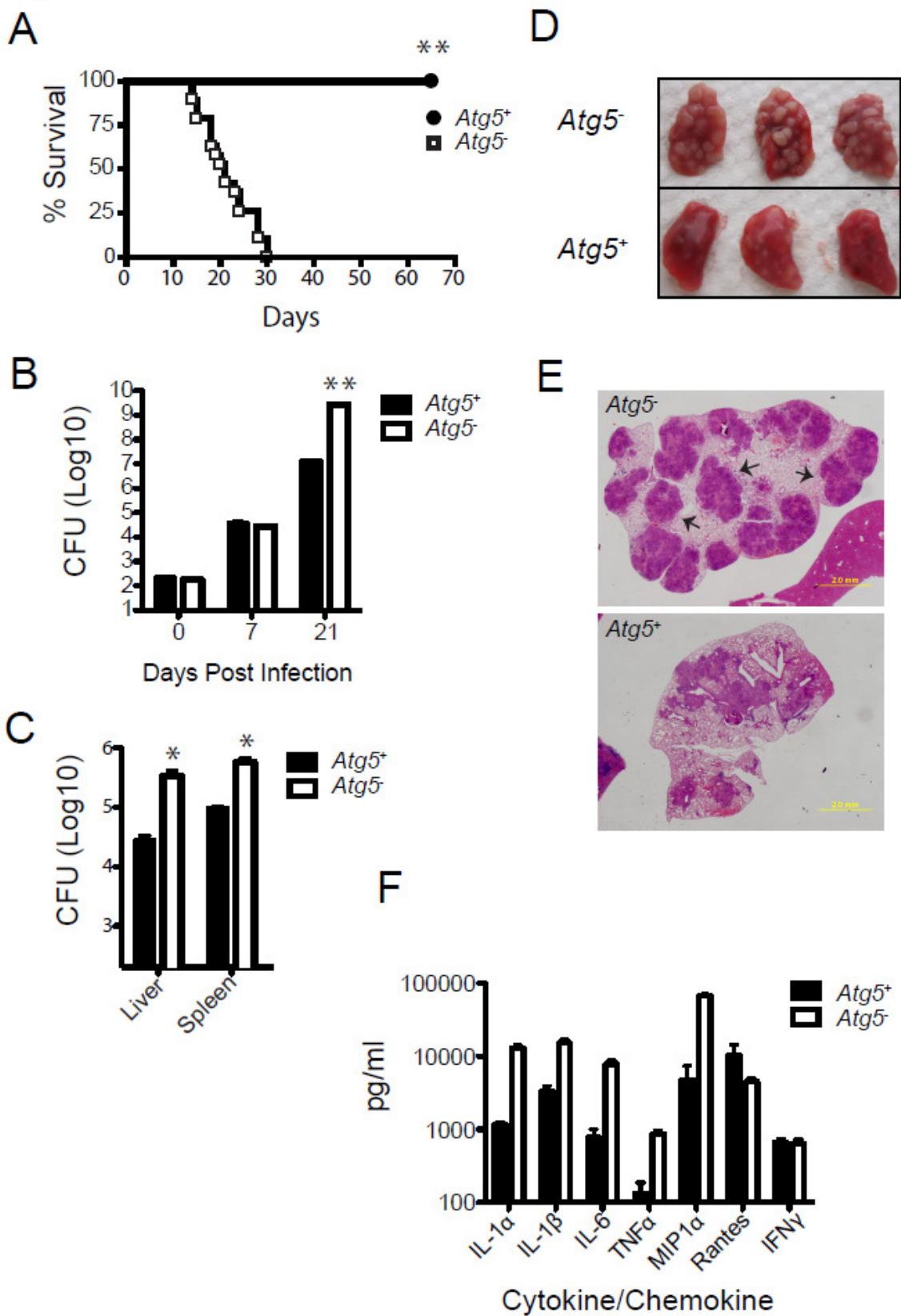
Figure 2.8 *M. tuberculosis* **and** *M. marinum* **targeting to autophagosomes requires phagosomal permeabilization via ESX-1.**

(A) Fluorescence images of RAW 264.7 cells stably expressing GFP-LC3 (green) infected for 6 hours with mCherry-expressing wild-type *M. tuberculosis* or Δesat-6 *M. tuberculosis* (red).

(B) Quantitative analysis of GFP-LC3 colocalization with wild-type *M. tuberculosis* and Δesat-6 *M. tuberculosis* at indicated times after infection. Results are the means ± SEM of three independent experiments.

(C) Fluorescence images of BMDMs infected with for 4 hours with either mCherry-expressing wild-type *M. tuberculosis* or Δ*esat-6 M. tuberculosis* (red) and immunostained with anti-LC3.

(D) Quantitative analysis of LC3 colocalization with wild-type *M. tuberculosis* or Δesat-6 *M. tuberculosis* and wild-type *M. marinum* or ΔRD1 *M. marinum* at indicated times after infection. Results are the means ± SEM of three independent experiments.

(E) Fluorescence images of RAW 264.7 cells stably expressing GFP-LC3 (green) infected with either mCherry-expressing wild-type *M. marinum* or ΔRD1 *M. marinum* (red) corresponding to 6 hours post-infection.

(F) Quantitative analysis of GFP-LC3 colocalization with wild-type *M. marinum* or ΔRD1 *M. marinum* at indicated times after infection. Results are the means ± SEM of three independent experiments.

(G) Fluorescence images of RAW 264.7 infected with for 4 hours with either mCherry-expressing wild-type *M. tuberculosis* or Δ*esat-6 M. tuberculosis* (red) and immunostained with anti-ATG12.

(H) Quantitative analysis of ATG12 colocalization with wild-type *M. tuberculosis* or

Δesat-6 *M. tuberculosis* and wild-type *M. marinum* or ΔRD1 *M. marinum* at indicated

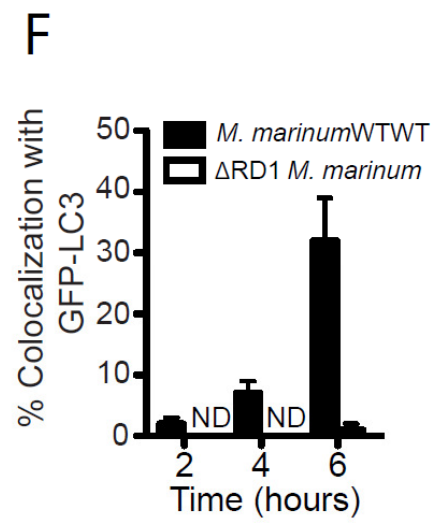times after infection. Results are the means ± SEM of three independent experiments.

Figure 2.8

Figure 2.8

E

| WT *M. marinum* | GFP-LC3 | merge |
| ΔRD1 *M. marinum* | GFP-LC3 | merge |

F

G

| WT *M. tuberculosis* | ATG12 | merge |
| *Δesat-6* *M. tuberculosis* | ATG12 | merge |

H
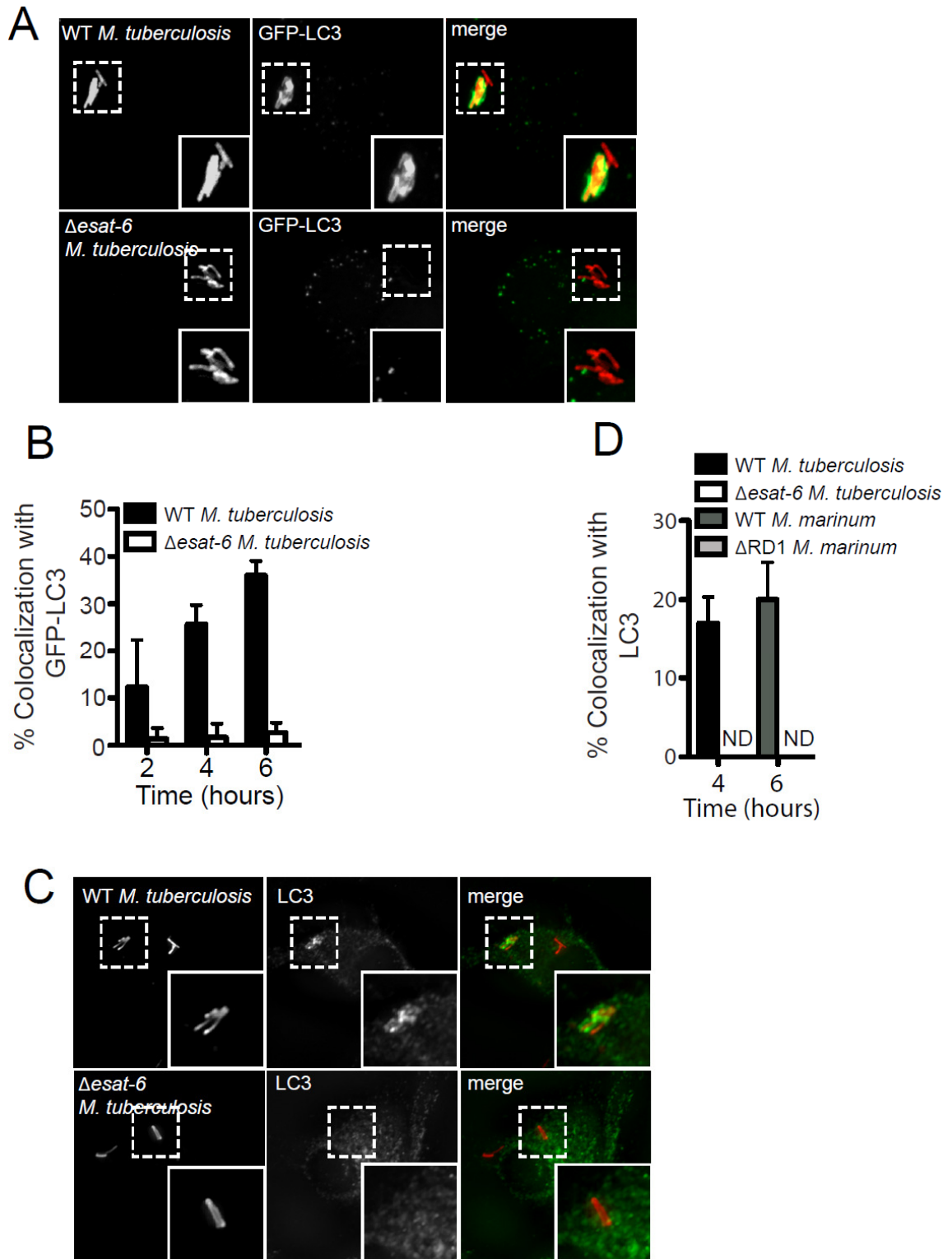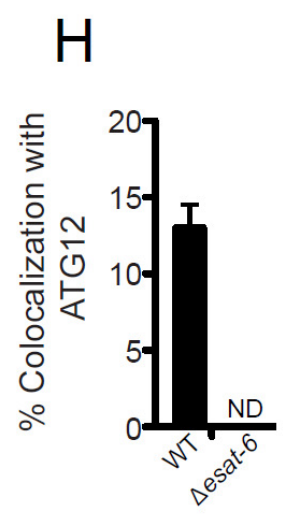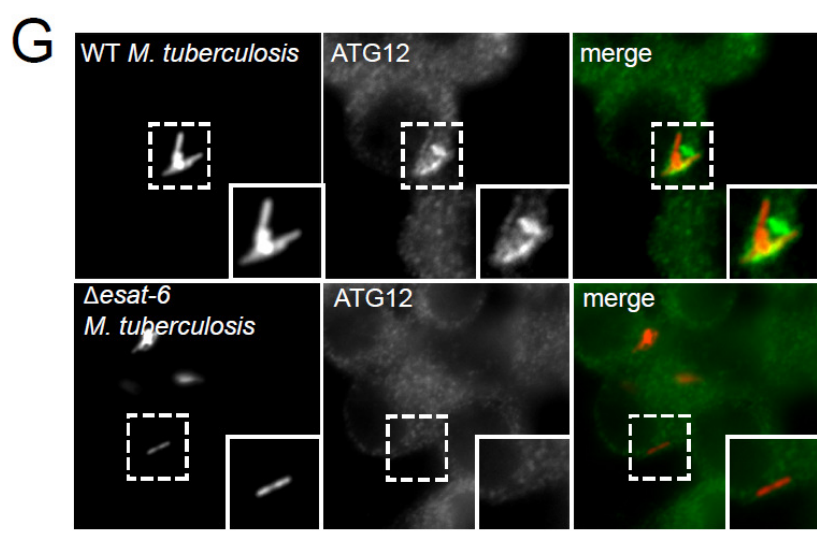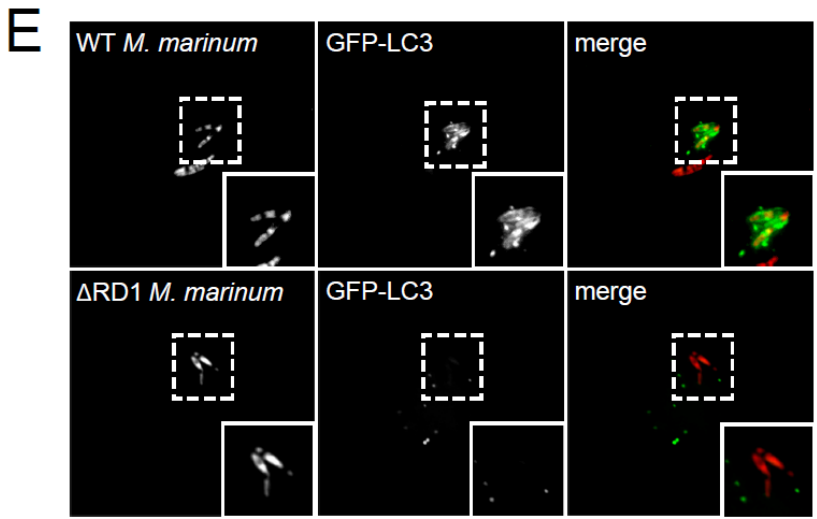
Figure 2.9 Ubiquitin, but not LC3, is localize to *M. tuberculosis* in ATG5⁻

macrophages.

(A) Fluorescence images of Atg5⁺ and Atg5⁻ BMDMs infected for 4 hours with mCherry-expressing wild-type *M. tuberculosis* (red) and immunostained with anti-LC3 (green) and anti-ubiquitin (blue).

(B) Quantitative analysis of LC3 and ubiquitin colocalization with wild-type *M. tuberculosis* in Atg5⁺ and Atg5⁻ BMDMs. Results are the means ± SEM of three independent experiments.

Figure 2.9

A

M. tuberculosis — ubiquitin — LC3 — merge — Atg5+

M. tuberculosis — ubiquitin — LC3 — merge — Atg5-

B

% Colocalization with marker

LC3
ubiquitin

Atg5+

Atg5-

ND
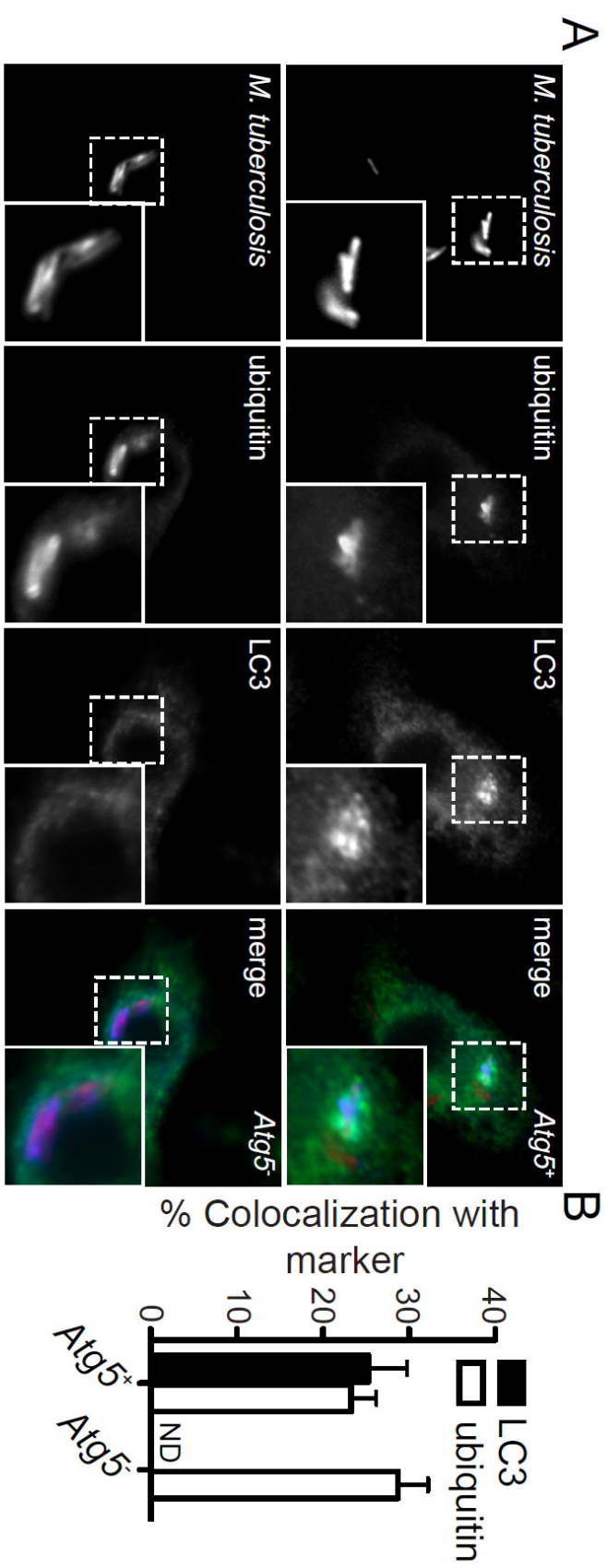
Figure 2.10 The LC3+ population of Rv1596::Tn and moaB1::Tn colocalize with ubiquitin. Fluorescence images of RAW 264.7 cells stably expressing GFP-LC3 (green) infected for 6 hours with mCherry-expressing Rv1596::Tn and moaB1::Tn (red) and stained with anti-ubiquitin (blue).

Figure 2.10
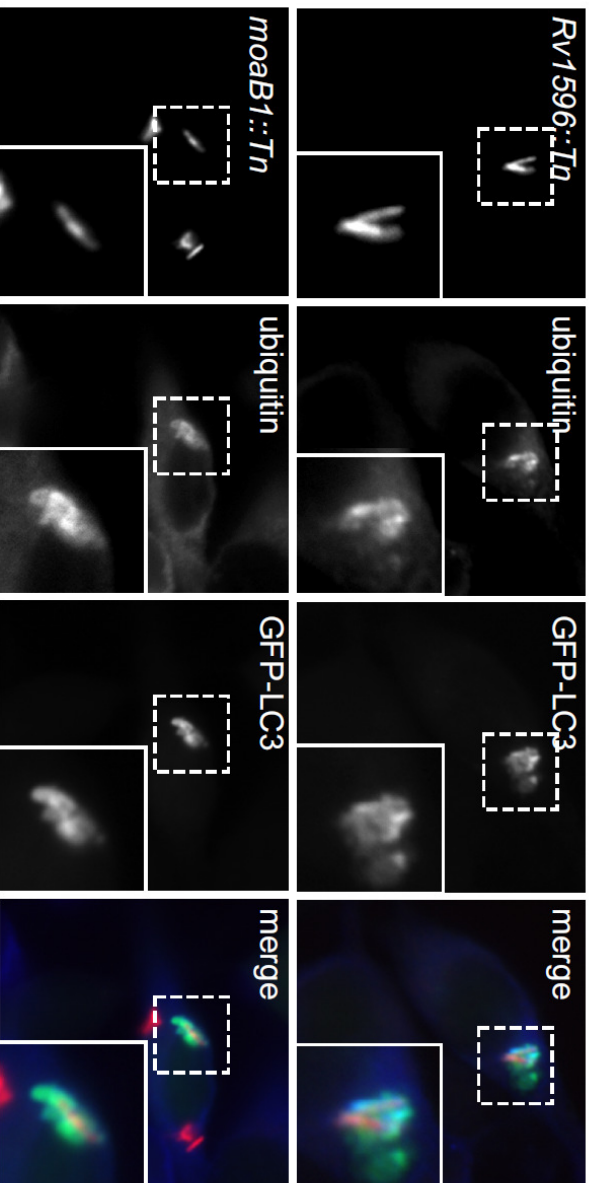
Figure 2.11 Transcript levels of p62 or NDP52 in shRNA knockdown cells.

GFP-LC3 RAW 264.7 cells were transduced with lentiviral constructs expressing shRNAs targeting p62, NDP52, or scrambled shRNA (control), and mRNA levels were assessed by RT-qPCR amplification. Data is expressed as a percentage relative to control knockdown cells.

Figure2.10
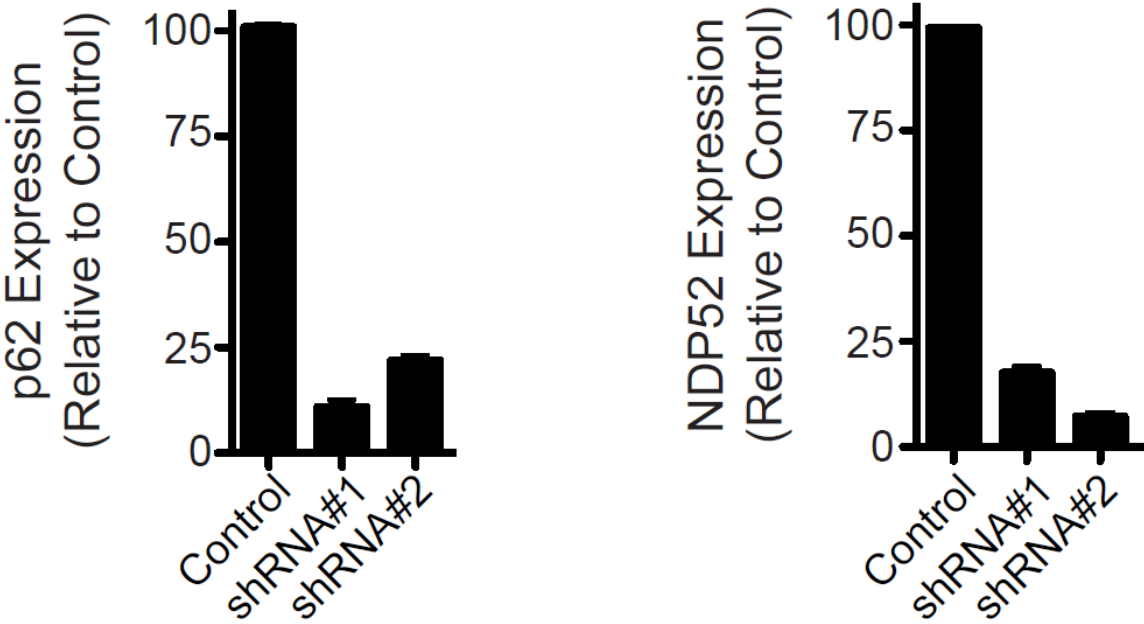
Figure 2.12 Cytosolic double stranded DNA induces autophagy and recruits LC3 in an Atg5 dependent manner.

(A) Fluorescence images of GFP-LC3 RAW 264.7 cells at 4 hours post-transfection with designated nucleic acid. Plasmid DNA was introduced by either lipofection (Plasmid-lipo) or by electroporation (Plasmid-electro), and all the other nucleic acid species were introduced by lipofection. Cells were also treated with lipfection reagent alone (Lipo) or DNA without transfection reagent (DNA only).

(B) Flourescence images of $Atg5^+$ and $Atg\ 5^-$ BMDMs 4 hours-post transfection with Cy3-labelled plasmid DNA (red) and immunostained with anti-LC3 (green).

Figure 2.12

A

| Plasmid-Lipo | E. coli | PolydG:dC | PolydA:dT | Lipo |
| GFP-LC3 nucleus | GFP-LC3 nucleus | GFP-LC3 nucleus | GFP-LC3 nucleus | GFP-LC3 nucleus |

| Plamid-electo | 5'p-dsRNA | ssRNA | ssDNA | DNA only |
| GFP-LC3 nucleus | GFP-LC3 nucleus | GFP-LC3 nucleus | GFP-LC3 nucleus | GFP-LC3 nucleus |

B

Atg5⁺   LC3 DNA

Atb5⁻   LC3 DNA
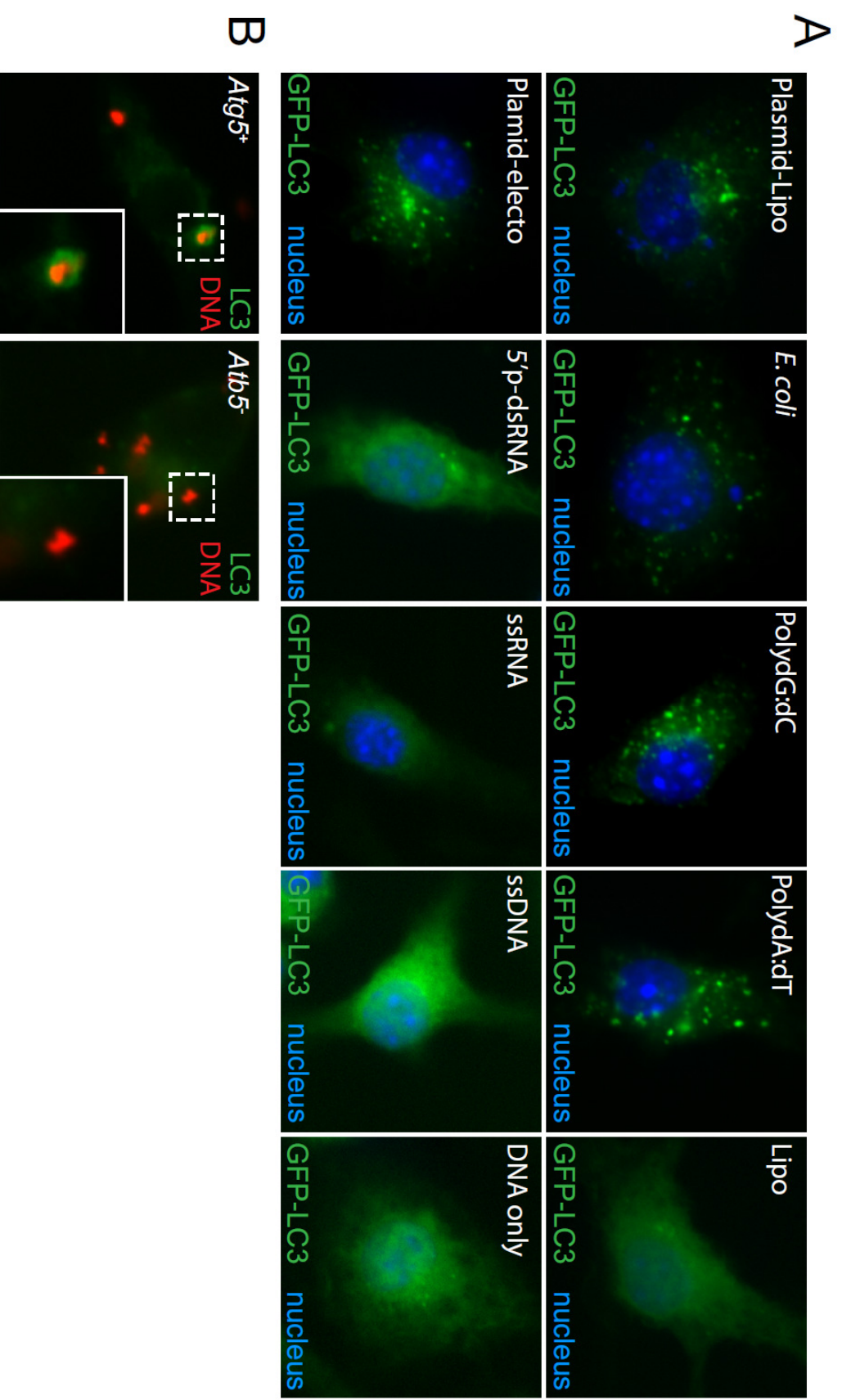
Figure 2.13 Cytosolic double stranded DNA LC3+ population also colocalizes with ubiquitin.

(A) Fluorescence images of BMDMs 4 hours post-transfection with Cy3-Labelled plasmid DNA (red) and immunostained with anti-LC3 (green), and anti-ubiquitin (blue).

(B) Quantitative analysis of M. tuberculosis colocalization with ubiquitin and LC3 at 4 hours post-infection. Results are the means ± SEM of three independent experiments.

(C) Fluorescence images of BMDMs 4 hours post-transfection with Cy3-Labelled plasmid DNA (red) and immunostained with anti-K63 and anti-K48 ubiquitin (green).

(D) Quantitative analysis of K63 and K48 ubiquitin colocalization with Cy3-Labelled plasmid DNA at 4 hours post-transfection. Results are the means ± SEM of three independent experiments.

Figure 2.13
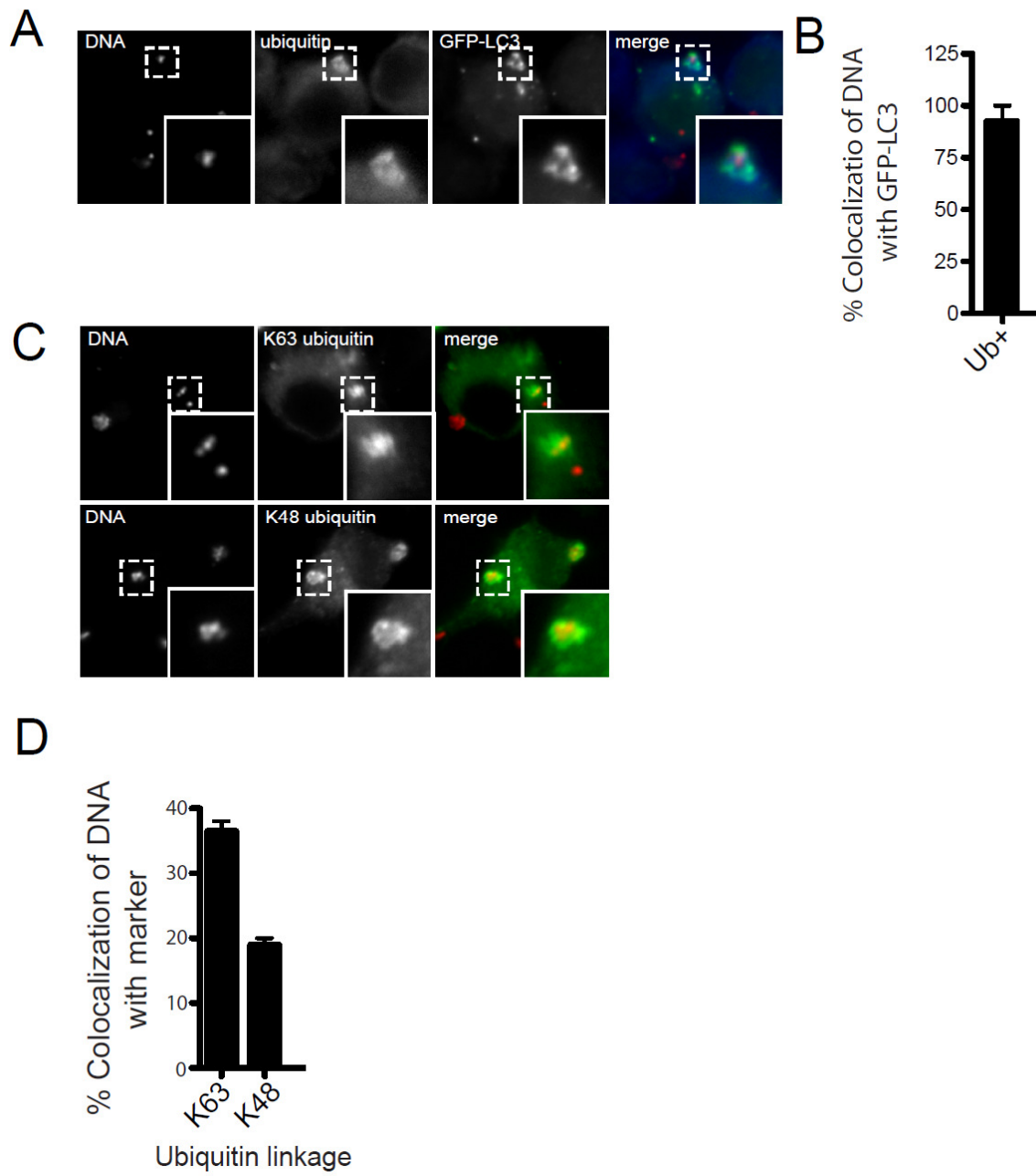
Figure 2.14 Quantitative analysis of *M. tuberculosis* colocalization with ubiquitin and LC3 in various knockout macrophages.

BMDMs of the indicated genotype were infected with wild-type *M. tuberculosis* for 4 hours and colocalization of M. tuberculosis with ubiquitin **(A)** and LC3 **(B)** was quantified.

Figure 2.14

A

B
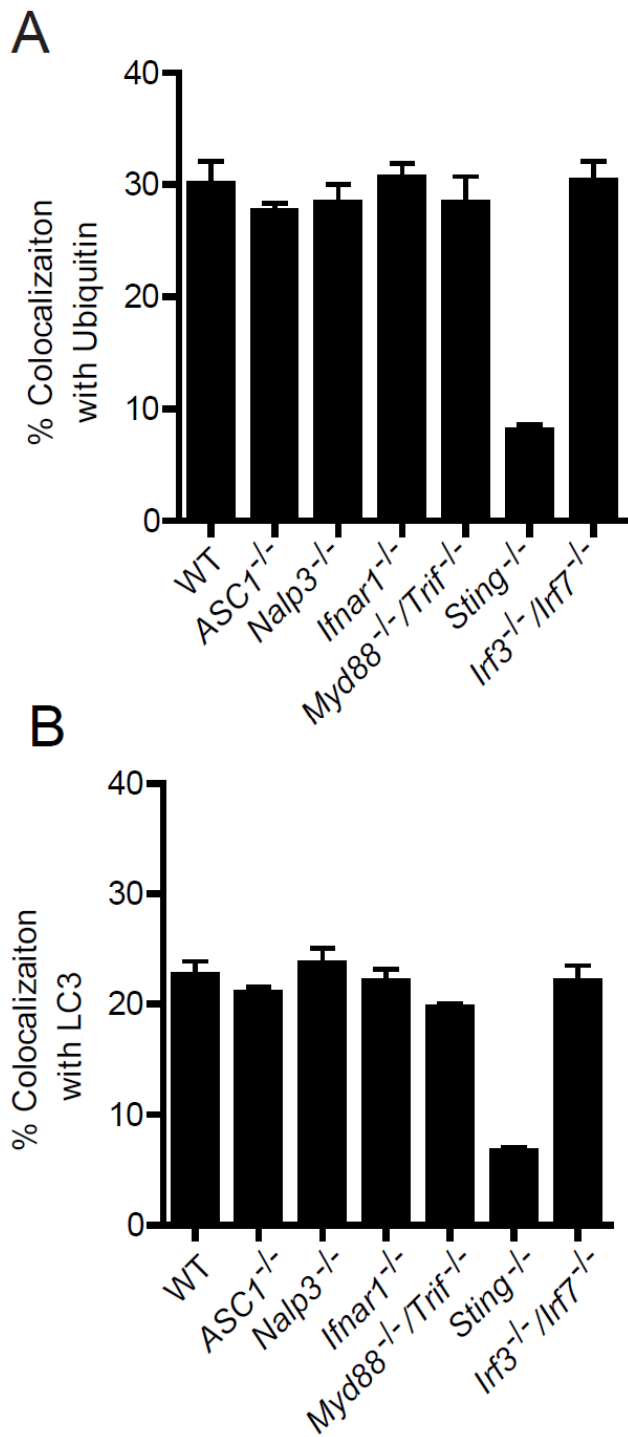
Chapter 3.

The ubiquitin ligase PARKIN is required for autophagy and host resistance to intracellular pathogens

Abstract

Ubiquitin-mediated targeting of intracellular bacteria to the autophagy pathway is a key immune mechanism of innate resistance to invading microbes[1,2], including the important human pathogen *Mycobacterium tuberculosis*[3]. The ubiquitin ligases responsible for catalyzing ubiquitin chains that surround cytosolic intracellular bacteria are unknown. We surmised that a mechanism by which eukaryotic cells target and destroy their eubacterial-derived mitochondria (mitophagy)[4] might be similar to the way they eliminate intracellular bacterial pathogens (xenophagy). PARKIN is a RING domain E3 ubiquitin ligase that has a well-established role in mitophagy[4], and null mutations in the gene encoding PARKIN (*Park2*) lead to autosomal recessive, juvenile Parkinson's disease[5,6] due to progressive loss of dopaminergic neuron viability. Surprisingly, mutations in the *Park2* regulatory region have also been associated with increased susceptibility to intracellular bacterial pathogens in humans, including *Mycobacterium leprae*[7] and *Salmonella typhi*[8], but the functional role of PARKIN in immunity has not been explored. Here we show that PARKIN plays an obligatory role in innate immune defense by marking *M. tuberculosis* with K63-linked ubiquitin chains. PARKIN-deficient macrophages fail to target *M. tuberculosis* to the autophagy pathway and to the lysosome. PARKIN-deficient mice are exquisitely sensitive to *M. tuberculosis* infection, and fail to control infection by *Listeria monocytogenes*, another intracellular pathogen. PARKIN appears to play a conserved role in metazoan innate defense, as PARKIN-deficient flies are also susceptible to microbial infections. Thus, PARKIN regulates both neuronal disease due to its role in mitophagy, and resistance to pathogens via its unexpected role in xenophagy.

Introduction

The key step in mitophagy is the marking of damaged mitochondria by PARKIN, which directly ubiquitinates proteins on the surface of the organelle[4]. Ubiquitin-tagged mitochondria are directed into the general autophagy pathway via the action of the adaptor protein p62[9,10], which binds both ubiquitin and the autophagosome-associated protein, LC3[11], although other factors are likely required[12]. Once LC3 is targeted to the cargo, other components of the general autophagy pathway, including ATG proteins such as ATG5, function to form autophagosomes and deliver the organelles to the lysosome for destruction[4]. Intracellular bacterial pathogens, including *M. tuberculosis*, *L. monocytogenes*, and *Salmonella enterica* serovar Typhimurium (*S.* Typhimurium), are also eradicated via ubiquitin-associated autophagy targeting[2]. Intracellular pathogens become surrounded by conjugated ubiquitin chains, which presumably recruits ubiquitin-binding autophagy adaptors such as p62, NDP52, and optineurin, ultimately delivering bacteria to lysosomes for destruction[1,3,13]. While ubiquitin binding adaptors are required for autophagy of bacteria[3,13,14], it is unknown whether ubiquitin itself directly mediates bacterial autophagy as the identities of the ubiquitinated substrate(s) and ligase(s) responsible for coating cytosol-exposed bacteria have not been identified.

Results

We have shown previously that upon infection of macrophages, *M. tuberculosis* bacilli that puncture phagosomal membranes and gain access to the host cytosol become

enveloped by conjugated ubiquitin chains and are targeted to autophagosomes via p62 and NDP52[3]. Because of the commonalities between mitophagy and autophagy of intracellular mycobacteria, and the links between *Park2* mutations and increased susceptibility to bacterial infection in humans, we hypothesized that PARKIN may be required for ubiquitin-mediated autophagy of *M. tuberculosis*. To test this, we infected bone marrow-derived macrophages (BMDMs) isolated from wild-type and *Park2*^{-/-} mice with wild-type *M. tuberculosis* expressing mCherry, and performed immunofluorescence co-localization experiments using antibodies that recognize polyubiquitin. As shown in Fig.3.1a and Fig.3.2, *Park2*^{-/-} BMDMs were severely defective for *M. tuberculosis* ubiquitin colocalization as compared to control macrophages, resulting in an 80-90% reduction in ubiquitin-positive mycobacteria. Likewise, shRNA knock-down of PARKIN expression in the human U937 macrophage cell line also resulted in a drastic reduction in ubiquitin localization with *M. tuberculosis* cells, (Fig. 3.1c-d) indicating that PARKIN plays a conserved role in innate defense in mice and humans. Expression of wild-type *Park2* in *Park2*^{-/-} cells fully restored *M. tuberculosis* ubiquitination (Fig. 3.1e). In contrast, *Park2*^{-/-} BMDMs expressing either of two pathogenic RING domain mutant alleles that inactivate PARKIN's E3 ligase activity, T240R or P437L[6,15], failed to restore ubiquitination of *M. tuberculosis* (Fig. 3.1e). These data demonstrate that the E3 ligase activity of Parkin is critical for ubiquitination of intracellular *M. tuberculosis* cells during infection.

We showed previously that both K63- and K48-linked polyubiquitin chains accumulate around *M. tuberculosis*[3]. Because PARKIN is known to catalyze K63-linked ubiquitin chains[4,16], we sought to determine the nature of the residual ubiquitin

surrounding *M. tuberculosis* in *Park2*^{-/-} BMDMs. Using ubiquitin linkage-specific

antibodies, we found that in wild-type BMDMs, approximately 90-95% of all ubiquitin-

positive bacilli co-localized with K63 ubiquitin, and only roughly 10% stained for K48,

demonstrating that K63-linked ubiquitin is the predominant ubiquitin-linkage

surrounding *M. tuberculosis* (Fig. 3.3a). In *Park2*^{-/-} BMDMs, however, there was a

specific defect in K63[+] mycobacteria, while the proportion of the K48[+] population

remained unaffected (Fig. 2b-c). These results are consistent with the notion that

PARKIN directly catalyzes the K63 linked ubiquitin chains surrounding *M. tuberculosis*,

although this awaits further study. These data also show that another, unidentified

ubiquitin ligase works independently of PARKIN to catalyze the K48-linked

ubiquitination that surround a minor population of *M. tuberculosis* cells.

Ubiquitination coincides with autophagic targeting of *M. tuberculosis* and other

intracellular pathogens[3,17], but a causal relationship has not been demonstrated. To

determine whether Parkin-mediated ubiquitination directs autophagic targeting of *M.*

tuberculosis, we infected wild-type and *Park2*^{-/-} macrophages with *M. tuberculosis* and

measured colocalization of bacilli with multiple markers of autophagy. Proteins involved

in ubiquitin recognition (NBR1, NDP52, p62, phospho-TBK1) all failed to colocalize

with *M. tuberculosis* in *Park2*^{-/-} macrophages (Fig. 3.3d-e), demonstrating that PARKIN-

mediated ubiquitination directly leads to the recruitment of the proximal ubiquitin-

adaptors that facilitate autophagic targeting of mycobacteria. Likewise, mycobacterial

cells within infected *Park2*^{-/-} BMDMs had reduced colocalization with autophagic

proteins LC3 and ATG12 relative to infection of wild-type BMDMs (Fig. 3.4a-b),

demonstrating that the K63-linked polyubiquitin catalyzed by PARKIN is required for

delivery of *M. tuberculosis* to autophagosomes. Consistent with this notion, *Park2$^{-/-}$* cells were defective in conversion of LC3 to its activated, lipidated form, LC3-II, during *M. tuberculosis* infection, further demonstrating that Parkin is required for autophagy of mycobacteria (Fig. 3.4c).

The autophagy pathway serves to limit *M. tuberculosis* replication in macrophages by delivering bacilli to the lysosome[3]. To determine if PARKIN mediated ubiquitination is required for autophagic targeting of *M. tuberculosis* to lysosomes, we infected BMDMs with *M. tuberculosis* and monitored co-localization with the lysosomal marker, Lamp-1. During *M. tuberculosis* infection of wild-type BMDMs, approximately 30% of bacilli stained positive for Lamp-1 at 6 hrs post-infection (Fig. 3.4d-e). In contrast, only 2-5% of bacilli colocalized with Lamp-1 during *M. tuberculosis* infection of *Park2$^{-/-}$* macrophages. This was similar to macrophages deficient for the essential autophagy protein, ATG5 (Fig. 3.4d-e)[3]. To test whether these differences led to changes in bacterial survival, we infected *Park2$^{-/-}$* and *Atg5$^{-/-}$* BMDMs with wild-type *M. tuberculosis* and determined bacterial viability by enumerating colony-forming units (CFUs). Infection of BMDMs deficient for either PARKIN or ATG5 resulted in a 3-fold increase in bacterial numbers relative to control BMDMs (Fig. 3.4f) by 16 hours post-infection. Likewise, knock-down of PARKIN expression in U937 cells also led to a similar increase in bacterial replication during infection (Fig. 3.4g). Taken together, our data demonstrates that PARKIN-mediated ubiquitination leads to the autophagic targeting of *M. tuberculosis* and is essential for inhibition of mycobacterial replication in macrophages.

Polymorphisms within the regulatory region of *Park2* in human populations have been identified as a common risk factor for increased susceptibility to leprosy and salmonella infection[7,8], suggesting that PARKIN plays an important role *in vivo* against a broad range of intracellular bacterial infections. We began to test this by first determining whether PARKIN was required *in vivo* during *M. tuberculosis* infection of mice. We performed a low-dose aerosol infection of wild-type and *Park2*^{-/-} knockout mice and determined mouse survival and bacterial burden within infected tissues. In comparison to infected wild-type mice, *Park2*^{-/-} knockout mice had a 10-fold increase in bacterial CFUs within infected lungs, spleens and liver by 21 days post-infection (Fig. 3.5a, b). Furthermore, survival studies revealed that *Park2*^{-/-} mice were extremely susceptible to *M. tuberculosis* infection as all infected mice succumbed to death by 85 days post-infection, while all infected wild-type mice remained alive and displayed no-overt signs of weight-loss or stress (Fig. 3.5c). Importantly, *Park2*^{-/-} mice were also highly susceptible to another intracellular pathogen, *L. monocytogenes*, resulting in 10-20 fold higher bacterial burdens relative to wild-type mice within infected spleens and liver (Fig. 3.5d). Taken together, this data demonstrates that PARKIN is essential *in vivo* for controlling intracellular bacterial pathogens.

Park2 is present in all metazoans[18], including *Drosophila melanogaster* and *Caenorhabditis elegans*, with well-characterized functions in mitochondrial maintenance and in models of Parkinson's disease. To determine whether PARKIN also plays an evolutionarily conserved role in immunity, we analyzed PARKIN-deficient *D. melanogaster* using models of bacterial systemic infection. We obtained two mutant fly lines with independent disruptions of the *Parkin* gene (*Park*[f01950], *Park*[c00062]) and infected

them with *L. monocytogenes,* which has previously shown to induce autophagy within

flies[19]. In contrast to wild-type infected flies, *Parkin* mutant flies were severely defective

in ATG8/LC3 processing during infection (Fig. 3.5e), suggesting that *Parkin* plays an

obligate role in autophagy in flies. Consistent with our results in mice, *Parkin* mutant

flies were also highly susceptible to *L. monocytogenes* infection and to 10-50 fold

increases in bacterial burdens relative to wild-type infected flies (Fig. 3.5f). This was

accompanied with decreased survival, with a median lifespan of two days following

infection (Fig. 3.5g). In addition, *Parkin* mutant flies were also susceptible to other

intracellular pathogens such as *S*. typhimurium and *M. marinum*, further delineating a

role of PARKIN against intracellular bacterial infection (Fig. 3.6a,b,c).

Discussion

Our findings reveal that PARKIN regulates a common cellular program by which

metazoans mediate quality control of endogenous mitochondria (self) and eradicate

harmful bacterial pathogens (non-self). Although these two activities are seemingly

disparate, the evolutionary origin of mitochondria from a bacterial endosymbiont

suggests that perhaps mitochondrial dysfunction triggers the recognition of the organelle

as non-self. For example, mitochondria (and bacterial endosymbionts) may actively

evade PARKIN surveillance, but these inhibitory processes are overridden upon

organelle damage. Our results also provide a molecular explanation for the susceptibility

of humans with mutations in the *Park2* regulatory region, revealing an unexpected

connection between mitochondrial-based neuronal disorders and susceptibility to

bacterial infection in humans.

While this study highlights the importance of Parkin in mycobacterial mediated autophagy and host defense, the question of whether Parkin directly or indirectly mediates ubiquination of the mycobacterial phagosome remains unknown. Attempts to analyze the subcellular localization of endogenous Parkin during *M. tuberculosis* were unsuccessful. Commercially available anti-Parkin antibodies were found to be unsuitable for use in immunofluorescence. Furthermore, I was unsuccessful in generating either human or mouse macrophage cell lines expressing GFP-Parkin or mCherry-Parkin, as overexpression of Parkin alone proved to be highly toxic to macrophages(data not shown). Thus, Parkin's direct effect on ubiquination of the mycobacterial phagosome is unknown and warrants further investigation.

Materials and Methods

Mice and macrophages

Park2^{-/-} mice on the C57L/B6 background were a gift from K. Nakamura (Gladstone Institute). Wild-type C57BL/6 mice were purchased from Jackson laboratories. BMDMs were obtained from mouse femurs as previously described[3] and cultured in DMEM H-21 supplemented with 20% FBS and 10% MCSF derived from 3T3-MCSF cells. U937 cells were obtained from ATCC and were stimulated overnight with 20ng/ml of PMA (Sigma) prior to infections.

Antibodies

The following antibodies were used: LC3B (Invitrogen), NDP52 (Novus Biologicals), mouse p62(Abnova), rabbit anti-drosophila ATG-8 (Gift from S. Cherry, U Penn), phospho-TBK1 (Cell Signaling), poly-ubiquitin (Enzo FK1), Parkin and ATG12 (Cell

Signaling), humanized rabbit monoloncal antibodies specific for K63 or K48 (Gift from

E. Brown lab at Genentech), tubulin (Cell Signaling), and actin (Abcam) antibodies.

Bacterial strains

The following bacterial strains were used: *M. tuberculosis* (Erdman), *L. monocytogenes*

(10403s), *M. marinum* (M), and *S*. typhimurium (SL1344). Mycobacteria expressing

mCherry was previously described[3].

Macrophage infection

For infections with *M. tuberculosis*, macrophages were infected as previously described[3].

Briefly, *M. tuberculosis* cultures were washed twice with PBS, gently sonicated to

disperse clumps, and resuspended in DMEM supplemented with 10% horse serum.

Media was removed from cells, monolayers overlaid with the bacterial suspension, and

centrifuged for 10 min at 1,000 RPM. Cells were washed twice in PBS and returned to

macrophage media. For determination of bacterial viability following infection, cells

were lysed in 1% Triton-X 100 and plated on 7H10 agar plates.

Western blotting

Protein lysates from cells and flies were obtained by lysis in RIPA buffer (Sigma) at the

indicated time points. Micro BCA protein kit (Pierce) was used to measure protein levels

and equal amounts of protein were electrophoresed on 4-20% Tris-HCL Criterion gels

(Biorad), and transferred onto nitrocellulose membranes. Western blots were analyzed

using an Odyssey Imager (Licor) according to manufacturer's instructions. Western blot

figures are a representative of at least two independent experiments.

Immunofluorescence

Infected cells were immunostained and visualized as previously described[3]. Briefly, macrophages were seeded onto poly-lysine coated coverslips and infected with *M. tuberculosis* as described above. Cells were infected at an MOI of 1, and fixed in 4%PFA for 20 min at the indicated time points. Cells were incubated with indicated primary antibodies for 2 h at room temperature in 5% milk, 0.05% saponin and visualized using secondary Alexa-fluor488 antibodies. Colocalization studies were performed as blinded experiments, with a minimum count of 200 cells per coverslip and performed in triplicate. Data shown is the mean ± SD.

Mouse infection

Mice were infected with *M. tuberculosis* via low-dose aerosol infection (200 CFU) as previously described[20]. Lungs, liver and spleens were harvested, homogenized, and plated on 7H10 agar plates. For survival experiments, infected mice were euthanized when they had lost 15% of their maximal body weight. For *L. monocytogenes* infections, mice were infected via intraperitoneal injection with 4 x 10^5 bacteria. 96 hours post infection, liver and spleen from infected mice were homogenized and serial dilutions were plated onto BHI agar plates. All mice were housed and treated humanely using procedures described in an animal care protocol approved by University of California, San Francisco, Institutional Animal Care and Use Committee.

Fly strains and infections

The white1118 strain (Bloomington stock center, stock 6326) was used as the wild-type parental strain for all experiments. The *Park*[c00062] and *Park*[f01950] alleles are from the Exelexis piggyBac transposon collection[21]. *Park*[c00062] was obtained from Bloomington

stock center and $Park^{f01950}$ was obtained from the Exelexis collection at Harvard. Infections were done as previously described[22]. Male 5 to 7 day-old files were anesthetized with CO2 and injected *L. monocytogenes* (1000 CFU), *S.* typhimurium (2500 CFU), or *M. marinum* (1000 CFU) in 50 nl of culture into the anterior abdomen. Infected flies were homogenized in PBS supplemented with 1% Triton X-100 and serial dilutions were plated onto solid media. For survival analysis, the number of dead flies was counted daily and analyzed via log-rank test.

Lentiviral virus knockdown and complementation

Lentivirus expressing shRNAs targeting human *Park2* transcripts were generated using the Mission PLKO.1 lentivirus system from Sigma (shRNA#1 TRCN0000000285, shRNA#2 TRCN0000000283). A lentivirus expressing a non-targeting scrambled shRNA was used as a control. U937 cells were transduced with lentivirus per manufacturer's instructions and stable cell lines were generated via selection with puromycin. For transgene expression of *Park2* mutants, full length *Park2* was cloned into pBluescript vector and RING domain mutants were generated using Quick-Change site directed mutagenesis kit (Stratagene). Lentivirus expressing PARKIN constructs were generated using the pLentiX-CMV-puro system[3]. $Park2^{-/-}$ macrophages expressing PARKIN constructs were generated by transducing marrow cells from knockout mice with lentivirus followed by differentiation into macrophages as described above. During day 3 of differentiation, cells were selected with 5ug/ml of puromycin.

<u>References</u>

1. Zhao, Z. *et al.* Autophagosome-independent essential function for the autophagy protein Atg5 in cellular immunity to intracellular pathogens. *Cell Host & Microbe* **4**, 458–469 (2008).

2. Deretic, V. & Levine, B. Autophagy, immunity, and microbial adaptations. *Cell host & microbe* **5**, 527–549 (2009).

3. Watson, R. O., Manzanillo, P. S. & Cox, J. S. Extracellular M. tuberculosis DNA Targets Bacteria for Autophagy by Activating the Host DNA-Sensing Pathway. *Cell* **150**, 803–815 (2012).

4. Youle, R. J. & Narendra, D. P. Mechanisms of mitophagy. *Nat Rev Mol Cell Biol* **12**, 9–14 (2011).

5. Kitada, T. *et al.* Mutations in the parkin gene cause autosomal recessive juvenile parkinsonism. *Nature* **392**, 605–608 (1998).

6. Martin, I., Dawson, V. L. & Dawson, T. M. Recent advances in the genetics of Parkinson's disease. *Annu Rev Genomics Hum Genet* **12**, 301–325 (2011).

7. Mira, M. T. *et al.* Susceptibility to leprosy is associated with PARK2 and PACRG. *Nature* **427**, 636–640 (2004).

8. Ali, S. *et al.* PARK2/PACRG polymorphisms and susceptibility to typhoid and paratyphoid fever. *Clin Exp Immunol* **144**, 425–431 (2006).

9. Komatsu, M. *et al.* Homeostatic levels of p62 control cytoplasmic inclusion body formation in autophagy-deficient mice. *Cell* **131**, 1149–1163 (2007).

10. Geisler, S. *et al.* PINK1/Parkin-mediated mitophagy is dependent on VDAC1 and p62/SQSTM1. *Nature cell biology* **12**, 119–131 (2010).

11. Pankiv, S. *et al.* p62/SQSTM1 binds directly to Atg8/LC3 to facilitate degradation of ubiquitinated protein aggregates by autophagy. *J Biol Chem* **282**, 24131–24145 (2007).

12. Narendra, D., Kane, L. A., Hauser, D. N., Fearnley, I. M. & Youle, R. J. p62/SQSTM1 is required for Parkin-induced mitochondrial clustering but not mitophagy; VDAC1 is dispensable for both. *Autophagy* **6**, 1090–1106 (2010).

13. Wild, P. *et al.* Phosphorylation of the Autophagy Receptor Optineurin Restricts Salmonella Growth. *Science* **333**, 228–233 (2011).

14. Ponpuak, M. *et al.* Delivery of cytosolic components by autophagic adaptor protein p62 endows autophagosomes with unique antimicrobial properties. *Immunity* **32**, 329–341 (2010).

15. Chen, D. *et al.* Parkin mono-ubiquitinates Bcl-2 and regulates autophagy. *J Biol Chem* **285**, 38214–38223 (2010).

16. Lim, K.-L. *et al.* Parkin mediates nonclassical, proteasomal-independent ubiquitination of synphilin-1: implications for Lewy body formation. *J Neurosci* **25**, 2002–2009 (2005).

17. Thurston, T., Ryzhakov, G., Bloor, S., Muhlinen, von, N. & Randow, F. The TBK1 adaptor and autophagy receptor NDP52 restricts the proliferation of ubiquitin-coated bacteria. *Nat Immunol* (2009).doi:10.1038/ni.1800.

18. Marín, I. & Ferrús, A. Comparative genomics of the RBR family, including the Parkinson's disease-related gene parkin and the genes of the ariadne subfamily. *Mol. Biol. Evol.* **19**, 2039–2050 (2002).

19. Yano, T. *et al.* Autophagic control of listeria through intracellular innate immune recognition in drosophila. *Nat Immunol* **9**, 908–916 (2008).

20. Voronin, D., Cook, D. A. N., Steven, A. & Taylor, M. J. Autophagy regulates Wolbachia populations across diverse symbiotic associations. *Proceedings of the National Academy of Sciences* **109**, E1638–46 (2012).

21. Goldberg, M. S. Parkin-deficient Mice Exhibit Nigrostriatal Deficits but Not Loss of Dopaminergic Neurons. *J Biol Chem* **278**, 43628–43635 (2003).

22. Ohol, Y. M. *et al.* Mycobacterium tuberculosis MycP1 protease plays a dual role in regulation of ESX-1 secretion and virulence. *Cell Host & Microbe* **7**, 210–220 (2010).

23. Thibault, S. T. *et al.* A complementary transposon tool kit for Drosophila melanogaster using P and piggyBac. *Nat Genet* **36**, 283–287 (2004).

24. Ayres, J. S. & Schneider, D. S. A Signaling Protease Required for Melanization in Drosophila Affects Resistance and Tolerance of Infections. *PLoS Biol* **6**, e305 (2008).

25. Watson, R. O., Manzanillo, P. S. & Cox, J. S. Extracellular M. tuberculosis DNA targets bacteria for autophagy by activating the host DNA sensing pathway. *Cell* 1–65 (2012).

Figure 3.1 PARKIN activity is required for *M. tuberculosis* ubiquitin colocalization during macrophage infection. a, Images of wild-type (WT) and *Park2*$^{-/-}$ BMDMs infected with mCherry-expressing *M. tuberculosis* for 4 h and immunostained for polyubiquitin. **b,** Quantification of ubiquitin-positive *M. tuberculosis* from **(a)**, expressed as a percentage of the values obtained from WT cells. Results are the means ± SEM of three independent experiments (*P<0.001 as determined by Student's t-test). **c,** Images of U937 human macrophages expressing a scrambled shRNA (Control) or one of two different shRNAs targeting *Park2* (shRNA#1, shRNA#2) infected with mCherry-expressing *M. tuberculosis* for 12 h and immunostained for polyubiquitin. **d,** Quantification of ubiquitin positive *M. tuberculosis* from (**c**), expressed as a percentage of the values obtained from control cells. Results are the means ± SEM of three independent experiments (*P<0.005 as determined by Student's t-test). **e,** *Park2*$^{-/-}$ BMDMs were transduced with lentivirus expressing BFP (-), wild-type PARKIN (WT), or two separate mutant PARKIN isoforms (T240R, P437L). Cells were infected with mCherry-expressing *M. tuberculosis* for 4 h and ubiquitin-*M. tuberculosis* colocalization was quantified and expressed relative to control BMDMs. Results are the means ± SEM of three independent experiments (*P<0.005 as determined by Student's t-test).

Figure 3.1

Figure 3.1

d

e
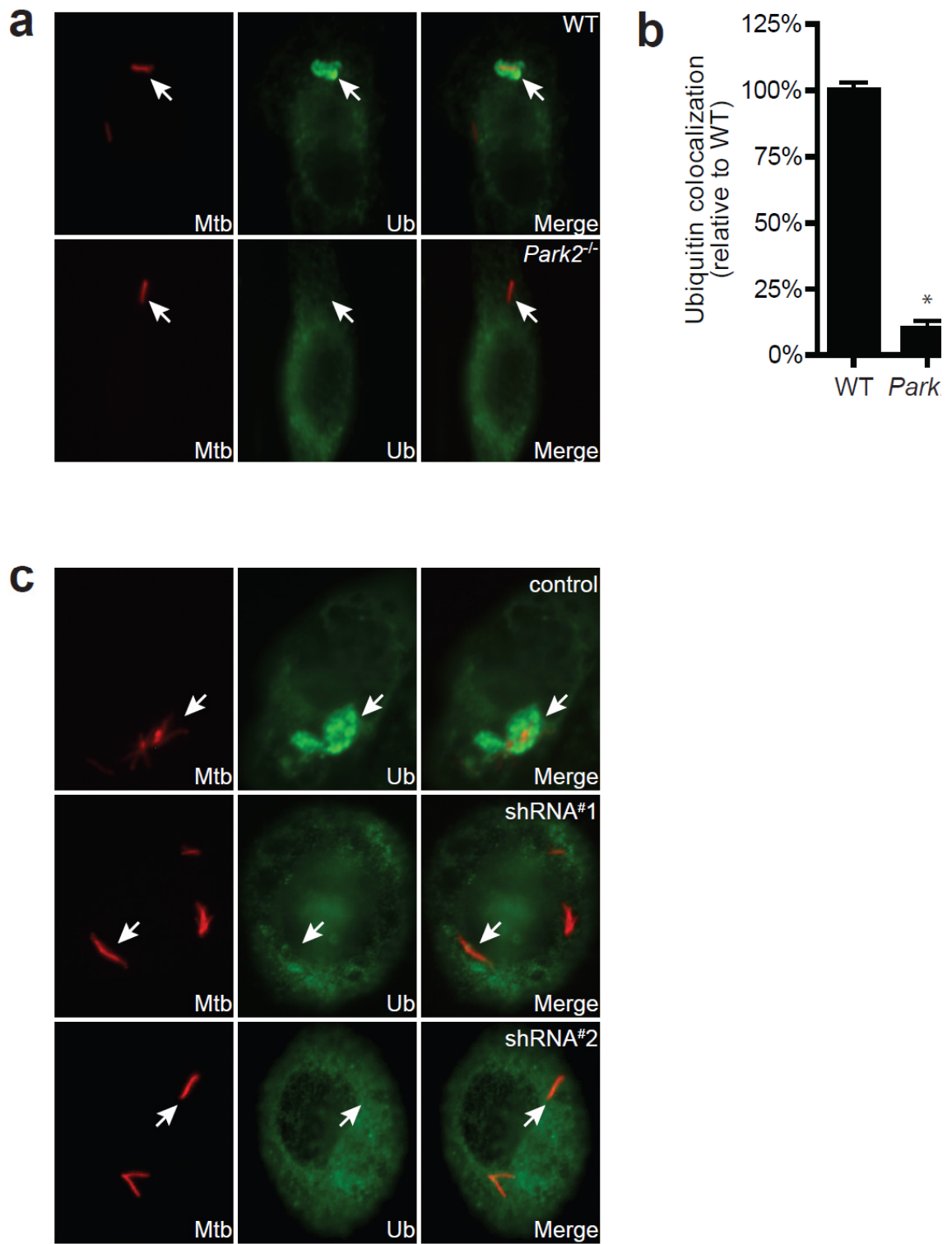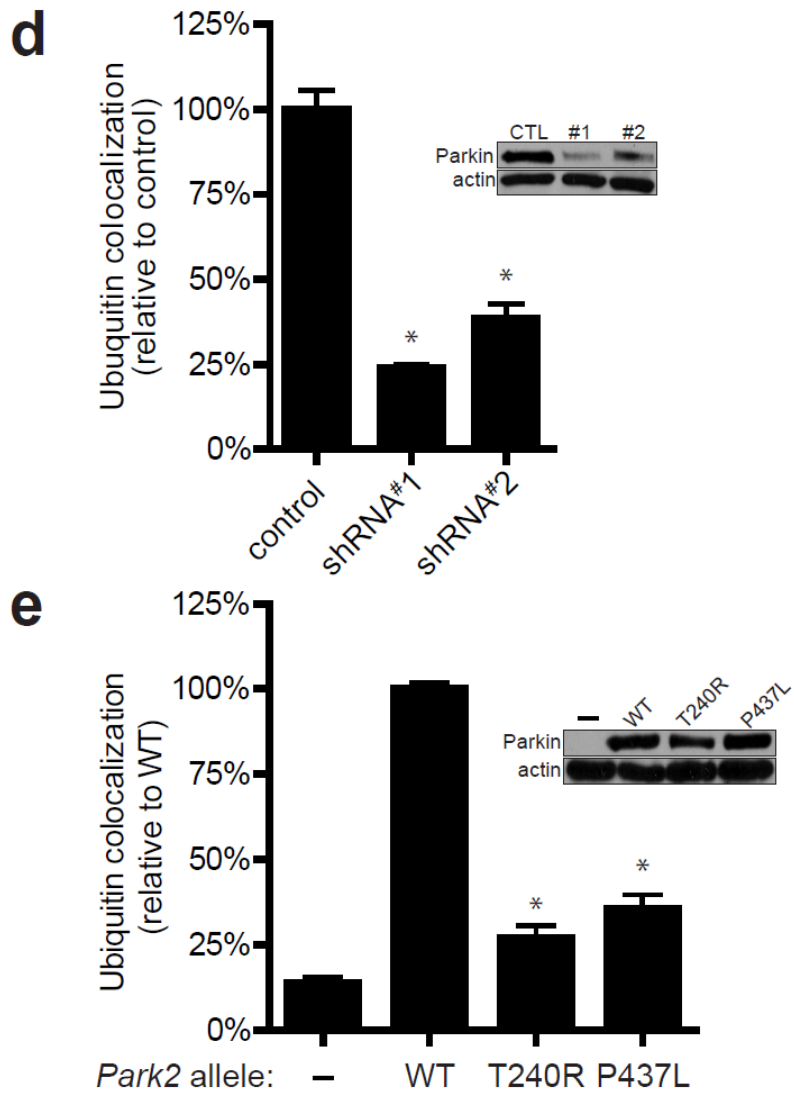
Figure 3.2 Time course analysis of ubiquitin and LC3 recruitment. a, Wild-type (WT

) and *Park2⁻/⁻* BMDMs were infected with mCherry-expressing *M. tuberculosis* and the

colocalization of LC3 and ubiquitin was quantified at the indicated time points via

immunofluorescence . Data shown is the percent of ubiquitin or LC3 positive bacteria
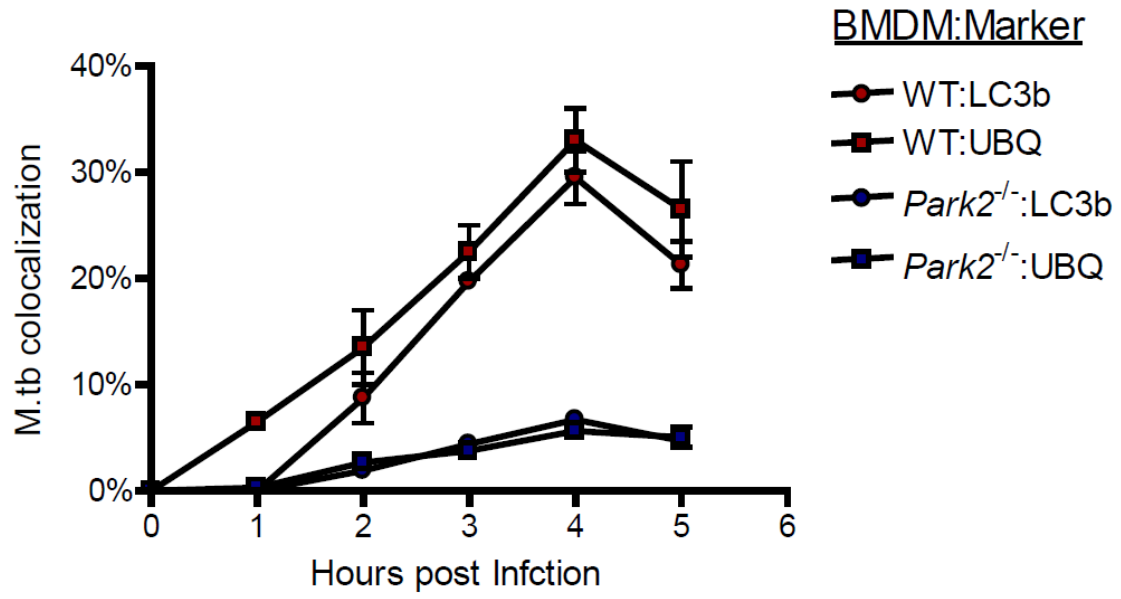
during the course of an infection.

Figure 3.2

Figure 3.3 PARKIN mediates K63-ubiquitin colocalization of *M. tuberculosis* and recruitment of ubiquitin-autophagy receptors. a, Wild-type (WT) BMDMs were infected with *M. tuberculosis* for 4 h and the percent of polyubiquitin positive bacteria that colocalize specifically with K63 or K48 ubiquitin chains was quantified (n=3 per group, *P < 0.001). **b,** Images of WT and *Park2*$^{-/-}$ BMDMs infected with mCherry-expressing *M. tuberculosis* for 4 h and immunostained for either K63 or K48 ubiquitin. **c,** Quantification of K63 or K48 ubiquitin positive *M. tuberculosis* from (**b**). Data is expressed as the percent of K48 or K63 positive cells relative to WT control cells (n=3 per group, *P < 0.001). **d,** Images of WT and *Park2*$^{-/-}$ BMDMs infected with mCherry-expressing *M. tuberculosis* for 4 h and immunostained for NDP52, p62, phospho-TBK1, and NBR1. **e,** Quantification of colocalization from (**d**), expressed relative to control WT cells (n=3 per group, *P < 0.001).

Figure 3.3
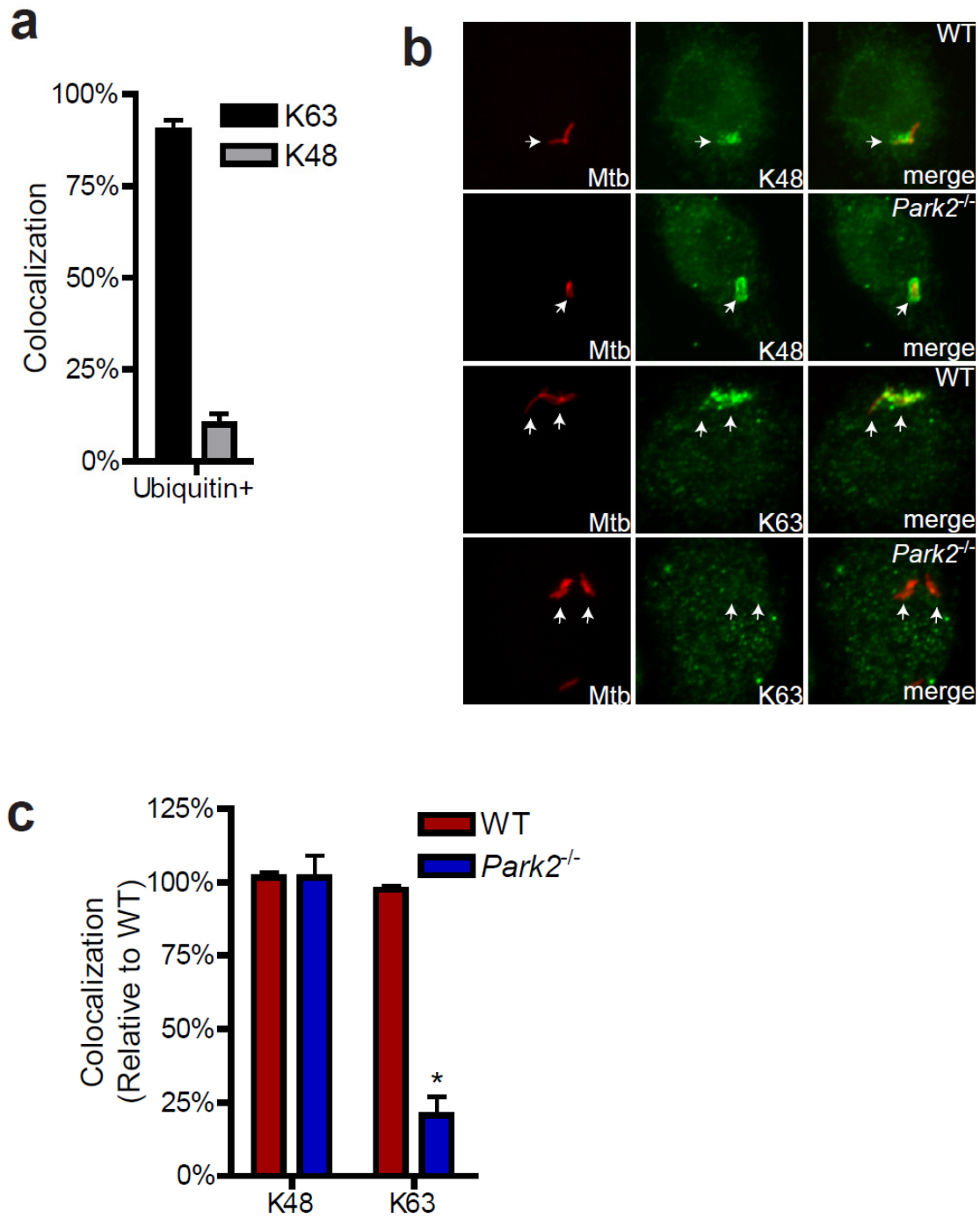
Figure 3.3
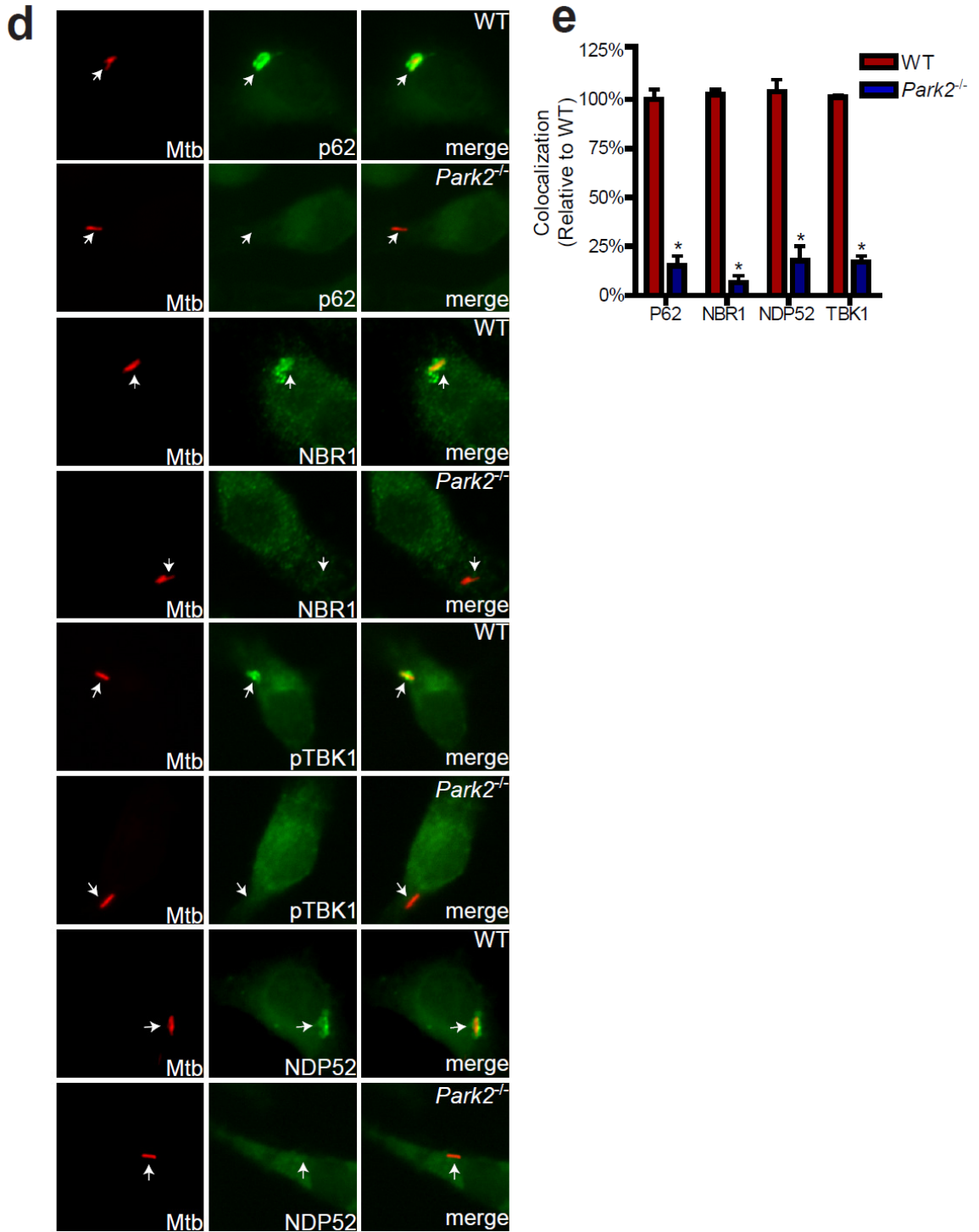
Figure 3.4 PARKIN mediates autophagic targeting of *M. tuberculosis* to lysosomes and limits bacterial replication. a, Images of wild-type (WT) and *Park2^{-/-}* BMDMs infected with mCherry-expressing *M. tuberculosis* for 4 h and immunostained for LC3 or ATG12. **b,** Quantification of ATG12- and LC3-positive *M. tuberculosis* from **(a)** expressed as a percentage of the values obtained from WT BMDMs (n=3 per group, *P < 0.001). **c,** LC3b cleavage was monitored by western blotting of lysates generated from **(a). d,** Images of BMDMs from knockout mice of the indicated genotypes infected with mCherry-expressing *M. tuberculosis* for 6 h and immunostained for Lamp1. **e,** Quantification of Lamp1 positive *M. tuberculosis* from **(a)** expressed as a percentage of the values obtained from control BMDMs (n=3 per group, *P < 0.001). **f,** BMDMs of the indicated genotypes were infected with WT *M. tuberculosis* at t=0 and colony forming units (CFU) were determined by plating cell lysates on solid media at t=0 and t=16 h. Results are the means ± SEM of three independent experiments and expressed as the percentage of CFU at t=16 compared to t=0 for each macrophage genotype (n=3 per group, *P < 0.02). **g,** U937 human macrophages expressing either a scrambled shRNA (control) or one of two different shRNAs targeting *Park2* (shRNA#1, shRNA#2) were infected with wild-type *M. tuberculosis* for 36 h and CFU were determined. Results are the means ± SEM of three independent experiments and expressed similarly as in **(f)** (n=3 per group, *P < 0.02).
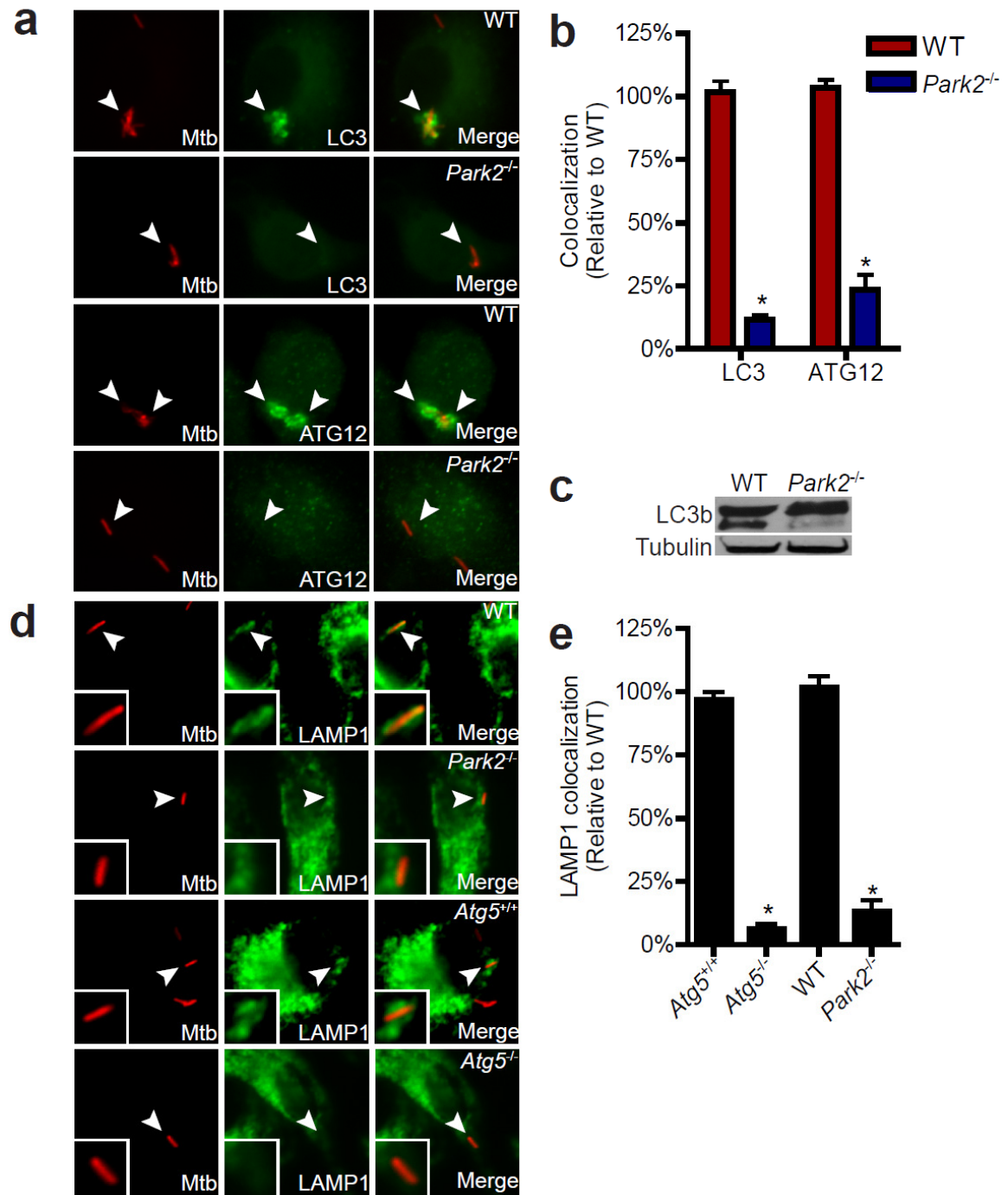
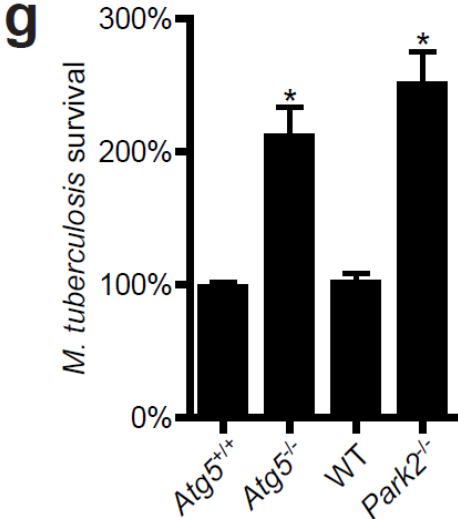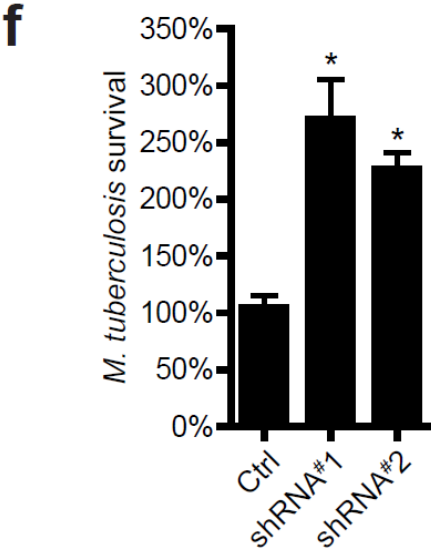# Figure 3.4

Figure 3.4

f

g

Figure 3. 5 PARKIN is required for control of bacterial infection *in vivo*. **a,** Wild-type (WT) and *Park2$^{-/-}$* mice were infected with wild-type *M. tuberculosis* via aerosol and lung bacterial burdens were determined at various time points by plating. Data is expressed as the mean ± SD (N=5 per group, *P<0.02 by Student's t-test). **b,** Enumeration of liver and spleen CFU from mice infected in (**a**) 21 days post-infection. Data shown is the mean ± SD, (N=5 per group, *P<0.03 by Student's t-test). **c,** Survival analysis of WT and *Park2$^{-/-}$* mice infected with wild-type *M. tuberculosis* (*P<0.001 by log-rank test). **d,** WT and *Park2$^{-/-}$* mice were infected with WT *L. monocytogenes* via IP injection and bacterial burdens in livers and spleens were determined by plating. Data shown is the mean ± SD (N=7 per group, *P<0.04 by Student's t-test). **e,** WT and two *Parkin* deficient *D. melanogaster* lines (*Park^{c00062}*, *Park^{f01950}*) were infected with *L. monocytogenes* via anterior abdomen injection. ATG8 processing was monitored by Western blot analysis of whole-fly protein lysates. **f,** Bacterial burdens of WT and *Parkin* deficient flies (*Park^{c00062}*, *Park^{f01950}*) infected with *L. monocytogenes*. Data shown is the mean ± SD (N=3-5 per group, *P<0.001 by Student's t-test). **g,** Survival of WT and *Parkin* deficient *D. melanogaster* flies (*Park^{c00062}*, *Park^{f01950}*) infected with *L. monocytogenes*. *P<0.001 by log-rank test.
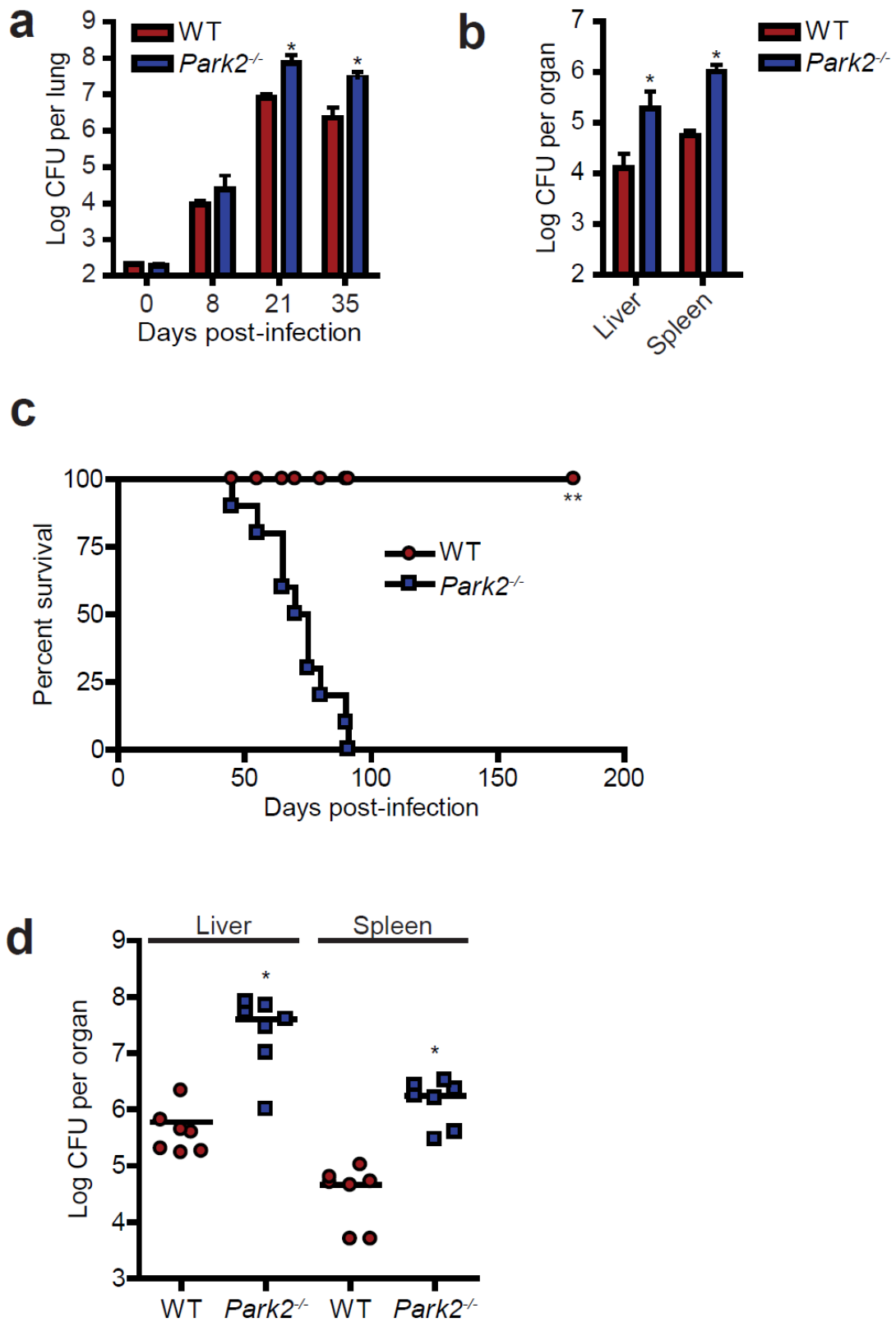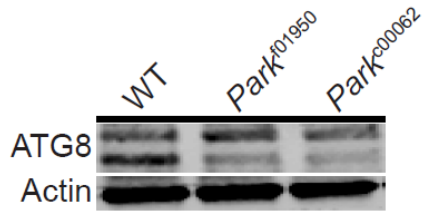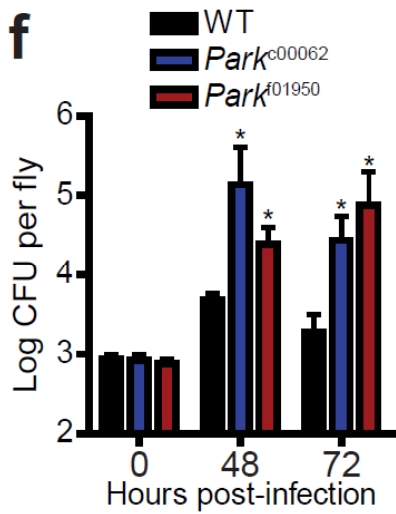
Figure 3.5

Figure 3.5
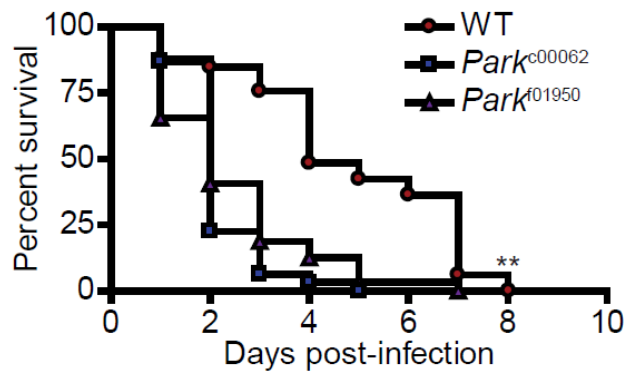
e

f

g

Figure 3.6 PARKIN is required for control of S. typhimurium and *M. marinum* infection within flies. **a,** Survival of WT and *Parkin* deficient *D. melanogaster* flies (*Park*^c00062^, *Park*^f01950^) infected with S. typhimurium. **P<0.001 by log-rank test. **b,** Bacterial burdens of WT and *Parkin* deficient flies (*Park*^c00062^, *Park*^f01950^) infected with S. typhimurium. Data shown is the mean ± SD (N=3-5 per group, *P<0.009 by Student's t-test). **c,** Survival of WT and *Parkin* deficient *D. melanogaster* flies (*Park*^c00062^, *Park*^f01950^) infected with *M. marinum*. **P<0.0045 by log-rank test.

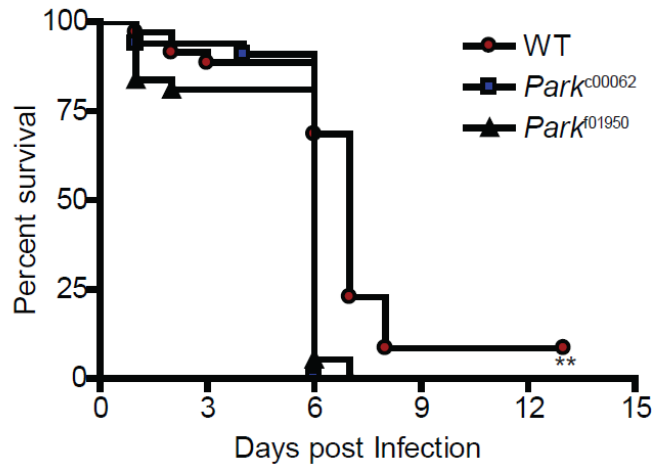# Figure 3.6

a
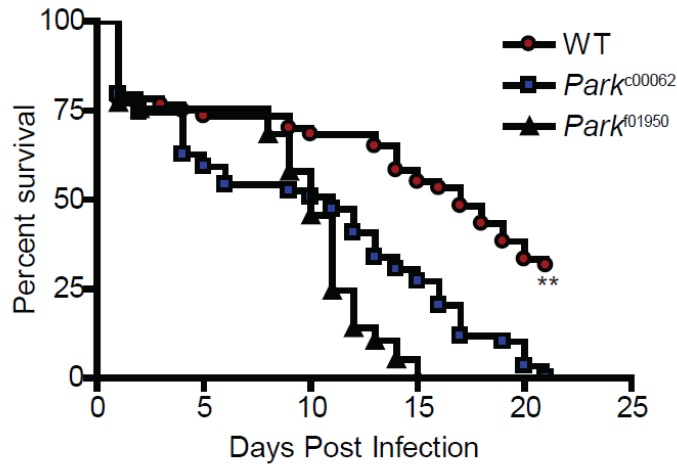
b
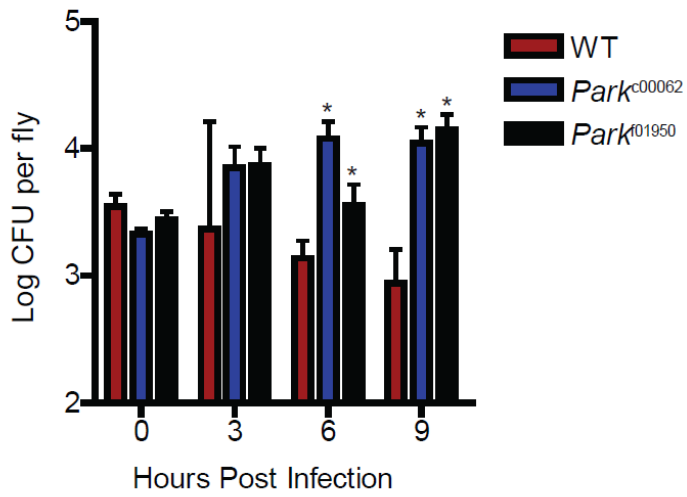
c

Chapter 4.

Conclusions and perspectives

In this thesis, I've detailed the molecular mechanisms of two clinically important host responses to *Mycobacterium tuberculosis* infection, the induction of interferon stimulatory genes (ISGs) and selective autophagy of *Mycobacterium tuberculosis*[1-3]. During the course of my thesis work, several groups have shown that ISG gene induction in PBMCs and peripheral blood can serve as a biomarker for active mycobacterial infection in humans[2-4]. These findings are of high clinical importance as current methods for determining whether humans are infected with active or latent *Mycobacterium tuberculosis* are currently unavailable[3]. Additionally, recent studies have also extended the importance of ISG gene induction to infection with other pathogenic mycobacteria, *Mycobacterium leprae* and *Mycobacterium bovis*[4, 5]. As both leprae and bovis species of mycobacteria contain a functional ESX-1 secretion system, it is likely that the mechanism for induction of ISGs is identical to that of *Mycobacterium tuberculosis* infection through activation of the STING-TBK1-IRF3 pathway. Thus, ISG induction appears to be a common host response to pathogenic mycobacteria and warrants future investigation into the mechanisms of how type I interferon and other ISGs affect the host and pathogen during the course of mycobacterial infection.

In addition to the mechanism of ISG gene induction, I've also shed light on the mechanism of autophagic targeting of *Mycobacterium tuberculosis* during infection of macrophages. Prior to our studies, several groups have published that chemical induction of autophagy could be used as a therapeutic against *Mycobacterium tuberculosis* infection[6, 7]. Our work is the first to show that autophagy plays a clear role *in vivo* in mouse models of mycobacterial infection, providing credence to the idea of targeting the

host autophagy pathway for treatment of mycobacterial infection. Lastly, our work highlights the novel relationship between DNA sensing and autophagy. Phylogenetic analysis of the protein components of cytosolic DNA sensing and autophagy appear to be evolutionarily conserved and are found in many organisms such as the Sea anemone which lack adaptive immunity and type I interferon signaling (unpublished data)[8]. Since DNA is present within the host nucleus and mitochondria, selective autophagy of cytosolic DNA may be an ancient mechanism to restore cellular homeostasis during organelle damage and sterile inflammation. Future work is needed to address the biological significance of selective

References

1. Ernst, J.D., *The immunological life cycle of tuberculosis.* Nature reviews. Immunology, 2012. **12**(8): p. 581-91.
2. Ottenhoff, T.H., et al., *Genome-wide expression profiling identifies type 1 interferon response pathways in active tuberculosis.* PloS one, 2012. **7**(9): p. e45839.
3. Berry, M.P., et al., *An interferon-inducible neutrophil-driven blood transcriptional signature in human tuberculosis.* Nature, 2010. **466**(7309): p. 973-7.
4. Teles, R.M., et al., *Type I Interferon Suppresses Type II Interferon-Triggered Human Anti-Mycobacterial Responses.* Science, 2013.
5. Killick, K.E., et al., *Genome-wide transcriptional profiling of peripheral blood leukocytes from cattle infected with Mycobacterium bovis reveals suppression of host immune genes.* BMC genomics, 2011. **12**: p. 611.
6. Deretic, V. and B. Levine, *Autophagy, immunity, and microbial adaptations.* Cell Host Microbe, 2009. **5**(6): p. 527-49.
7. Kumar, D., et al., *Genome-wide analysis of the host intracellular network that regulates survival of Mycobacterium tuberculosis.* Cell, 2010. **140**(5): p. 731-43.
8. Ouyang, S., et al., *Structural analysis of the STING adaptor protein reveals a hydrophobic dimer interface and mode of cyclic di-GMP binding.* Immunity, 2012. **36**(6): p. 1073-86.

Publishing Agreement

It is the policy of the University to encourage the distribution of all theses, dissertations, and manuscripts. Copies of all UCSF theses, dissertations, and manuscripts will be routed to the library via the Graduate Division. The library will make all theses, dissertations, and manuscripts accessible to the public and will preserve these to the best of their abilities, in perpetuity.

Please sign the following statement:

I hereby grant permission to the Graduate Division of the University of California, San Francisco to release copies of my thesis, dissertation, or manuscript to the Campus Library to provide access and preservation, in whole or in part, in perpetuity.

03/05/2013

_____ _____

Author Signature   Date